GCA-TR-68-18-N

ATMOSPHERIC NITRIC OXIDE MEASUREMENT TECHNIQUES

R. O. Carpenter C. Schuler J. Pressman

Bedford, Massachusetts

FINAL REPORT
CONTRACT NO. NAS12-85

PREPARED FOR
NATIONAL AERONAUTICS AND SPACE ADMINISTRATION
ELECTRONICS RESEARCH CENTER
CAMBRIDGE, MASSACHUSETTS

NOVEMBER 1968

GCA-TR-68-18-N

ATMOSPHERIC NITRIC OXIDE MEASUREMENT TECHNIQUE

R. O. Carpenter
C. Schuler
J. Pressman

GCA CORPORATION
GCA TECHNOLOGY DIVISION
Bedford, Massachusetts

FINAL REPORT

Contract No. NAS 12-85

November 1968

Prepared for:

NATIONAL AERONAUTICS AND SPACE ADMINISTRATION
Electronics Research Center
Cambridge, Massachusetts

TABLE OF CONTENTS

1. INTRODUCTION

The principal objective of the program reported herein has been the investigation and development of a suitable laser technique for the measurement of the vertical number density distribution of neutral nitric oxide in the earth's atmosphere.

Although NO represents a minor constituent of the upper atmosphere, it is believed to play a major role in the formation of the D and lower E regions of the ionosphere (Ref. 1,2). In addition, the chemiluminescence reaction between NO and O may be important in the generation of the observed night airglow continuum (Ref. 1). Finally, ion molecule reactions involving NO^+ and NO are important in determining the final steady state conditions prevailing in these ionospheric regions. Clearly, it is of prime importance to establish both the concentration and vertical distribution of this important constituent as well as its variations with time and other pertinent aeronomic parameters. On this basis, a number of recent experimental (Ref. 3,4,5) and theoretical (Ref. 1,2,6) investigations have been undertaken to perform this task. However, considerable uncertainties still remain concerning many quantitative aspects of this problem.

The first experimental measurement of NO in the earth's atmosphere was reported by Barth (Ref. 4) wherein the total content above 85 km was established by employing a rocket-borne scanning spectrometer to observe the gamma band ultraviolet fluorescence from solar illuminated NO. An analysis of the data indicated that the total measured column count amounted to about 1.7×10^{14} molecules/cm^2-column (above 85 km). Earlier, Jursa (Ref. 7) had attempted to measure the NO content by absorption spectroscopy using a rocket spectrograph with a solar-pointing control. Although NO was not detected, it was possible to estimate an upper limit of 10^{15} molecules/cm^2 resident within the altitude range of 63-87 kms. Subsequent measurements by Barth (Ref. 3) yielded local molecular number densities of between 4×10^7 cm^{-3} to 6×10^6 cm^{-3} throughout the altitude region between 110 km to 125 km. Finally, sunrise measurements by Smith (Ref. 5) yielded neutral NO number density estimates of about 10^7 cm^{-3} between 130 km to 150 km. Owing to the recent development of laser technology, the feasibility of utilizing the laser as an atmospheric probing tool has been demonstrated (Ref. 8-20) with varying degrees of success. The techniques employed involve detection of laser illuminated atmospheric constituents (including dust) via Rayleigh (Ref. 8-20), Raman (Ref. 18,19), Mie (Ref. 8-20) and/or resonance-fluorescence scattering (Ref. 16,20). Only the latter phenomenon can be employed for the detection of minor atmospheric constituents (i.e. NO) owing to their relatively low concentrations. Resonance-fluorescence scattering offers the potentials of both enhanced selective scattering (large cross sections) and specific species identifying radiation.

Various general aspects of a suitable laser radar probe are considered in Section 2. The effects of atmospheric attenuation, laser pulse length, quantum transitions and signal-to-noise considerations are presented. In addition, the interplay between several different parameters is examined. The resultant evaluation of a practical laser probe is given for selected transitions. In this regard, a detailed evaluation was performed on the characteristics of the nitric oxide energy states, including transition rates and branching probabilities, resonance and Rayleigh scattering cross sections, etc. On this basis, it was decided that the two optimum probe wavelengths were the ultraviolet 2155Å [gamma (1-0) electronic vibration transition] and the IR 5.33μ [vibration-rotation (0.1) transition].

Section 3 is devoted to the theoretical examination of several techniques of producing laser radiation for NO gas transition involving a ground state which is sufficiently populated in ambient atmospheric NO, and simultaneously possesses characteristics that are compatible to the development of a suitable probe. The two systems considered were those of the NO ground state fundamental at 5.33μ and the NO gamma band at 2155Å as selected in Section 2.

Two basic techniques were considered. The first involved the direct generation of the desired frequencies by a suitably arranged discharge configuration which required consideration of several physical processes including Franck-Condon pumping, photodissociation, chemical reactions, etc (Ref. 21,22). The second technique involved the generation of the desired frequencies by frequency shifting techniques. In this regard, selected wavelengths can be produced by shifting or tuning currently available lasers (e.g., CO_2, ruby, neodymium, etc.) by combinations of harmonic generation, sum, frequency production, stimulated Raman scattering, temperature turning, or mode selection. For example, the required 5.33μ radiation can be produced by generating the harmonic of the CO_2 laser radiation (10.6μ) while 2155Å radiation can be produced by generating a frequency approximately 5 times that of the Neodymium-in-glass laser (10,600Å).

A detailed account of the laboratory effort performed under the present program is presented in Section 4. The specific problems investigated include the lasing of NO itself, the harmonic generation in the CO_2 laser, and harmonic generation and mixing experiments with the Neodymium glass laser.

In Section 5, the results of this investigation are summarized and discussed in terms of the feasibility of producing a suitable NO atmospheric laser probe. It is concluded that little immediate promise exists for the development of a direct laser generator with sufficient power and other required field capabilities. However, it is shown that shift-tuning techniques can be applied to the generation of suitable laser wavelengths. Furthermore, the generation of suitable power levels requires the use of higher power lasers and thus further development. Finally, some recommendations for future work are presented in those areas which appear to offer the most promise.

2. THE PROBLEM OF DEVELOPING AN ATMOSPHERIC LASING PROBE — GENERAL CONSIDERATIONS

The problem of developing a suitable atmospheric lasing probe for a specific constituent is complex and detailed. However, there are a number of elements which are common to any lasing probe and which must be considered in sufficient detail in order to evaluate the feasibility of developing a specific probe. Thus, this section includes a sufficiently detailed discussion of a number of common elements for subsequent application to the present problem, i.e., the development of atmospheric lasing probe for measuring NO in the earth's atmosphere.

2.1 Resonant-Fluorescent and Rayleigh Scattering from Laser-Illuminated Atmospheric Constituents

The application of recent laser technology to atmospheric probing (Ref. 8-20) has demonstrated the feasibility of detecting laser illuminated constituents (and/or dust) by Rayleigh (Ref. 8-20), Raman (18, 19), Mie (Ref. 8-20) and/or resonance-fluorescence scattering (Ref. 16,20). For the case of minor atmospheric constituents (i.e., NO) only the latter phenomenon is applicable since it offers the enhanced selective scattering cross sections and associated signature radiation which are necessary for detection against the background radiations. Thus, in practice it is necessary to evaluate the ratio of resonant-fluorescent signal (from the trace species) to the Rayleigh scattered signal (from the total atmospheric composition) since this value establishes the basic threshold limit for trace detection by an active probe. In the following discussion the roles of resonant, fluorescent and Rayleigh scattering are considered individually; then the appropriate ratios are determined.

2.1.1 Resonant-scattering from laser illuminated species. — Assume that a laser transmitter emits a pulse of shape $P_\nu(\nu,t)$ (watts cm^{-1}) in time and spectrum, spectral energy $E_\nu = \int P_\nu(\nu,t)\,dt$ and total energy $J = \int\int P_\nu(\nu,t)\,d\nu\,dt$. For the present purpose, a square pulse approximation is employed so that $P_\nu = J/(\Delta\nu\ \Delta t)$ where $\Delta\nu$ and Δt are the transmitter spectral band pass and time constant, respectively. Additionally, the transmitter anular divergence shape which is assumed to be small, is taken to be a cond of $\Delta\Omega$ steradians.

Assume the receiver time constant Δt_R, spectral pass band $\Delta\nu_R$, and angular aperture $\Delta\Omega_R$ are all larger than the corresponding transmitter Δt, $\Delta\nu$, and $\Delta\Omega$-values. The range resolution of the optical radar is $\Delta R = c\ \Delta t_R/2$, and a general expression for the received laser signal is

$$S(t,R) = \frac{c\, n(R)\, A_R\, \tau^2}{8\pi R^2}\, \eta(R) \int E_\nu\, \sigma_\nu\, d\nu \ \text{(watts)} \qquad (2\text{-}1)$$

where

$S(t,R)$ = signal received by the detector at time t due to resonant scattering of laser illuminated species, i.e., NO at a range distance R,

c = velocity of light

$n(R)$ = population of molecules (i.e., NO) in the appropriate resonance energy level resident at R,

A_R = area of detector collecting surface,

τ = one-way transmission factor,

$\eta(R)$ = an efficiency factor defined subsequently (see Equation 2.2)

E_ν = energy in pulse per spectral unit,

σ_ν = absorption cross section.

In the above expression, the linewidth and shape depend on the combination of natural, Doppler, collision, multiplet structure, and other broadening effects. For low density upper atmosphere applications, the Doppler width is often the controlling feature. In the case of NO, the Doppler width between half-maxima is given approximately by $\Delta\nu_D \approx \nu\ 10^{-6}(T/273)^{1/2}$ which dominates the collision width in air if the density $n_a < 1/16$ NTP. For the present purposes, then, it is adequate to approximate the peak cross section by $\sigma_p = \alpha/\Delta\nu_D$ where $\alpha = \int \sigma_\nu\, d\nu$ = integrated absorption cross section. Finally, Equation (2-1) can also be expressed in terms of photons per second by multiplying by $(1/hc\nu)$ (photons/joule).

2.1.2 Fluorescent scattering from laser illuminated species. — In the previous discussion, the resonant scattering process for a molecule, such as NO, was considered. The initial action in this process consists of the absorption of a photon (from a transmitted electromagnetic beam) by a molecule in the appropriate lower state. When subsequent spontaneous emission to a different energy level occurs, the process results in fluorescent scattering of the laser pulse. Under certain conditions the intensity of this scattered radiation can dominate over the contribution due to resonant scattering.

In expression (2-1) it is assumed that the lifetime of the resonantly excited state is less than the receiver time constant Δt_R (the case where this assumption is not valid is considered later). In any event, a fluorescent efficiency factor may now be defined as

$$\eta(R) = \frac{A_{12}}{\Sigma_j A_{1j}} \quad (E_j < E_1) \tag{2-2}$$

which gives the fraction of the absorbed energy which is re-emitted spontaneously in the receiver pass band, the remainder decaying by other mechanisms. It should be recognized that there may be some non-radiative processes which may "quench" the excitation before the resonance time $(\Sigma A_{1j})^{-1}$ has elapsed. In general, these may be included in the "effective rates" A_{1j} with the understanding that these rates may depend on concentrations of other species and other parameters of the experimental situation. The simplest example applicable to radiative fluorescence in a molecular electronic band would be a laser emission of the vibrational (v',v'') component, raising the molecule to the upper v' level, from which it can fluoresce to all the lower vibrational levels; in many case $A_{v',v}$ may be greater than $A_{v',v''}$ $(v \neq v'')$ so that significant fluorescence results. It is evident that the precision of match and the relative widths of σ_ν and E_ν are critical in this situation. For the case where the spectral width of the laser pulse is narrower than the absorption line doppler width (which is not subject to system control), the maximum value for the final integral in Equation (2-1) is namely $J\sigma_p \approx \alpha J/\Delta\nu_D$. Thus, for the present case, Equation (2-1) may be written as

$$S(t,R) = \frac{c\tau^2}{8\pi} \frac{A_R}{R^2} \frac{\alpha J}{\Delta\nu_D} \left[\eta(R)\ n(R)\right] = \frac{K}{R^2} \left[\eta(R)\ n(R)\right] \tag{2-3}$$

where

$$K = \frac{c\tau^2}{8\pi} A_R \frac{\alpha J}{\Delta\nu_D}$$

For the constraints indicated, Expression (2-3) can be employed for estimating contributions from resonant and/or fluorescent scattering.

2.1.3 Rayleigh scattering from laser illuminated species. — The Rayleigh scattering of the standard atmospheric composition may be considered as a slowly varying spectral cross section $\sigma_{Ray}(\nu)$, and accurate quantitative data has been assembled by Penndorf (Ref. 23). The well-known λ^{-4} $(0 + \nu^4)$ spectral variation may be extracted from the data by writing

$$\sigma_{Ray}(\nu) = 4(2\pi\bar{a}\nu)^4 \cdot \overline{\pi a^2} = 128\ \pi^5\ \bar{a}^6\ \nu^4$$

where $\bar{a}(\nu)$ is an "effective" average molecular radius, deduced from Penndorf's detailed spectral considerations.

As in the case of resonance and fluorescence signals, the Rayleigh signal return is also given by Equation (2-1) by insertion of both the appropriate cross section, σ_{Ray} and <u>total</u> molecular density, n_t at the altitude and range at which the return is being analyzed in the range gate. Thus, for this case

$$S(t,R) = \frac{c\tau^2}{8\pi} \frac{A_R}{R^2} [\eta(R)\ n_t(R)] \int E_\nu\ \sigma_{Ray}\ d\nu \qquad (2\text{-}4)$$

For the Rayleigh scattering return, the line match integral is simply $J\sigma_{Ray}$, and the efficiency factor is $\eta \equiv 1$ so that Equation (2-4) can now be rewritten as:

$$S(t,R) = \frac{c\tau^2}{8\pi} \frac{A_R}{R^2} J\sigma_{Ray}\ n_t \qquad (2\text{-}5)$$

<u>2.1.4 The ratio of S(resonant)/ to S(Rayleigh).</u> – In practice, a major limiting factor of minor constituent detectability involves the ratio of the signals due to resonant and Rayleigh scattering. Thus, it is evident that for the present case

$$\frac{S(resonant)}{S(Rayleigh)} = \frac{\eta(R)\ n(R) \int E_\nu\ \sigma_\nu\ d\nu}{n_t\ J\sigma_{Ray}} \qquad (2\text{-}6)$$

which for an imperfect match (so that $\int E_\nu\ \sigma_\nu\ d\nu$ optimizes to $\approx \alpha J/\Delta\nu_D$ for a narrow, well-matched transmitter line) Expression (2-6) becomes

$$\frac{S(resonant)}{S(Rayleigh)} \approx \frac{\eta(R)\ n(R)\ \alpha}{n_t(R)\ \sigma_{Ray}\ \Delta\nu_D} \qquad (2\text{-}7)$$

On the basis of Equation (2-7) the following comments apply:

(1) As state, optimization requires $\Delta\nu$ (laser) $< \Delta\nu_D$. For other estimated laser shapes, the loss can be estimated from $\int E_\nu\ \sigma_\nu\ d\nu$, and is approximately $\Delta\nu_D/\Delta\nu$ (laser) for $\Delta\nu$ (laser) $\gg \Delta\nu_D$.

(2) With everything else the same, the lower temperature at the scattering point is favored by the Doppler width $\Delta\nu_D$ in Equations (2-7) and (2-3). This, however, is not subject to the control of the experimenter control in a given situation. An additional temperature factor is present from the equilibrium Boltzmann effect on the ratio n/n_t. This favors lower temperature for a ground state absorption, but higher temperature otherwise.

(3) Therefore, a principal factor in evaluating suitable laser transitions in NO will involve a comparison of the factor $n\alpha/\nu^5$ times the n/n_t ratio (the latter to be determined by the Boltzmann population factor in the appropriate lower state of the considered resonance transition). The ν^5 factor arises from $\sigma_{Ray}\ \Delta\nu_D$ in Equation (2-7). For future reference, it is convenient to distinguish the total NO density from the density in an appropriate energy state by writing $n(R) = p[NO]$, p expressing the Boltzmann distribution factor.

(4) Since higher laser energy will concommitantly increase resonant and Rayleigh scattering (other design factors having been optimized), Equation (2-7) for optimizing the resonant/Rayleigh signal ratio is independent of the laser energy magnitude. Alternatively, the absolute resonant or Rayleigh scattered signal is clearly directly proportional to the laser energy magnitude by Equations (2-1) and (2-4), and its effect in overcoming shot noise and internal receiver noise is considered subsequently. The effects of other background sources are also deferred for later consideration.

(5) All the above arguments assume the action of the direct resonant scattering process. A more detailed analysis is required to assess each case independently to ascertain whether the resonant excitation is "quenched" by fast collision processes during the lifetime of the excited resonant state. However, at the high altitudes involved (or low densities) significant quenching becomes less likely.

If a fluorescence transition should be more efficient than direct resonance, the receiver spectral filter could be tuned to the fluorescence line. This would have two advantages (1) there would be no Rayleigh scattering background return, and (2) both optical interference and saturation in the receiver from the transmitted pulse would be reduced. The fabrication of complex receiver filters accepting several fluorescent lines as well as the direct resonance, can be conceived. Unless continuous spectral background sources are present, only moderate shaping will be required. The effect of including fluorescent scattering is clearly to increase the factor of η towards unity. Next, one can conceive of the molecular laser generator having several vibrational components essentially equal in gain so that they simultaneously lase, or at least sequentially jump from one to the other (multimoding). Estimation of the effective fluorescent efficiency is relatively complex in such cases. In any event, because of the multiplicity of line frequencies in a complete molecular band, fluorescent efficiency estimation

represents a critical problem for successful signal intensity predictions. Finally, it is important to evaluate the effect of relatively long radiation lifetimes associated with fluorescence of the power return from laser illuminated constituents as discussed below in greater detail.

2.1.5 Effect of fluorescent radiation lifetime on power level of signal scattered from laser illuminated specie. – The purpose of the following brief analysis is to examine the consequences of relatively long (compared to the transmitted pulse time constant, τ_T) fluorescent radiative lifetimes on the time-history of the return from a laser radar utilizing resonant-fluorescent scattering from the illuminated molecule. As a pertinent example, molecular nitric oxide is considered wherein the pertinent transition is the fundamental vibration-rotation band of the ground state. The lifetime of the upper state is $\tau(v) = 0.088 \text{ sec}/(v'-1)$ whereas the typical pulse transit time (for an NO layer of 10 km thickness will be ≈ 30 μsec. For this case then, the previously presented laser radar formulae for power return are not applicable since the return from each resolution element (in height) has a unique position in time insofar as detector response is concerned.

First, consider a laser probe wherein the initial absorption of the pulse photons occurs within a region of width $dR = c\Delta t_R/2$ (where Δt_R is the receiver time constant). Thus one may write

$$dP_{Abs} = \frac{c\tau^2}{8\pi} A_R \frac{\alpha}{\Delta\nu_D} J [\eta(R)\ n(R)] = K\{\eta(R)\ p(R)\ [NO(R)]\} \quad (2\text{-}8)$$

where K and n(R) have been defined previously. The power at the receiver at time $t > 2R/c$ (from the 10-km layer of illuminated NO) is given by

$$dP_r = \frac{K}{\tau_F} \frac{f(R)}{R^2} \exp [-(t - 2R/c)/\tau_F] \quad (2\text{-}9)$$

where $f(R) = \eta(R)\ p(R)\ [NO(R)]$ and
τ_F = fluorescent radiative lifetime

However, at time, t, all the layers below the slice at R are also contributing owing to the relatively long fluorescence lifetime. Consequently, these contributions must be summed as follows

$$P_r(t) = K\ \tau_F^{-1} \exp(-t/\tau_F) \int_0^{ct/2} R^{-2} f(R) [\exp(2R/c\tau_F)]\, dR \quad (2\text{-}10)$$

Here what is sought is f(R) and one way of proceeding is to make trial estimates of f(R) that fit the shape of $P_r(t)$. A more elegant procedure is to proceed by differentiation.

$$\frac{\tau_F}{K}\frac{d}{dt}\left[P_r(t)\ \exp\ (t/\tau_F)\right] = 2c^{-1}\ t^{-2}\ \exp\ (t/\tau_F)\ f(R) \qquad (2\text{-}11)$$

$$f(R) = f(ct/2) = \frac{ct^2\ \tau_F}{2K}\left[\frac{dP_r(t)}{dt} + \frac{P_r(t)}{\tau_F}\right] \qquad (2\text{-}12)$$

The population factor p(R) and the fluorescence efficiency factor including quenching and multiple radiative paths can be determined theoretically from our knowledge of the atmosphere. Inserting the value of K

$$[NO(R)] = \frac{4\ t^2\ \tau_F\ \Delta\nu_D}{\alpha\ J\ A_R\ \eta(R)\ p(R)}\left[\frac{dP_r(t)}{dt} + \frac{P_r(t)}{\tau_F}\right] \qquad (2\text{-}13)$$

$$\propto t^2\left[\tau_F\ \frac{dP_r(t)}{dt} + P_r(t)\right] \qquad (2\text{-}14)$$

Equation (2-13) is an appropriate formula for the nitric oxide density at R = ct/2 expressed in terms of both the signal and the time derivative of the signal at time t. The t^2 factor arises from the inverse square law. The formula has the proper behavior for times after the pulse has arrived at the scattering region. Here [NO(R)] should equal zero for $t > 2R_{max}/c$ where R_{max} represents the upper limit of the scattering region. Since the pulse transit time is 10 km thick so that it is relatively small compared to the fluorescence lifetime, the fluorescing NO region behaves similar to a single decaying source described by

$$n/n_o = \exp\ (-t/\tau_F) \qquad (2\text{-}15)$$

$$\frac{dn}{dt} = (n_o/\tau)\ \exp\ (-t/\tau_F) = -\ n/\tau \qquad (2\text{-}16)$$

Equation (2-16) implies that Equation (2-14) will be zero as appropriate when the scattering layer has been traversed by the light pulse. Moreover Equation (2-14) also indicates that the information desired, namely the altitude distribution of NO can only be obtained from the noise of the signal pulse since for later times Equation (2-14) yields a zero result. Consequently Δt_R should be less than τ_T by an adequate

margin. Since $\tau_T = 30$ μsec, Δt_R should be no greater than 1 μsec yielding 30 resolution elements or 30 points defining the NO distribution.

On the basis of these expressions it is a relatively straightforward task to assess the effect of diminution of signal power owing to the fluorescent radiation lifetime factor. For example, Equation (2-1) can be recast to express the energy, E_T, scattered from a pulse of width τ_p during a period τ_r

$$E_T = B\ \tau_p\ \tau_r \tag{2-17}$$

where $B = \dfrac{P_n(R)\ A_R\ \tau^2}{4\pi R^2}\ \eta\ p\ [NO]\ \dfrac{c}{2}$, $P = \dfrac{J}{\tau}$

$$S_T = B\ \tau_p \tag{2-18}$$

The originally scattered energy, E_T in τ_R is now spread over the fluorescent lifetime τ_F. Dividing Equation (2-5) by τ_F one obtains the new signal power S_{TF}

$$S_{TF} = B\ \frac{\tau_p \tau_r}{\tau_F} \tag{2-19}$$

Taking ratios $$S_{TF} = \frac{\tau_r}{\tau_F} \quad ST = D_1\ S_T \tag{2-20}$$

where $D_1 = \dfrac{\tau_R}{\tau_F}$. This is merely the contribution from a region of width τ_r.

For the NO vibration-rotation lines and $\tau_R = 1$ μsec the diminution, D, is 10^{-5}. However, other layers located below that at (R - ct/2) are also contributing. If τ_T represents the transit time, the number of these layers runs from 1 to τ_T/τ_r and the diminution D_T for this total effect is given by

$$\frac{\tau_r}{\tau_F} \leq D_T \leq \frac{\tau_T}{\tau_F} \tag{2-21}$$

For NO: $10^{-5} \leq D_T \leq 3 \times 10^{-4}$

The maximum value that τ_T can assume is τ_F, since this is the time period within which the addition effects occur. Generally, for the upper atmosphere $\tau_T < 100$ km/c = 300 μsec since the scale height is of the

order of 10 kilometers and one simply runs out of atmosphere. The foregoing approximation has assumed uniform distribution of scatterers within the scattering region and uniform decay but nevertheless it represents a reasonable approximation to the exact solution of Equation (2-10) for the signal level.

2.2 Calculation of Selected Parameters Involved in Evaluating the Feasibility of a Laser Atmospheric Probe

An evaluation on the feasibility of developing a useful laser atmospheric probe involves the assessment of a number of pertinent parameters. These include: (1) Calculation of signal intensity estimates due to resonant fluorescent and Rayleigh scattering by laser illuminated species, (2) signal-to-noise estimates involving receiver noise, ambient background effects, (3) atmospheric attenuation, (4) atmospheric content and distribution of the probe species, and finally (5) a survey of the possible modes of generating the required lasing capability.

For the case of NO in particular, Items (3) and (4) have been discussed in detail elsewhere (Ref. 24,25), while Item (5) constitutes the subject matter of Section 3 of this report. Thus, in the present section, Items (1) and (2) are discussed in detail with reference made to the other items where pertinent.

2.2.1 Estimates for the S(resonant)/S(Rayleigh) ratio for some selected lasing transitions in NO. — In the following analysis, estimates are obtained for the S(resonant)/S(Rayleigh) ratios for three specific transitions in NO, each of which involve a specific type of lasing possibility. First, it is necessary to collect and assess some pertinent spectroscopic data on the NO molecule. This has been accomplished, and the material is presented in Tables 2-1 and 2-2 and in Figure 2-1. The constants associated with some electronic states of NO are summarized in Table 2-1 (the potential curves for the states are presented in Figure 2-1), whereas Table 2-2 includes data on the M-bands of NO as well as the frequencies of some ground state NO vibration-rotation bands. The three specific transitions considered in detail are: (1) the $(v'-v'')0, 0$ and $0,4$ M-bands (due to the electronic-vibration transition: $a\ ^4\Pi \rightarrow X\ ^2\Pi$) (2) the $(v-v'')0,0$ and 1.0 γ bands (due to the electronic vibration transition $A\ ^2\Sigma \rightarrow X\ ^2\Pi$) and, finally (3) the 1,0 vibration-rotation transition in the electronic ground state, $X\ ^2\Pi$, of NO. For (1) the 0,0 and 0,4 M band transitions occur at 2635 and 3265Å, respectively; for (2) the 0,0 and 1.0 γ bands occur at 2269 and 2155Å, respectively; and for (3) the 1,0 vibration-rotation band occurs in the IR at 5.33 microns.

The data shown in Table 2-1 are due to Gilmore (Ref. 26) and are applicable to the far UV transitions for the γ bands, while the information in Table 2-2 is due to Broida, et al. (Ref. 27). The m-bands transitions of present interest also lie in the far UV. Concerning the IR

TABLE 2-1

SOME ELECTRONIC STATES OF NITRIC OXIDE

State	Electron Configuration					Ω	T_e (cm^{-1})	Vibrational Constants			Rotational Constants			Vib.-Tot. Lifet Coupling
	3σ	1π	$1\pi^*$	$3\sigma^*$	Other			ω_e	$\omega_e x_e$	$\omega_e y_e$	B_e	α_e	r_e (A)	A
X $^2\Pi_r$	2	4	1	0		1/2 3/2	0 121.1	1904.03 1903.68	13.97	-0.0012	1.7042	0.01725	1.1508	123
a $^4\Pi_i$	2	3	2	0		5/2 3/2 5/2	37965±25	1019.0	12.8		1.14	0.02	1.407	
A $^2\Sigma^+$	2	4	0	0	$3s\sigma$	1/2	43965.7	2371.3	14.48	-0.28	1.9952	0.0164	1.0637	
B $^2\Pi_r$	2	3	2	0		1/2 3/2	45918.0 45946.7	1036.96 1038.41	7.603	+0.0967	1.076 1.177	0.0116 0.0189	1.415	
C $^2\Pi$	2	4	0	0	$3p\pi$	1/2 3/2	52148.0	2347.0	15.0		1.955	0.030	1.062	
D $^2\Sigma^+$	2	4	0	0	$4p\sigma$			2323.9	22.885		2.0026	0.021	1.062	

TABLE 2-2

M-Bands (ν_{oo} = 37,962 ± cm^{-1})			Frequency Table for NO Vibration-Rotation Bands (cm^{-1})										
v',v''		From IR	v'' →	0	1	2	3	4	5	6	7	8	9
0,1	(-14cm^{-1})	36,086	v' 1	1876	-	-	-	-	-	-	-	-	-
0,2		34,238	2	3724	1848	-	-	-	-	-	-	-	-
0,3		32,416	3	5546	3668	1820	-	-	-	-	-	-	-
0,4	30,626	30,625	4	7337		3612	1792	-	-	-	-	-	-
0,5	28,860	28,861	5	9101			3556	1764	-	-	-	-	-
0,6	27,121	27,124	6	10838				3500	1736	-	-	-	-
0,7	25,425	25,416	7	12546					3444	1708	-	-	-
0,8	23,751	23,735	8	14227						3389	1680	-	-
0,9	22,104	22,082	9	15880							3333	1652	-
0,10	20,481	20,457	10	17505								3277	1624

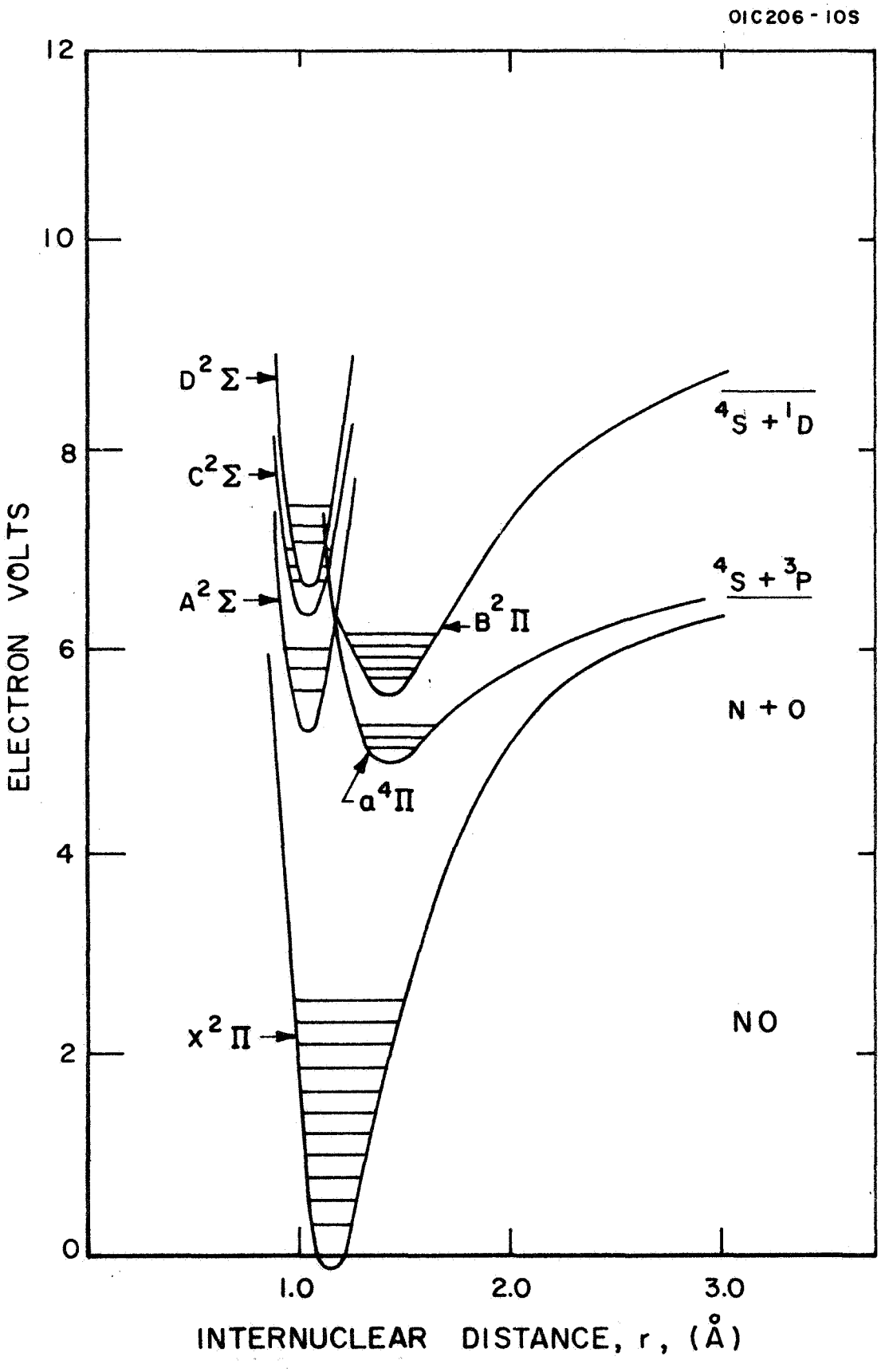

Figure 2-1. Potential energy curves for a number of selected electronic states for NO.

possibility, Carpenter and Franzosa (Ref. 28) have published a detailed analysis of the vibrational-rotational terms, frequencies, transition probabilities, and equilibrium thermal populations of the ground states $X\ ^2\Pi_{1/2,3/2}$ of NO. This work is too laborious to attempt for many excited states, although it can be performed for special cases of specific importance. Some of the frequencies of the fundamental transitions, $\nu_{v'v''}$ (cm^{-1}), of nitric oxide are shown in Table 2-2 for reference. These data are rounded off to one wavenumber as taken from Reference 19 and unpublished data tables compiled during the conduct of that previous investigation. Also shown in Table 2-2 are the M-band frequencies observed by Broida (Ref. 27). Since all the observed frequencies have the upper vibrational state $v' = 0$, Broida's data have been re-analyzed to derive only the single new constant $\nu_{oo} = 37{,}962 \pm 3\ cm^{-1}$, from which the other M-band centers are derived from the presumably more accurate IR-band data. The M-band is partially forbidden by the selection rule $\Delta s=0$, thus the "a" state (see Figure 2-1) has a "metastable" long lifetime, and at least some of the high M(0 - v") transitions may be lasable. However, the results of the following analysis indicate that they do not represent promising techniques for atmospheric probe applications.

Similarly, one can tabulate accurately the relative frequencies (0 - v") of other permitted nitric oxide transitions, ending on ground state γ, β, δ, ϵ, etc., the absolute position depending on the accuracy of knowledge of the term value T_e in Table 2-1. The γ-band would be particularly interesting for probe applications but will be difficult to lase.

A knowledge of the absolute radiative transition probabilities is desirable in any attempt to analyze atomic or molecular laser possibilities and active resonant probes for trace species. It is not expected that such data will be as complete and accurate as frequency data. Such data enter into the analysis in determining the relative laser gains, the resonant scattering cross section, and in the competition between various fluorescent and quenching mechanisms in the probe, and pumping mechanisms in the laser.

The quantum mechanical computation of the electronic transition moment, R_e of molecular transitions has not proven practical at present. However, in most cases the electronic-vibrational interaction is small and the transition probability between vibrational states can be separated into (Ref. 20)

$$A_{v'v''} = (hc\nu)^3\ R_e^2\ q_{v'v''} \qquad (2\text{-}22)$$

where

$$q_{v'v''} = \left| \int \psi_{v'} \psi_{v''}\ dt \right|^2 \qquad (2\text{-}23)$$

is the integrated overlap of vibrational wave functions called the "Franck-Condon factor." The assumption involves the fact that R_e is not highly sensitive to (v',v") within a given molecular electronic transition, so that the Franck-Condon factor yields reasonable estimates of relative transition probabilities within a band. Then a single experimentally determined band intensity can be employed to give absolute transition probabilities. Nicholls (Ref. 29) has applied the above technique and has published a list of absolute transition probabilities for the NO β and γ bands. In addition, Nicholls (Ref. 30) has computed the Franck-Condon factors for the M bands of NO, but these "forbidden" transitions are very weak and have not been observed under conditions where a reliable intensity value can be obtained (Ref. 18). For purposes of estimation, an upper limit has been determined in the following way:

From the failure to observe the M(0c0) band in laboratory absorption in pure NO up to 30 meters path at 1 atm., one may set an upper limit for $A_{oo} < 0.1\ sec^{-1}$. The Franck-Condon factors of Nicholls (Ref. 30) then give consistent limits for other M-band components, for estimating transition probabilities and fluorescent efficiencies.

For IR vibration-rotation bands, the absorption strength has been determined experimentally with perhaps 10 percent accuracy, which determines absolutely A_{10} (see References 28, 31, and 32). For a harmonic potential function, the Franck-Condon integral for the fundamental transitions is expressed by

$$q_{v',v'-1} \propto v'$$

Breene (Ref. 33) has performed some calculations for nitric oxide vibrational matrix elements for an harmonic (Lippincott) potentials and a three-term dipole moment expansion. His values differ slightly from the harmonic oscillator approximation, the difference increasing at higher v', but it is difficult to establish the reliability of his models and calculations. Therefore the above harmonic oscillation rule was adopted for the transition probabilities for the IR band for nitric oxide as follows:

Upper v':	0	1	2	3	4	etc.
$A_{v',v'-1}$:	11.4	22.8	34.2	45.6	57	(sec^{-1}) etc.

The key parameters for evaluating the ratio of resonant to Rayleigh scattering for five specific bands of NO are presented in Table 2-3. Calculations were based on the optimum (well-matched) form of Equation (2-7):

TABLE 2-3

ESTIMATE OF RESONANT/RAYLEIGH RATIO IN NITRIC OXIDE ATMOSPHERE PROBE

Band	M	M	Vibrational-Rotational	γ-Bands		Notes & Ref.
v', v''	0,0	0,4	1,0	0,0	1,0	(1)
$\lambda_{v'v''}(\mu)$	0.2635	0.3265	5.33	0.2269	0.2155	
$\nu_{v'v''}(cm^{-1})$	37,962	30,640	1876	44,100	46,450	
$A_{v'v''}(sec^{-1})$	< 0.1	< 50	11.4	5.15×10^{5}	1.14×10^{6}	(2)
$f_{v'v''}$	$< 1.70 \times 10^{-10}$	$< 1.30 \times 10^{-7}$	4.86×10^{-6}	4.14×10^{-4}	7.88×10^{-4}	(2)
α (cm)	$< 1.50 \times 10^{-22}$	$< 1.10 \times 10^{-19}$	4.27×10^{-18}	3.50×10^{-16}	7.00×10^{-16}	(2)
$\Delta\nu_D(cm^{-1})$	3.00×10^{-2}	2.50×10^{-2}	1.50×10^{-3}	3.50×10^{-2}	3.70×10^{-2}	
σ(Ray) (cm^{-2})	1.00×10^{-25}	4.00×10^{-26}	5.80×10^{-31}	2.10×10^{-25}	2.50×10^{-25}	(3)
$p(v'', j'' = 5\frac{1}{2})$	0.069	$0.069 \times e^{-65}$	0.069	0.069	0.069	(4)
Fluorescent (P6)	7.10×10^{-5}	0.036	0.53	0.073	0.154	(5)
Efficiency (η) (Q5)	0.56×10^{-5}	0.0027	0.04	0.0055	0.0116	(5)
(R4)	6.50×10^{-5}	0.029	0.43	0.060	0.125	(5)
S(resonant)/ S(Rayleigh)	$< 7.00 \times 10^{-9}$	$< 10^{-28}$	5.00×10^{8}	690	2400	
Lifetime (sec)	$> 10^{-3}$	$> 10^{-3}$	0.088	0.26×10^{-6}	0.26×10^{-6}	

$$\frac{S(\text{resonant})}{S(\text{Rayleigh})} = \frac{np\ [NO]\ \alpha}{\eta_{air}\ \sigma_{Ray}\ \Delta\nu_D}$$

the required estimate of the content and distribution of atmospheric NO can be obtained as follows. Barth (Ref. 3) has measured the column density of NO above 86 km by observation of the fluorescence scattering in the γ(1-0) band of solar illuminated NO. From the results one may deduce that

$$\int_{85\ km}^{\infty} [NO]\ dh = 1.7 \times 10^{14}\ \text{molecules/cm}^2$$

Although the distribution of local density [NO] was not measured it is generally accepted that the distribution peaks in the vicinity of 90 km. The layer thickness is probably 1 or 2 scale heights, which at 90 km is about 5 km. Thus, it is assumed that the effective layer thickness

$$\Delta h = \int [NO]\ dh/[NO]\ (\text{peak}) \approx 10\ \text{km}$$

so that $n[NO]_{max} \approx 1.7 \times 10^8\ cm^{-3}$. At 90 km, according to the ARDC model atmosphere, $n(air) = 5.92 \times 10^{13}\ cm^{-3}$, $T = 166^{\circ}K$. At this temperature the Doppler width for NO is $\Delta\nu_D \approx 0.8 \times 10^{-6}\ \nu$.

The tabulated (see Table 2-3) parameters and the [NO], n and T-values presented above were employed to calculate the required S(resonant)/S(Rayleigh) ratios shown in line 12 of the table. It is evident that for the transitions considered, favorable values obtain only for the 5.3μ vibration-rotation and γ-band transitions. Thus, on the basis of the pertinent spectroscopic constants, it appears that these two possibilities deserve further consideration. The problem of obtaining the required lasing wavelength is discussed in greater detail in Sections 3.1, 3.2 and 4.1 of this report. For completeness, some pertinent notes and references are presented below for data associated with the entries in Table 2-3.

(1) v' = upper, v'' = lower state.
(2) α,f,A are related by Equation (2-1):

$$\alpha = \int_{line} \sigma(\nu)\ d\nu = \frac{1}{8\pi\ c\nu_{21}^2} \cdot \frac{g_2}{g_1} A_{21} = \frac{\pi e^2}{mc^2} f_{abs}\ [cm]$$

In particular, α,f differ only by $\pi e^2/mc^2 = 8.83 \times 10^{-13}$ cm where f is the non-dimensional "oscillator absorption strength" and α is the "integrated cross section."

(3) R. Penndorf, JOSA 47, 176 (1957), Reference 23.

(4) The ground state of NO is an electronic doublet, $^2\Pi_{1/2}$ at $T_e = 0$, and $^2\Pi_{3/2}$ at $T_e \approx 121$ cm^{-1}. Therefore, the electronic partition function Q_e is $1 + \exp(-hc\, T_{3/2}/KT) \approx 1.53$ at 166°K with 65.3 percent in $^2\Pi_{1/2}$, 34.7 percent in $^2\Pi_{3/2}$. (Corresponding bands of these two states are separated a few tenths wavenumber which exceeds the Doppler width at 90 km.) The more populated $^2\Pi_{1/2}$ state is selected for the laser transmitter. The vibrational excitation at 166°K is negligible, i.e., all molecules are in $v'' = 0$ state. The population for $v'' = 4$ is $\approx \exp(-4hc\, \omega_e\, KT) \approx e^{-65}$, which is a key problem for the M (0,4) band. Of the 65.3 percent in $^2\Pi_{1/2}$ ($v'' = 0$) the maximum population will be in the rotational state (Ref. 26)

$$J_{max} \approx \frac{KT}{2hcB} - 1/2 \approx 5\,\frac{1}{2} \text{ for NO at } 166^{\circ}K$$

The rotation partition function will be

$$Q_R \approx \frac{KT}{hcB} \approx 68 \text{ at } 166^{\circ}K$$

The rotational energy $T_J(5.5) = 58.9$ cm^{-1}, and the relative population (Ref. 34)

$$\frac{n_J}{n} = \frac{(2J + 1)}{Q_R} \exp(-hcT_J/KT)$$

Thus, the overall Boltzmann factor for the state ($^2\Pi_{1/2}$, $v'' = 0$, $j'' = 5\ 1/2$) is

$$p \approx 0.069$$

(5) The overall fluorescent efficiency $\eta = \eta_e\, \eta_v\, \eta_r\, \eta$ (quenching). Most molecular lasers listed by Bennett (Ref. 35) more readily lase on the P-branch. It is assumed that a single line P(5.5) is transmitted. Then the resonantly excited molecule in the upper state will be $j' = 4.5$. From this level, three rotational components can radiate spontaneously, P(5.5), Q(4.5), and R(3.5). Their relative statistical weights are given by the Hönl-London formulae (in terms of upper J):

$$H_P(j) = \frac{j'(j'+2)}{j'+1} = 5.32$$

$$H_Q(j) = \frac{2j'+1}{j'(j'+1)} = 0.40$$

$$H_R(j) = \frac{(j'-1)(j'+1)}{j'} = 4.28$$

$$(2j'+1) = \text{sum} = 10.00 \qquad (2\text{-}24)$$

Therefore, the fluorescent efficiencies for the three rotational components are

$$\eta_P = 0.53, \qquad \eta_Q = 0.04, \qquad \eta_R = 0.43$$

The fluorescent efficiencies for biration are given by

$$\eta_v = A_{v'v''}/\Sigma_{v'}A_{v'v''} \qquad (2\text{-}25)$$

Barth (Ref. 3) has calculated $\eta_v = 0.292$ for the $\gamma(1\text{-}0)$ band. Since $A \rightarrow a$ is forbidden, no alternate electronic decay of significance exists. Thus, the overall n for the $\gamma(1\text{-}0)$ band is estimated as 0.154(P), 0.0116(Q), and 0.125(R). Values for $\gamma(0\text{-}0)$ are similarly estimated to be $\eta_v(0,0) = 0.138$.

For the vibration-rotation (1-0) band transition, the only competition for radiative decay would arise from the pure rotational transition, e.g., $j = 5 \rightarrow 4$, although absolute rotational probabilities are small compared to vibrational transitions. Thus, it is assumed that the overall efficiency is represented by the above values of η_R for the vibration-rotation band.

The appropriate η_v for the m bands have been calculated from Nicholls' Franck-Condon factors and frequencies.

2.2.2 Estimates of signal strength, receiver noise, and ambient background sources. — A preceding section contained a discussion of the ratio of resonant signal-from-trace species to the Rayleigh scattered signal from the total atmospheric composition which establishes one of the limits to threshold for trace detection by an active probe. Since both these signals are directly proportional to laser pulse energy, this ratio is independent of energy. In the present section, absolute signal levels are estimated in order to establish the signal threshold levels as limited by the detector noise (S/N depends on the transmitted laser

energy), and limits due to extraneous radiation backgrounds, such as the Rayleigh scattered sunlight, atmospheric thermal excitation, fluorescence from solar illuminated species, airglow, etc.

First, numerical estimates of signal strength are derived for the case of the IR 5.3-micron band. In this case, since the NO layer thickness is estimated to be $\Delta h \cong 10$ km, the transit time $(\Delta h/c) \approx 67$ μsec, whereas the fluorescent lifetime is $\tau_F = 0.088$ sec. Under these conditions, the actual signal at the receiver telescope is given approximately by

$$S(t,R) = \left(\frac{c\alpha A_R J}{8\pi}\right)\left(\frac{\tau^2 \eta \rho [NO]}{R^2 \Delta\nu_D}\right)\left(\frac{2\Delta h}{c\tau_F} \exp\ [-t/\tau_F]\right) \qquad (2\text{-}26)$$

That is, the effect of the fluorescent delay is to attenuate the received amplitude by $(2\Delta h/c\Delta\tau_F)$. At this point, it is instructive to rewrite the amplitude of

$$S(t,R) = \left(\frac{J}{\tau_F}\right)\left(\frac{A_R}{4\pi R^2}\right)(\tau^2 \eta \rho)\left(\frac{\alpha [NO]\Delta h}{\Delta\nu_D}\right) \qquad (2\text{-}27)$$

In this form one can now interpret J/τ_F as the average transmitter power over the effective fluorescent time constant; $A_R/4\pi R^2$ as the effective fractional solid angle intercepted by the receiver τ^2 np as certain nondimensional efficiencies depending upon transmission, fluorescent loss, and population factor. In addition, $\alpha[NO]\Delta h/\Delta\nu_D$ defines the nondimensional "optical absorption depth" of the $[NO]\Delta h$ layer, since $\alpha/\Delta\nu_D$ represents the peak absorption cross section, σ_p. The following assumed or estimated parameters have been employed:

$$\alpha = 4.27 \times 10^{-18}\ \text{cm}^2$$
$$A_R = 1000\ \text{cm}^2$$
$$J = 1\ \text{joule (or } 2.6 \times 10^{19}\ \text{photons)}$$
$$\tau = 1$$
$$\eta = 0.53$$
$$p = 0.069$$
$$[NO]\Delta h = 1.7 \times 10^{14}\ \text{cm}^{-2}$$
$$R = 90\ \text{km}$$
$$R^2 = 81 \times 10^{12}\ \text{cm}^2$$
$$\Delta\nu_D = 0.0015\ \text{cm}^{-1}$$

Substitution of these values into Equation (2-27) yields a return signal amplitude of $S(t,R) \approx 2 \times 10^{-12}$ watts or 5.2×10^{7} photons/sec.

The "noise equivalent power," NEP, of the photovoltaic InSb detectors marketed by Texas Instruments, Inc. is estimated for ready comparison. These highly developed detectors (cooled by liquid nitrogen) are relatively sensitive to the cutoff wavelength of about 5.5 microns, so that they are appropriate to employ for the 5.3-micron spectral region. The NEP is best described in terms of the conventional figure of merit, $D^* \approx 1.5 \times 10^{10}$ watts^{-1} cm cps$^{1/2}$, with NEP $\approx (A\ \Delta f_R)^{1/2}/D$ where A is the detector area (fabrication of this D is practical in the range 10^{-3} to 10 cm^2), and $\Delta f_R = (1/2\ \Delta t_R)$ describes the electrical bandpass or time constant of the detector and associated circuitry (the pv - InSb material at 77°K is limited to $\Delta t = > 0.5$ microsecond).

Low NEP or noise is favored by small A and long Δt_R, whereas range resolution requires short Δt_R. Assuming typical laser transmitter beam divergence $\Delta\Omega = 16^{-6}$ steradian (receiver telescope same) and telescope F/D = 1, $A_R = 10^3$ cm^2, then the minimum practical A $\approx 10^{-3}$ cm^2 can be achieved. First, consider that Δt x 100 μsec, which is adequate to observe the layer [NO]Δh, (though it will not be adequate for high resolution of local density NO). Thus with these suggested parameters NEP $\approx$ 1.5×10^{-10} watts or 3.9×10^{9} photons/sec.

When this value is compared with the previously estimated signal of 2×10^{-12} watts, it appears somewhat discouraging. At first glance, it is not obvious why one cannot detect 5200 photons in 100 μsec with a high quantum efficiency detector such as pv-InSb. The basic reason is that the background photons from the assumed (or laboratory) 300°K background in the calibration of D provides an effective background of about 10^{-6} watts; it is the shot noise associated with this background which provides the major obstacle.

This analysis would suggest operation of a practical probe wherein the instrument walls and optics are maintained at a sufficiently low temperature to significantly reduce the thermal radiation background. In this regard, a previously reported (Ref. 16) analysis which considered the atmospheric attenuation of the 5.3-micron radiation as well as the ambient thermal background radiation has indicated that the practical operation of a 5.3-micron laser probe would be performed at high aircraft altitudes (about 40,000 to 45,000 ft) whereby the thermal background (T $\approx$ 220°K) radiation is reduced by about two orders of magnitude, Thus, under these admittedly stringent conditions it appears that favorable S/N ratios can be obtained.

---

*For information on low temperature detection problems, and properties of InSb and other IR quantum detectors, see Texas Instruments, Inc. bulletin "Infrared Devices," and such texts as Kruse, et al., "Elements of IR Technology," or Jamieson, et al., "IR Physics and Engineering."

An analagous S/N determination (Ref. 25) involving the 0,0 γ-band radiation has also indicated a requirement to operate at high aircraft altitudes. However, in this case, the major factor is not thermal background radiation but atmospheric attenuation. The study (Ref. 25) has also indicated that fluorescence of solar illuminated NO as well as day and/or night airglow emissions present no background problem for performing 0,0 γ-band lasing probe measurements.

Thus, it appears that favorable S/N ratio values obtain for both the IR 5.3-micron and UV 2155Å lasing wavelengths so long as operation is performed above high operational aircraft altitudes.

2.2.3 Discussion of minimum power requirements as a function of frequency for the NO laser. – In the following discussion, the effect of frequency on the power requirements of the NO laser is considered in different portions of the electromagnetic spectrum. The development employed is similar to that due to Schawlow and Townes (Ref. 36).

Any ensemble of excited systems which is capable of producing coherent amplification at very high frequencies must also be expected to emit the usual amount of spontaneous emission. The power in this spontaneous emission increases relatively rapidly with frequency since it is proportional to ν^4 if the width $\Delta\nu$ is due to Doppler effects or as ν^6 if the width is produced by spontaneous emission. By proper selection of a low transition probability, $\Delta\nu$ can be limited to that associated with the Doppler effect. However, the increase in spontaneously emitted power as rapid as ν^4 is unavoidable.

The minimum power, P, which must be supplied in order to maintain n systems in excited states is given by

$$P = \frac{nh\nu}{\tau} = \frac{ph\nu}{t} \tag{2-28}$$

where τ = lifetime of state
p = number of modes which are effective in producing spontaneous emission
t = time constant for rate of decay in cavity
h = Planck's constant
ν = frequency

$$p(\nu)\, d\nu = \frac{8\pi\, \nu^2\, \nu\, d\nu}{c^3} \tag{2-29}$$

For a Lorentzian line shape

$$p = \frac{8\pi^2\, \nu^2\, V\, \Delta\nu}{c^3} \tag{2-30}$$

while for a Doppler shape the corresponding number of effective modes is

$$p = \frac{8\pi^2 \nu^2 V \Delta\nu}{(\pi \ell n\ 2)^{3/2} c^3} \qquad (2\text{-}31)$$

The cavity decay time t is given by

$$t = 6\ V(1 - \alpha)\ Ac \qquad (2\text{-}32)$$

where V = volume
α = reflective coefficient
A = cross section
c = velocity of light

For a Doppler line width

$$\Delta\nu_p = \frac{2\nu}{c}\sqrt{\frac{2\ kT\ \ell n\ 2}{M}} \qquad (2\text{-}33)$$

while for the natural line width

$$\Delta\nu_N = \frac{A_{ab}}{4\pi} \qquad (2\text{-}34)$$

where

$$A_{ab} = \frac{64\pi^4 \nu^3}{3h\ c^3} |R_{ab}|^2 = \text{matrix element for the dipole transition between states a and b} \qquad (2\text{-}35)$$

Substituting Equations (2-33) and (2-34) into Equations (2-31) and (2-32) respectively, where Equation (2-35) has been used in Equation (2-34) one obtains

(a) $P \sim \nu^4$ for a Doppler profile
(b) $P \sim \nu^6$ for a natural line profile (2-36)

as stated above.

For a laser of one centimeter length, 1 cm^2 cross section, $\lambda = 50{,}000\text{Å} = 5\mu$ (the NO vibration rotation band) and broadenind due to the Doppler effect, Equation (2-28) gives minimum power requirements of

$$P_{VR} = 1.3 \times 10^{-6} \text{ watts}$$

If lasing is attempted at the M bands or the γ bands of NO (at approximately 0.2μ) the power requirements become

$$P_M = (5\mu/0.2\mu)^4 P_{VR} = 3.9 \times 10^5 P_{VR}$$

or between five and six orders of magnitude greater

$$\simeq 4 \times 10^{-1} \text{ watts}$$

On the basis of these arguments, it appears that the use of the M or γ-band radiations is contra-indicated. Thus, from the view point of power requirements alone, it appears that employment of the IR 5.3-micron wavelength offers the optimum possibility for a practical NO radar probe at least in light of present technology. In this regard, the following section surveys a number of possibilities and mechanisms for obtaining lasing action in both the IR and UV spectral regions.

3. STUDY AND EVALUATION OF PROBING TECHNIQUES

3.1 Analysis of Mechanisms for Lasing Action in the Vibrational-Rotational States of the NO Ground Electronic State ($X\ ^2\Pi_r$)

The purpose of this section is the presentation of a relatively detailed discussion of the possible mechanisms by which lasing action can be obtained either through total or partial inversions in the ground electronic state ($X\ ^2\Pi_r$) of NO. This initial systematic investigation would serve then as a basis for the selection of the most promising approaches to those problems which could be isolated for further analysis as required. Additionally, this analytical material assists in the design of an appropriate experimental setup characterized by sufficient versatility to explore various type of inverting mechanisms. The variety of possibilities for achieving the required inversions involve the lasing in ground state NO by: (1) direct discharge, (2) vibrational-rotational transfer via inelastic collisions, (3) electronic-vibrational transfer via inelastic collisions, (4) chemical reactions resulting in selective vibration-rotation enhancement, (5)Franck-Condon pumping involving electronic-vibrational transitions, (6) photodissociation and fluoriescence for selective inversion, (7) thermal excitations and non-equilibrium cooling, and (8) direct excitation by blackbody radiation.

In the following discussion, the individual mechanisms are described in varying detail depending upon the present availability of supporting data (cross sections, collisional transfer, transition probabilities) and conceptual schemes for ealing with the calculations involved in the multiple competing processes. Finally, in some cases there will be a partial duplication in some of the categories whereas in other categories a detailed analysis is not performed with specific reference to NO owing to the necessary limitations in scope of the above orienting investigation.

3.1.1 Possible laser action of rotational-vibrational transitions in ground state nitric oxide by direct discharge. – To date there have been few reports of laser action in molecular systems in a direct discharge system. Of these, the system which has undergone the most intensive investigation is the first positive bands in nitrogen (Ref. 37,38). These are belived to terminate on excited vibrational levels in the $A\ ^3\Sigma_u^+$ electronic state. Since this state is metastable against radiative decay, the mechanism by which the inversions are maintained is of interest herein. The hypothesis (since at present the mechanism has not been validated completely) employed to expalin the observation is that the inversion exists only as a transient phenomenon during the buildup of the excitation pulse. Further data are required to substantiate this interpretation since the inversion duration does not satisfy the inequality $T < 2g_1/g_2\ A_{21}$ required in transient systems. The mechanism hypothesized (Ref. 37) is

$$N_2\ (X\ ^1\Sigma_g^+ + e \rightarrow N_2\ (a\ ^1\Pi_g) + e \qquad (3\text{-}1)$$

$$N_2\ (a\ ^1\Pi_g) + N_2\ (X\ ^1\Sigma_g^+) \rightarrow N_2\ (B\ ^3\Pi_g) + N_2\ (\text{other states}) \qquad (3\text{-}2)$$

$$N_2\ (B\ ^3\Pi_g) \rightarrow N_2\ (A\ ^3\Sigma_u^+) + h\nu \qquad (3\text{-}3)$$

In this system, the excitation is presumed due to electron impact in a discharge rather than by the atomic recombination mechanism described below in a subsequent discussion. As yet there does not appear to be sufficient evidence in favor of either mechanism for the observed population inversion. This lasing action is not strictly analogous to the NO vibration-rotation case since the lower laser level is an upper electronic state. However, it does represent a relatively metastable state which is of interest herein.

3.1.1.1 Carbon monoxide vibration-rotation lasing (direct pulsed discharge). – A pertinent lasing action is that involving rotational transitions of 10-9, 9-8, 8-7, 7-6, and 6-5 vibrational bands pertinent to the ground electronic state ($X\ ^1\Sigma^+$) of CO. Laser action is produced in a low-pressure CO pulsed discharge. A generalized treatment has been prepared of these transitions which are due to partial inversions (Ref. 39). It has been shown that it is advantageous to operate at as low a temperature as possible for the production of maximum gain. Analysis of the excitation mechanisms under pulsed operations has indicated that they are complicated and time-dependent. In general, it is considered that direct excitation of CO molecules from the ground electronic state, v = 0 level, to higher vibrational levels is not a predominant mechanism.

The currently favored mechanism is (Ref. 39)

$$CO\ (X\ ^1\Sigma^+) + e \rightarrow CO\ (B\ ^1\Sigma) + e \qquad (3\text{-}4)$$

$$CO\ (B\ ^1\Sigma) \rightarrow CO\ (A\ ^1\Pi) + \text{Angstom band} \qquad (3\text{-}5)$$

$$CO\ (A\ ^1\Pi) \rightarrow CO\ (X\ ^1\Sigma^+)_{v' > 1} \qquad (3\text{-}6)$$

$$CO\ (X\ ^1\Sigma^+)_{v' > 1} \rightarrow CO\ (X\ ^1\Sigma^+)_{v' - 1}\ (\text{lasing action}) \qquad (3\text{-}7)$$

This represents a type of Franck-Condon pumping by electron excitation in a discharge.

McFarlane and Howe (Ref. 40) have recently demonstrated lasing action in the ground state vibrational-rotational system of CO in mixtures

of CO and CO_2. These run from 12 to 11 to 6 to 5 in CO. Additional transitions were observed for CO_2 001 → 202 in which flow systems characterized by high current pulsed dc excitation were employed. No explanations were offered for the observations other than consideration should be given to "collisions of the second kind, absorption by CO molecules of hot band radiation from CO_2, and alteration of the chemical composition of the mixture." (Ref. 40). Here, it is suggested that similar systems with NO and NO_2 may operate successfully by analogy even though the mechanisms are not well understood.

3.1.2 Lasing of nitric oxide vibration-rotation fundamental lines by vibrational transfer. — Nitrogen activated by a high frequency discharge can result in relatively strong luminescence in the spectral region between 4 and 5 microns when mixed with CO, CO_2, or N_2O. Activated nitrogen contains a large percentage of nitrogen molecules vibrationally excited in the ground state. The analysis of previous results indicate strongly that the operative mechanism is a transfer of vibrational energy from molecular nitrogen to the modes of vibration of the molecules of CO, CO_2, and N_2O owing to resonant inelastic collisions. The resonance is due to the fact that the first vibrational level of N_2 is 2331 cm^{-1} while the appropriate states of CO, CO_2, and N_2O are located at 2143, 2349, and 2224 cm^{-1} respectively. The excellent coincidence of these levels facilitate a rapid transfer of energy from the nitrogen. This fact, as well as the observation that the vibration temperature is high (4600°K) while that of rotation is low, indicates that lasing capability may be possible, particularly in CO_2, because of the good match.

This has been borne out by the recent work of Patel (Ref. 37) on CO_2. In the case of CO, Patel has observed laser action upon interaction with excited N_2 but he does not attribute this to vibrational transfer from N_2 but rather to the dissociative action on the CO of the active nitrogen. Alternatively, Legay and Legay-Sommaire (Ref. 41) have observed the vibrational-rotational emission spectrum of CO in the ground electronic state up to $v = 4$ in a system where vibrational-energy transfer from N_2 to CO is believed responsible.

The effectiveness of the vibrational transfer depends upon the closeness of the resonance and also upon the allowedness of the interchange. In Quarterly Progress Report No. 1 (Ref. 24), the ω_e are presented for various diatomic molecules selected from Herzberg (Ref. 34) which closely match that for NO. It should be noted, however, that these values are different from the fundamental frequencies since

$$G_e(v) = \omega_e\left(v + \frac{1}{2}\right) + \omega_e x_e \left(v + \frac{1}{2}\right)^2 + \omega_e y_e \left(v + \frac{1}{2}\right)^3 \qquad (3\text{-}8)$$

Even a brief survey of diatomic molecules reveals that there are several others which have ω_e-values particularly close to that for NO.

In particular, BO (1885 cm^{-1}) and CuH (1904 cm^{-1}) should give good resonances for vibrational exchange where they operate analogous to the nitrogen in the nitrogen-carbon dioxide experiment.

It is now appropriate to consider the transition (vibrational) for $\Delta v = 1$ with spin change from 1/2 to 3/2. The energy jump for transition changes from 1876 without the spin transition to approximately 2000 cm^{-1}. Energetically the CO vibrational transitions from v = 10 to v = 9, v = 9 to v = 8, etc. match very closely (approximately 2000 cm^{-1}). However, a spin must be changed in the collision since the ground state of NO consists of the $^2\Pi_{1/2}$ and $^2\Pi_{3/2}$ components with a splitting of 121 cm^{-1}. There is little material on the vibrational change of energy between molecules with spin change involved. However, it has been shown by sound absorption measurements that the probability of spin-relaxation for NO per gas kinetic collision is 0.062 at 298°K. There is also some evidence on spin-relaxation of electronic species when quenched by molecules. In particular many experiments have been performed and speculation exists concerning the spin-relaxation in Hg

$$Hg\ (6\ ^3P_1) + M \rightarrow Hg\ (6\ ^3P_0) + M \qquad (3\text{-}9)$$

Theory indicates that the interactions of $^3P_1$ with a quenching molecule removes the degeneracy during the collision.[1] The interaction with a $^3P_1$ produces three molecular species, only one of which can undergo the radiationless transition to the $^3P_0$ complex. Consequently, for the NO vibrational transfer case where the transition of interest is the NO ($^2\Pi_{1/2}$, v = 0) → NO ($^2\Pi_{3/2}$, v = 1) of energy 2000 cm^{-1} such a transfer possibly may not be strongly forbidden. The lasing transition would then be NO ($^2\Pi_{3/2}$, v = 1) → NO ($^2\Pi_{3/2}$, v = 0).

Another molecule of interest is O_2^+ whose ω_e-value is only 28 cm^{-1} less than that of NO. However, the problem here involves obtaining adequate populations of O_2^+ whose coefficient of recombination being of the dissociative type ($\alpha \sim 10^{-7}$ cm^3 sec^{-1}) is extremely rapid.

It has been shown (Ref. 24) that for vibrational exchange some other molecules of interest in this regard are N_2, CO, BO, AgH, CuH.

Finally, it may be noted here that there are some advantages in attempting laser transitions from the S = 3/2 component of the nitric oxide ground state, 121.1 cm^{-1} above ground since the relative population in the 3/2 state varies from about 15 percent at 100°K to 36 percent at 300°K. Thus, it may be easier to invert the 3/2 transitions, e.g., in the pump removal technique, although the spin relaxation, 3/2 → 1/2, is relatively slow, since forbidden.

3.1.3 Electronic-vibrational transfer in an inelastic collision. — The present basic scheme involves the interaction of NO with an excited electronic species which transfers the vibrators from v = 0 to some excited level v > 1. As an example, the following two reactions are suggested:

$$Hg^* \ (6\ ^3P,\ 6\ ^3P_0) + NO \rightarrow Hg + NO^v \text{ (vibrationally excited) } v > 1 \quad (3\text{-}10)$$

$$Na^* + NO \rightarrow Na + NO^v \text{ (vibrationally excited) } v > 1 \quad (3\text{-}11)$$

These are reactions for which there is a large cross section for quenching and in which some degree of vibrational excitation may be expected [see Tables 3-2 and 3-3 in Quarterly Progress Report No. 1 (Ref. 24)]. For such a scheme, to insure lasing, it is desirable that v be greater than unit.

There has been one reaction to date in which this process has been demonstrated (Ref. 34):

$$Hg\ (6\ ^3P_1,\ 6\ ^3P_0) + CO_{v=0} \rightarrow Hg\ (6\ ^1S_0) + CO_{v=6-9} \quad (3\text{-}12)$$

In this experiment (Ref. 42), the mercury was excited by absorption of a 2537Å line and the infrared emission was studied. The rate of excitation into levels v = 7, 8 was more than an order of magnitude greater than into the level v = 2-5. The absolute efficiency is high and there is very little possibility that CO vibrational levels were created by cascading from an upper excited electronic state because of inadequate energy in the mercury.

The proposed mechanism is due to Polanyi (Ref. 42) and is illustrate in Figure 3-1 for Hg^* and CO which approach each other with thermal energy along electronic curve A. When the particles are close they cross over to the state $X(^1\Sigma)$ in which, as one can see from the steepness of the $r_{Hg\text{-}CO}$ coordinate, a relatively strong force becomes operative. The excitation of the CO is believed to occur here as the result of a sudden impulse. Regarding this interaction classically, conservation of linear momentum establishes an upper limit on the energy that can go into the relative motion of B with respect to C vibrational energy. If A^* is heavy, this fraction is $f_v = m_c/m_{BC}$ which for CO, is 0.43. For Hg^* $6\ ^3P_1$ as donor and approach from the O end the upper limit of excitation is v = 8; for an approach from the C end v = 11.

Similarly for NO, f_v = 0,42 and 0.53, the energy available is $E_v = f_v$ (40,000) cm^{-1} = 16,800 cm^{-1} and 21,200 cm^{-1}. The above contravenes the Landau-Teller theory of translational-vibrational transfer according to which the collisional transfer selection rules parallel the radiational ones. This occurs because the encounter is impulsive in which the collision duration is short compared to the vibrational period.

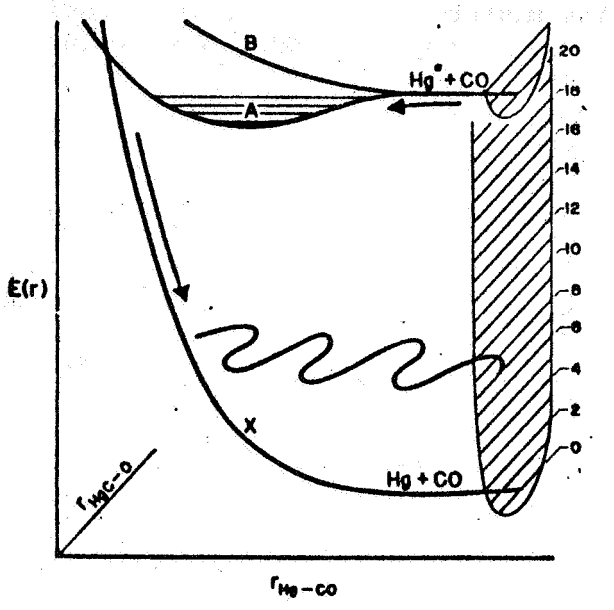

Figure 3-1. Schematic diagram of the potential energy curves $E(r_{Hg-CO})$, in the plane of the paper and $E(r_{HgCO})$, perpendicular to the plane of the paper. The impulse experienced by CO, following the crossing from curve A to X, induces vibration in the C-O bond, of energy equivalent to v = 6-9.

For the case of NO, several possibilities exist whereby use may be made of this process as enumerated below.

(1) Discharge through a mixture of nitric oxide and mercury. In this type of setup both the 6 $^3P_1$ and the 6 $^3P_0$ can excite the NO.

(2) Mingling in an interaction zone [similar to the Patel (Ref. 37) N_2-CO_2 setup] of a mercury discharge and cooled NO. The NO is cooled so that lasing on partial inversions may occur even if complete inversions do not. Here only the 6 $^3P_0$ would be effective owing to the short lifetime of the 6 $^3P_1$ state.

(3) High power flashing or steady-state excitation of 6 $^3P_1$ by a 2537Å lamp. The gas mixture in the laser will consist, at least initially, of a mixture of mercury and NO. Here again both the 6 $^3P_1$ and 6 $^3P_0$ would be effective.

The last process seems particularly attractive because of:

(a) High quenching cross sections of Hg 6 $^3P_1$, 6 $^3P_0$ by NO
(b) High population of 6 $^3P_0$ which is possible
(c) Excitation into higher vibrational levels by the interaction
(d) High power, 70 watts, is possible for photo-flashing.

3.1.4 Chemical reactions governing selective excitation of NO lasing in vibration-rotation bands. – This process involves those chemical reactions which selectively excite certain electronic or vibrational levels. For convenience, those types of reactions which occur in afterglow phenomena are viewed as a subclass and are treated separately below. In some cases, possible lasing action on electronic exciations will be indicated.

3.1.4.1 After glow phenomenon. – Afterglow investigations are often analyzed in terms of chemical reactions so that the role of electron excitation is omitted. This can be justified since the electron energies generally die down rapidly within a millisecond of the discharge excitation region or termination. Thus, in the following, interpretations are presented in terms of chemical reactions involved in the afterglow phenomena.

At low pressures (< 1 mm) preassociation reactions dominate so that

$$N + O \rightarrow NO\ (C\ ^2\Pi) + h\nu \qquad (3\text{-}13)$$

Through potential switching from the a $^4\Pi$ state to the $v' = 0$ level of the C $^2\Pi$ state, radiation to the X $^2\Pi$ ground state (δ bands) occurs, where the strongest bands are the (0,2) and (,3) bands at 2061 and 2141Å, each representing 25 percent of the total emission.

For pressure greater than 1 mm, the dominant reaction becomes

$$N + O + M \rightarrow NO + M \tag{3-14}$$

$$k_2 = 2 \times 10^{-32} \text{ cm}^6/\text{sec}$$

In addition, NO is removed by

$$N + NO \rightarrow N_2 \rightarrow O \tag{3-15}$$

so that

$$k_3 = 2 \times 10^{-11} \text{ cm}^3/\text{sec and}$$

$$[NO] = \frac{k_2}{k_3} [O] [M] \tag{3-16}$$

It should be pointed out that the δ bands are just border line in terms of lasing since by equating production and loss of $X\ ^2\Pi_{v'} = 3,2$

$$R_v = \frac{[NO\ (C\ ^2\Pi)]}{[NO\ (X\ ^2\Pi_{v'} = 3,2]} = 4\tau_\delta \times 2 \times 10^{-11} [N] \tag{3-17}$$

$$\approx \tau_\delta \times 10^6 \text{ for } [N] = 10^{16}$$

If $N > 10^{16}$ the chances are improved for lasing the δ bands.

Consider the possibility of inverting the rotation vibration bands. First, write

$$\frac{d[NO\ (X\ ^2\Pi_{v = 3,2}]}{dt} = \frac{NO\ (C\ ^2\Pi)}{\tau_\delta} - k_3\ [NO(X\ ^2\Pi_{v'} = 3,2)]\ [N] \tag{3-18}$$

$$\frac{d}{dt} [NO\ (C\ ^2\Pi)] = k_2\ [N]\ [O]\ [M] - \frac{[NO(C\ ^2\Pi)]}{\tau_\delta} - k_3 [NO(C\ ^2\Pi)]\ [N] \tag{3-19}$$

In the steady-state condition

$$[NO\ (C\ ^2\Pi)] = \frac{k_2\ [N]\ [O]\ [M]}{\frac{1}{\tau_\delta} + k_3\ [N]} \tag{3-20}$$

However since $1/\tau_\delta \gg k_3\ [N]$ for $[N] \sim 10^{16}$,

$$[NO\ (C\ ^2\Pi)] = \tau_\delta\ k_2\ [O]\ [M]\ [N] \qquad (3\text{-}21)$$

Inserting this value in Equation (3-18) yields

$$NO\ [X^2\Pi_{v\,=\,3,2}] = \frac{k_2\ [O]\ [M]}{k_3} = 10^{11} \text{ for } [N] = [O] = [M] = 10^{16} \qquad (3\text{-}22)$$

assuming that radiative decay ($\tau_v = 0.1$) of the v-r bands is too slow to count and also that interchange of energy between the r-v levels by collision is slower than vibrational energy exchange. This is interesting since it implies that the ($C\ ^2\Pi$) state shuttles rapidly into the ground v-r band. Using the formula below and assuming the lower level to be empty, for $\nu = 2 \times 10^3\ cm^{-1}$ (5μ)

$$\frac{\Delta N}{\tau} = \frac{4\pi^2}{3}\ c\ \frac{\Delta\nu}{\nu}\ \frac{(1 - R)}{L}\ \nu^3\ G$$

$$\Delta\nu = 0.04\ cm^{-1},\ R = 0.98,\ L = 10^2$$

$$\frac{\Delta N}{\tau} = 4 \times 10^{12}\ G$$

where G is the branching possible in the transition. It may run from approximately 2 to 40 depending upon the number of rotational levels fitted in the upper vibrational level and the number of vibrational levels to which the upper state can go. By cooling the tube G may be minimized since rotational equilibrium is established rapidly in one or two collisions. A first order approximation for the time behavior of the C state is

$$C = \beta_o\ \tau_\delta\ [1 - \exp - (t/\tau_\delta)]$$

where $\beta_o = k_2\ [O]_o [N]_o [M]_o$, τ_δ = lifetime of the δ state = 10^6.

Using values $[O]_o = [N]_o \sim [M]_o \sim 10^{16}$ and $\beta_o = 10^{16}$ equilbrium is attained in a microsecond. A similar equation applies to the concentration of the X state with a time constant of the order of 10^{-5} seconds. If $[N] = [O] = 3 \times 10^{16}$ and $[M] = 17$ then $[NO\ (X\ ^2\Pi_{v\,=\,3,2})] = 3 \times 10^{12}$.

Consequently, for these assumed initial values, the inversion is almost operable by the above derived criterion. Thus, the experiment is still an interesting one since:

(1) Partial inversion may be obtained, particularly with cooling of the tube.
(2) Presently achievable concentrations of [N]. [O], and [M] are within a factor of only three of the required amount.
(3) Over-loading with O_2 will increase the formation of atomic oxygen and increase the formation rate of the C state, but not increase the depletion of the X state which is only affected by N.

3.1.4.2 Other chemical processes resulting in complete or partial inversion. – In this class of reaction, there is a selective reaction into a vibrational level at a rate of $k_{\nu'} > k_{\nu}$ where $\nu' > \nu$. There are several serious problems here including:

(1) The k_{ν}'s are only known for a few reactions and the analysis of suitable reactions is consequently speculative.
(2) Cascading tends to saturate the lower levels since radiative and collisional transitions are generally higher for higher vibrational levels. Consequently, there is saturation of lower levels and pulse operation is much easier than CW operation. An alternative is to chemically react out the v = 0 or lower vibrational levels.

Polanyi (Ref. 42) has analyzed the general distribution of energy among the various products of simple types of chemical reactions by examining the dynamics of the formation and break up of the activated complex in the system below. The details of this analysis are presented in Figure 3-2.

$$A + BC \rightarrow AB + C + Q \text{ Kcal mole}^{-1}$$

(1) Attractive: In this case the major portion of the energy release occurs as A is attracted to B.
(2) Repulsive: The major portion of the energy release occurs as C is repelled away from AB
(3) Mixed: This is a reaction in which the repulsive and attractive phases are not well separated. Among this interesting class of reactions are those in which the configuration shift from a covalent to an ionic nature.
(4) Some Specific Suggestions: Two possible reactions are enumerated below:

$$Na + NO_2 \rightarrow NaO + NO$$

$$Na + NO\ C\ell \rightarrow NO + 61 \text{ Kcal/mole}$$

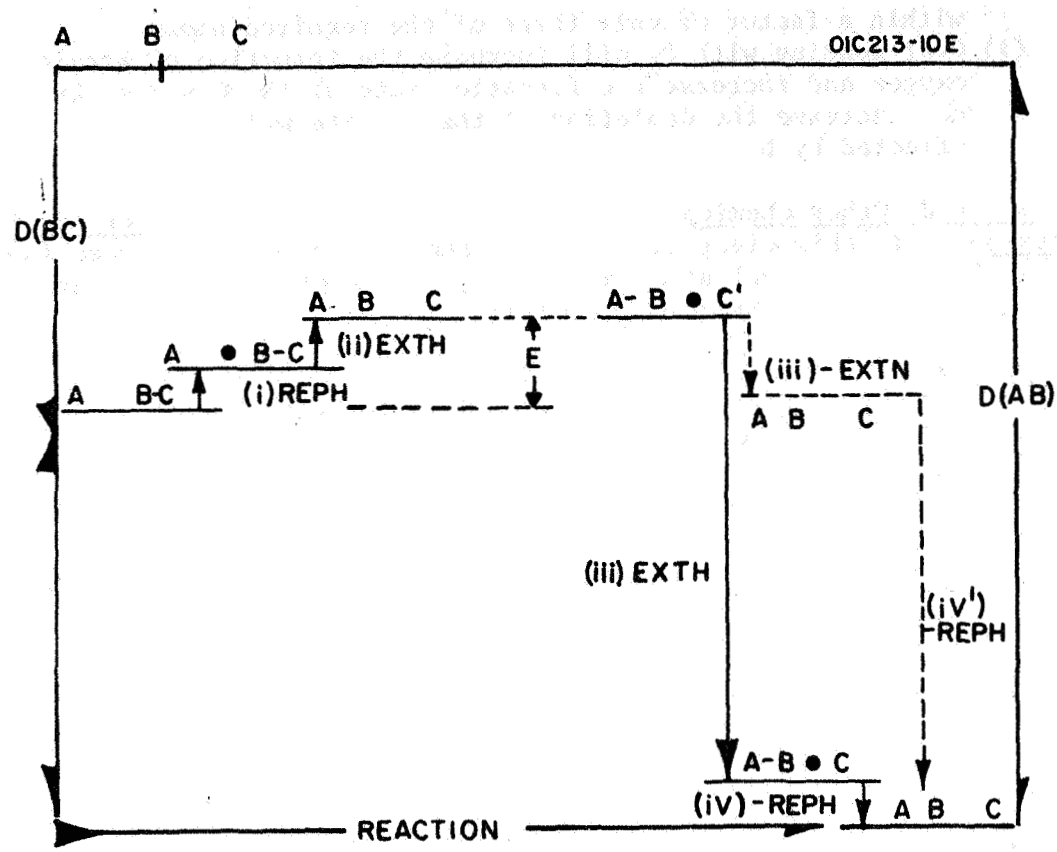

Figure 3-2. Potential energy changes during the course of an exothermic reaction A + BC → AB + C (proceeding from left to right in the drawing), divided into four stages: (i) A-B repulsion, (ii) B-C extension, (iii) A-B relaxation (termed "-extension"), and (iv) B-C relaxation (termed "-repulsion"). D(BC) is the dissociation energy of bond being broken, D(AB) that of the bond being formed; the difference Q, is the heat of reaction. E_c is the classical activation energy. In the scheme shown by solid lines the major part of the heat of reaction is liberated in stage (iii)(this behavior is termed"attractive"), in the scheme shown by a broken line the major part is liberated in (iv) (termed "repulsive"). In reality (iii) and (iv) need not take place consecutively but may be simultaneous (termed "mixed").

Although the preliminary analysis indicates that the bulk of chemical energy passes into the NaCℓ band the vibrational excitation of NO remains a possibility. Another possibility involves the reaction $H + NOC\ell \rightarrow HC\ell^* + NO^*$ which has been studied by Polanyi (Ref. 42). While the major emission originates from the HCℓ bands, emission has been observed from the NO v = 1-0 band of the ground state.

The above material is somewhat general and was intended solely for the systematic completion of pertinent data. A more careful examination of the theoretical laser and experimental results to date would be required to select the optimal type of chemical system for this type of inversion mechanism. However, any additional effort in this direction is not within the scope of the present survey.

3.1.5 Franck-Condon pumping. – The discrete absorption of radiation by molecules leads them from the ground electronic state to an excited electronic state. Subsequently, after emitting fluorescent radiation, the molecule can fall back to some other lower state or to the ground state. It has been suggested earlier (Ref. 43) that the absorption and emission of radiation by molecules may be used for obtaining population inversion between the rotational vibrational levels of the molecules. Since the relative probabilities of the above type of transition between two vibrational levels is governed by the Franck-Condon principle, it is designated as the method of Franck-Condon pumping for obtaining population inversion. Shuler, et al. (Ref. 44) have presented detailed discussions of this subject, the salient features of which are summarized briefly below.

Consider the radiative transitions between the vibrational levels of two electronic states (X and A) of a diatomic molecule (see Figure 3-3). When this molecule is placed in a radiation field with frequencies of radiation which can be absorbed by the molecule in the transition $A \leftarrow X$, a molecule in lower level, j, undergoes a transition to upper level, m. The normalized probability of such a transition is given by:

$$q_{mj} = \frac{U(\nu_{mj}) \mid R_{mj} \mid^2}{\sum_j U(\nu_{mj}) \mid R_{mj} \mid^2} \qquad (3\text{-}23)$$

where $U(\nu_{mj})$ is the radiation density at the frequency ν_{mj} and $|R_{mj}|$ is the transition moment matrix element. After attaining the upper level, m, the molecule will radiate spontaneously to the level i of the lower state X. The net result of this absorption-emission cycle is a transition of the molecule from the level j to that of i of the lower electronic state. Neglecting the effect of intermolecular collisions, the probability of the transition of molecules from the level j to level i as a result of absorption emission cycle is given by

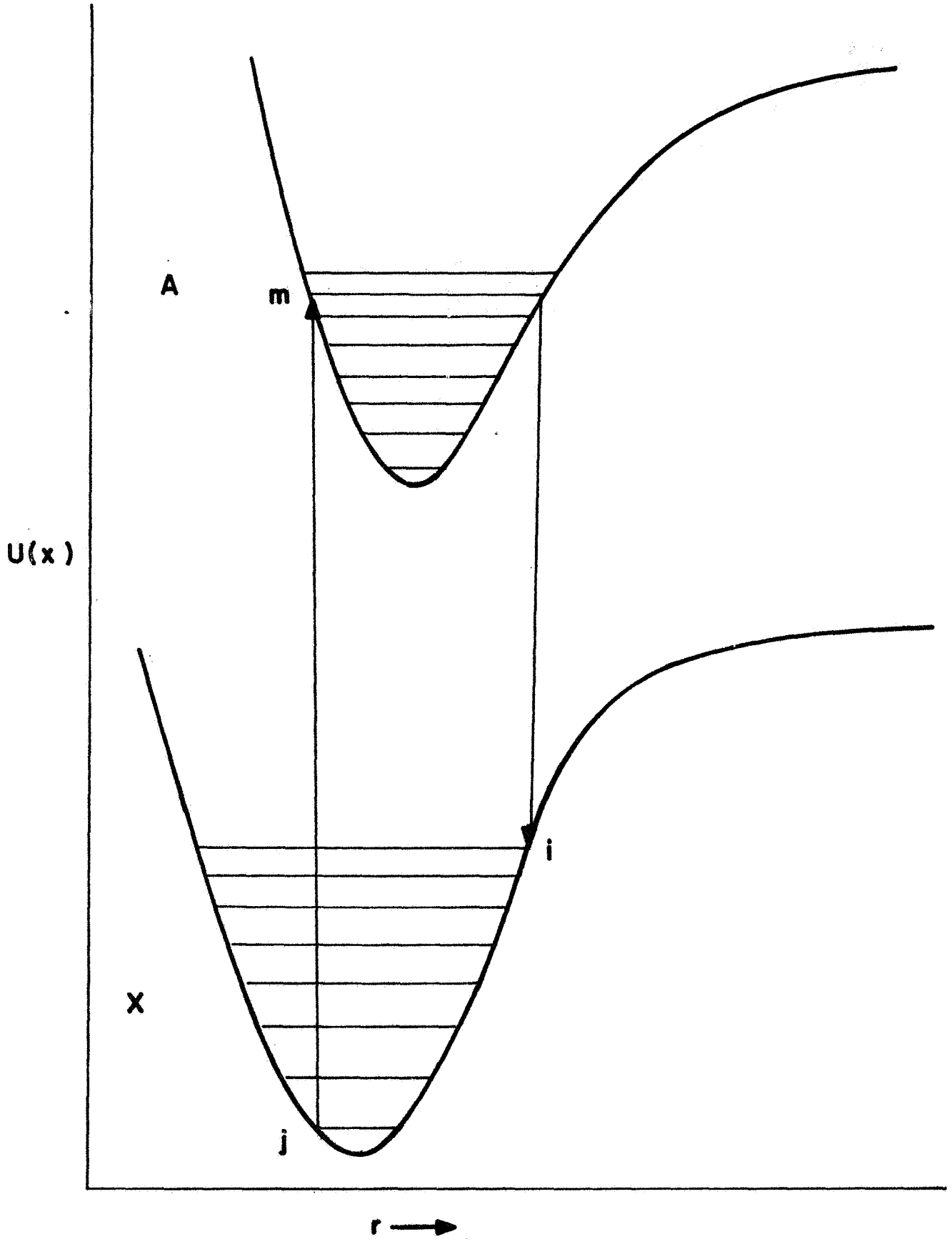

Figure3-3. Franck-Condon pumping of diatomic molecule.

$$P_{ij} = \sum r_{im} q_{mj} \qquad (3\text{-}24)$$

where r_{im} is the probability of transition between levels i and m and is given by

$$r_{im} = \frac{[8\pi\ hc^{-3}\ \nu_{im}^{3} + U(\nu_{im})]\ |\ R_{im}\ |^{2}}{\sum_{i} [8\pi\ hc^{-3}\ \nu_{im} + U(\nu_{im})]\ |\ R_{im}\ |^{2}} \qquad (3\text{-}25)$$

Following the method of Shuler, et al. (Ref. 44), the steady state distribution of molecules in different vibrational levels of the lower electronic state X can be calculated. Shuler, et al. (Ref. 44), have concluded that if the radiation density is independent of the frequency and, provided

$$\sum_{j} q_{mj} = 1 \text{ and } \sum_{m} r_{im} = 1, \qquad (3\text{-}26)$$

the distribution of molecules in different vibrational levels of the lower state is uniform under steady state illumination. However, the above condition may break down in some cases to yield an inverted population among the vibrational levels of the lower state. Moreover, the inversion of population may be sourght in the transient distribution produced soon after the initiation of pumping radiation. The inversion is particularly likely when the Franck-Condon parabolas are well separated, and when the pumping radiation excites a single electronic transition. In some cases, the molecules in a given upper level may undergo transitions into several nonadjacent vibrational levels. In such cases the populations of some adjacent vibrational level may be inverted. For a particular case, a careful examination of the Franck-Condon arrays will indicate the most favorable transitions for population inversion by Franck-Condon pumping. Extensive information regarding the Franck-Condon factors for various NO molecular transitions is available in the literature (Ref. 30). The energy level diagram showing some selected potential energy curves has been presented in Figure 2-1. Reference to that figure indicates that the lowest electronic states from which an electronic transition is allowed to the ground state of NO are A $^{2}\Sigma^{+}$ and B $^{2}\Pi_{r}$. The equilibrium internuclear distance of B $^{2}\Pi_{r}$ is significantly different from that of the ground state. This difference is reflected in the calculated arrays of Franck-Condon factors, q_{v}, given by Nicholls, et al. (Ref. 30). In addition, the tabulated $q_{v',v''}$ values of the β-system are higher for higher v'' value and therefore the absorption and re-emission of β-system can be employed more efficiently for pumping NO molecules to

higher vibrational levels. Thus, in principle at least, opportunities exist for acquiring selective enhancement of ground state vibrational states via Franck-Condon pumping.

3.1.6 Photodissociation and molecular fluorescence for lasing vibrational levels of the ground state NO molecule. — It has been demonstrated (Ref. 45) that the photodissociation of the nitrosyl halides NOCℓ and NOBr produces NO in high vibrational levels of the electronic state. This can serve as an example of possibly obtaining required vibrational inversions via photodissociation. Although in this particular case the mechanism has not been definitely established as yet, it is very likely that this pertains since high vibrational levels are strongly populated, and the rotational temperature is low. Furthermore, apparently the NO molecules are formed in levels up to $v'' = 11$ directly in the breakup of NOCℓ or NOBr. The employed light source was a flash lamp of duration about 25 microseconds, and dissipating 2000 joules per flash over a spectral range between 1900 and 2600Å. Another case of this type involved the flash photodissociation of CS_2, which yields vibrationally excited CS (Ref. 46). However, vibrational inversion in this case is relatively uncertain.

The general nature and some selected problems associated with this type of lasing are discussed below.

First, it is pertinent to inquire as to the distribution of energy in the fragments of photodissociated polyatomic molecules. Such distribution, in general, does not correspond to equilibrium at any single temperature. Theoretical investigation of the energy distribution has proceeded generally along two main lines. The first has involved the fact that the energy is distributed statistically among the degrees of freedom of the fragments consistent with the conservation of energy and angular momentum. This statistical or strong coupling approach (which nevertheless may show inversions) has shown fair agreement for the case of the OH radical rotational distribution in H_2O photodissociation. A second line of theoretical investigation has involved the case when the excited molecule has a short lifetime or interaction between the dissociation fragments in weak coupling. Such a process is almost equivalent to a collision and insight has been gained by work on molecular collisions both experimentally and theoretically.

In the molecular situation some of the problems are similar to that encountered in atomic fluorescence. There remains the requirement to deactivate the lower laser level usually by means of collision. Consequently, some degree of selectivity in deactivation is required although the upper level is also populated from above. In addition, the critical inversion density is proportional to the line width so that consequently the Doppler width of radiation emitted by the dissociation fragments is important. The kinetic energy of the fragments may differ considerably from that of a Maxwellian velocity distribution. Additionally, anisotropic effects are to be expected depending upon the orientation of the electric field of the exciting radiation, the dipole moment of the molecule, and the direction of viewing.

The large number of possible types of inversion are not reviewed here. Rather, for the present application, interest is confined to the following two possibilities: (a) inversion between rotational levels in different vibrational levels of the electronic ground state and (b) electronic transitions.

An example of Case (a) involves the photodissociation of the nitrosyl halides NOCℓ and NOBr which have been found to produce NO in high vibrational levels of the ground state under active wavelengths of 1900 and 2600Å. In addition, flash photolysis and dissociation of CS_2 yields vibrationally excited CS. The possibility also exists for both photodissociation and subsequent Franck-Condon pumping to occur. (The theory of Franck-Condon pumping has been treated previously in Section 3.1.5.) Such a mechanism is evidently involved in the photodecomposition of cyanogen $(CN)_2$ and cyanogen halide CNBr and CNI with respective wavelengths of 1900 and 2200Å and somewhat longer for the halide.

An example of Case (b) involves the photodissociation of H_2O (by 10 eV photons) which produces electronically excited $OH(A\ ^2\Sigma^+)$ molecules most of which are formed initially in high rotational levels of the lowest vibrational state with rotational distribution peaks at K = 22. However, in this case the population density in this level is not adequate for the present purpose. On the other hand, there are other cases which involve C_2N_2, CNBr, and similar molecules. In addition, the fluorescence of $NH(C\ ^1\Pi)$ produced in the photodissociation of NH_3 at wavelengths 1165 to 1295Å as well as electronically excited H or H_2 from photons of energy greater than 15 eV may be utilized for this purpose. Photodissociation is often followed by specific molecular fluorescence processes. In general, these are less advantageously employed than atomic fluorescence processes since in a molecule the intensity may be distributed over many frequencies due to (1) occupation in the electronic state of several vibrational and rotational levels, and (2) transitions downward to many v, J levels may occur. In some special cases (1) may be minimized because special v′, J′ levels may be found in photodissociation. The variation in (2) can be estimated from standard spectroscopic theory.

For each of the individual vibration-rotation components of an electronic transition, the line strength can be approximated by

$$S(2,v',J' \rightarrow 1,v,J) \simeq S(2 \rightarrow 1)\ S(v' \rightarrow v)\ S(J' \rightarrow J). \qquad (3\text{-}27)$$

where $\Sigma\ S(v' \rightarrow v) = 1$

$$\Sigma_j\ S(J' \rightarrow J) = 2J' + 1$$

and

$$\Sigma_{v,j} S(2,v';J' \rightarrow 1,v,J) = (2J' + 1)\ S(2 \rightarrow 1)$$

Here the electronic factor, $S(2 \rightarrow 1)$, may be comparable to the strength of an atomic line and is related to the molecular oscillator strength. The vibrational factor, $S(v' \rightarrow v)$, is the Franck-Condon factor discussed earlier whereas the rotational factor, $S(J' \rightarrow J)$ is usually denoted by S_j and called the Hönl-London factor.

With reasonable approximations the relative optical gain for the various v', $J' \rightarrow v$, J lines within the electronic transition is basically

$$\alpha \text{ real} \simeq S(v' \rightarrow v)\ [(N_{2v'J'}/g_2) - (N_{1vJ}/g_2)] \qquad (3\text{-}28)$$

From the above it can be seen that the total strength associated with each progression of $v' \rightarrow v$ lines is comparable to an atomic line. Often, the Franck-Condon factor (Ref. 21) puts most of the intensity in one or two members of each progression, e.g., the first positive and second positive bands of N_2 and the angstrom band of CO.

The line width of the fluorescent line represents an important parameter affecting the laser action of the system. In the case of atomic fluorescence excited by the photodissociation of the molecules it depends on the following factors: (1) thermal motions of the parent molecule, (2) the magnitude of the recoil velocity of the dissociated molecule, and (3) the angular distribution of the recoil velocity.

In the case of the photodissociation of molecules, the contribution from the first factor is negligible in comparison with the other two. The Doppler width due to the recoil velocity depends on the final relative kinetic energy E of the fragments of the parent molecule and is given by:

$$E = h\nu_p + E_{AB} - T_{AB} + \frac{1}{2}\ \frac{P^2}{\mu\ r_o^2} \qquad (3\text{-}29)$$

(here it is assumed the daughter molecule A is NO), where $h\nu_p$ is the energy of the pumping photon, E_{AB} is the sum of the dissociation energy of the A-B bond and the vibrational excitation energy of the daughter molecule A. The final term represents the energy due to the rotation of the parent molecule. It is desirable from the view point of laser action that the width of the fluorescent line should be a minimum, so that the larger fraction of the pumped power can be channelled to the laser radiation. The Doppler width of the fluorescent line can be a minimum if the

recoil energy is minimum. A technique of reducing the recoil energy of the dissociated daughter molecule is to employ the pumping radiation of narrow bandwidth so that $h\nu_p \sim T_{AB}$. However, this action seriously reduces the pumping efficiency. Another means of limiting the recoil velocity of A* is to select a molecule such that the mass of B greatly exceeds that of A. In case of polyatomic molecules the excess energy E can be shared by several degrees of freedom of the fragment B thereby reducing the velocity of the dissociated excited molecule A*. In some cases the anisotropy of the recoil velocity with respect to the incident radiation can be employed to reduce the observed width of fluorescent radiation. Finally, another possibility exists since in some cases the photodissociation of a molecule can provide a suitable method of pumping a daughter molecule into an excited state. For example, it may be possible to obtain a transient inversion if the buildup into an upper vibration is sufficiently fast, i.e., in a time less than the relaxation time of the upper vibrational state. Such a system would also lase by a cascading process, as shown in CO_2, even for a lower vibrational transition and, in particular, the 1-0 transition which is optimum on the basis of its utility as an atmospheric probe. As noted previously, even if T_v and T_r are significantly different lasing may still occur.

3.1.7 Thermal excitation and nonequilibrium cooling. — The objective here is to seek partial population inversion and consequent stimulated emission in a molecular material which is relaxing following a thermal pulse.

Furnaces of reasonably high temperature are available, e.g., zirconium carbide and hafnium carbide are capable of producing up to 4000°K, zirconium oxide to 2500°K, tungsten to 2000°K, etc. In a reasonable volume the Libby plasma torch achieves temperatures in a flowing system of between 30,000 and 40,000°K into which it is conceivable that NO could be passed. Highly extreme temperature would have to be avoided to prevent decomposition. With water-cooled walls and high axial temperatures the necessary ratio of T_v to T_r might be obtained for partial emission.

The basic scheme for lasing by nonequilibrium cooling was advanced by Polanyi (Ref. 42). More recently, Wells (Ref. 47) has suggested a variation in which a beam of hot molecules interacts with distant collisions with a cold gas of another species at relatively low pressure. Certain energy levels in the hot gas are cooled faster than others owing to coincidental resonances in the spectra of the two gases. In the partially cooled nonequilibrium state, population inversions are possible in the hot species. For example, initial analysis has indicated that the Schawlow-Townes conditions for maser action can be satisfied for $J = 3 \rightarrow 2$ transition in HF at 123.1 cm^{-1} or 81.25 microns.

The active medium in this concept is a gas which, like the working fluid of a heat engine, is active while in a nonequilibrium condition during passage from hot to cold heat reservoirs. The matching of the

resonant interaction levels for selective depopulation is indicated schematically in Figure 3-4(b) with the dashed line showing the ideal limit of the level population in the hot species of the resonant transfer.

Consideration of appropriate molecules leads to the conclusion that pure rotational transitions are optimal. The number of possibilities is narrowed further by eliminating: (1) molecules having no dipole moments, (2) molecules having large moments of inertia, and (3) asymmetric top molecules - too many energy levels and allowed transitions.

3.1.8 Creation of lasing action in vibration-rotational levels by direct excitation by blackbody radiation. — This scheme was first suggested and initially analyzed by Heil and Wagner (Ref. 48). Basically the concern here involves the degree of quenching of inverted populations in vibrational levels by collisional excitation transfer; such calculations have been performed for CO and HCℓ (Ref. 48). It was shown that the operation of lasers involving a vibronic or rotational transition in a molecular gas is inhibited strongly by the possibility of resonant excitation collision transfer. Electromaghetic transfer is hindered because of the unharmonicity in the energy levels which isolates the absorptive (v = 1 to v = 0 level) from the amplifying population (v = 2 to v = 1) and consequently constitutes no problem.

By analysis of the five dominant processes:

γ_e = loss of radiation from cavity,

γ_g = rate at which electromagnetic radiation in the cavity is amplified by a given excess of population in the second vibronic level relative to the first one,

γ_c = relates to the rate at which resonant inelastic collisions in which a molecule in the v = 2 vibronic level collides with a molecule in the v = 0 level producing two molecules in the v = 1 level,

γ_p = rate at which molecules in the v = 2 level are supplied and in Heil scheme are supplied by pumping with overtone radiation, and

γ_w = rate at which molecules are lost in the two excited vibronic levels from other than the resonant process,

the following is obtained:

(1) $\gamma_L = c\ (1 - r)/\ell$

r = reflectance coefficient of end mirror

ℓ = length of cavity

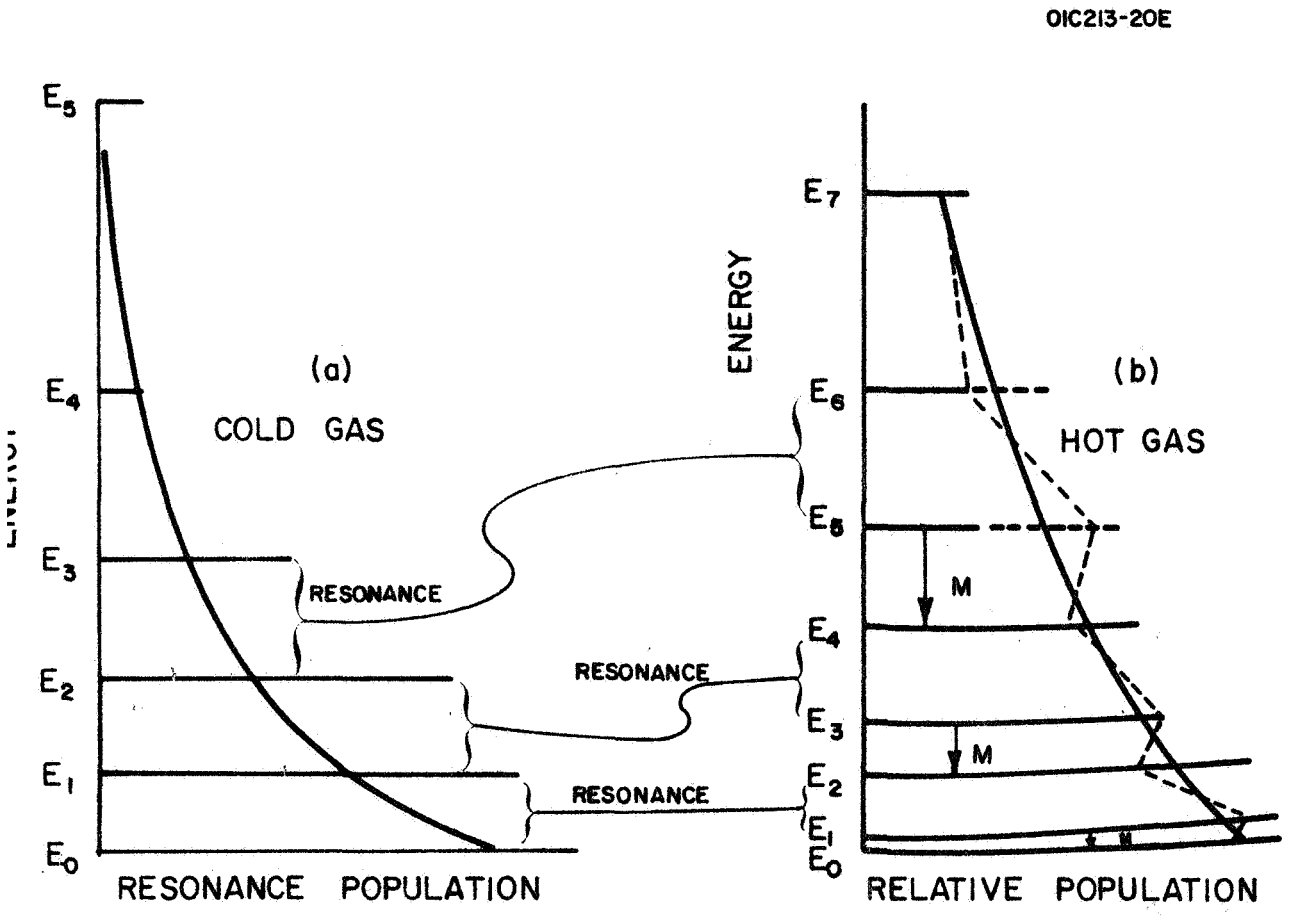

Figure 3-4. Population of energy levels. The solid curves are plots of the initial relative populations of levels in both a hot and cold species. The dashed line in part (b) shows the ideal limit of the level populations in the hot species after resonant transfer.

(2) $\gamma_g = 8\pi\ ed_{12}\ (n_2 - n_1)\ Rc/u$

α = fine structure constant

d_{12} = dipole moment between the v = 2 and v = 1 level,

e = elementrary charge

R = rotational dilution factor

u = relative velocity

(3) $\gamma_c = 2\pi\alpha ed_{o1}\ d_{12}\ n_o\ S$

n_o = ground vibronic population

S = Stueckelberz factor expressing the effective reactive cross section as a fraction of the exact resonant cross section

The supply rate of molecules in the second vibronic state is W

(4) $W \geq \alpha\ d_{02}^2\ \omega_{20}^3\ n_o/\{3\ c^2\ [\exp\ (h\ \omega_{20}/kT_s) - 1]\}$

For lasing

(5) $W \geq (\gamma_c + \gamma_\omega)\ n_2$ where it is assumed for pulsed operation that $n_1 = 0$ and $\gamma = 0$. Then the defining equation is

(6) $[\exp\ (h\ \omega_{20}/kT_s - 1]^{-1} \geq \sqrt{2}\ (1 - r)\ Su\ \tau/16\ \ell\ R\ A$

where $\tau = 3\ c^2/4\alpha\ d_{01}^2\ \omega_{10}^3$ is the lifetime of the fundamental.

While the temperatures (T_s) required for lasing CO in this fashion (10^{5o}K) are excessive, that for HCℓ (10,000°K) is not in light of Libby's recent development of plasma torches operating in the regime 30,000 to 40,000°K. Such calculations may be performed for NO to determine the requisite T_s.

It is pointed out by Heil, et al. (Ref. 48), that this concept is based upon the anharmonicity of the level system where the relevant parameter is A defined by $d_{02}^2 = A\ d_{01}^2$. Also important, although not stressed by Heil in the practical sense, is minimizing the pumping of the v = 1 level. This scheme does not seem suitable for the high energy requirements for the NO laser system (Ref. 48).

3.2 The Use of Shift-Tuning Techniques to Produce the Required Lasing Action

On the basis of the material presented in Section 3.1, it appears that the prospects are not particularly promising for a short range

development to produce a direct gaseous laser generator of sufficient power for a probe of atmospheric NO. A major reason for this conclusion is that the ideal probing transition would be one terminating in the ground states of NO, i.e., $X\ ^2\Pi_{1/2,3/2}$ (v = 0). Inversion on the ground state is far more difficult in any gaseous system than on upper level transitions (4-level laser). This is especially true in the case of nitric oxide since the first electronic levels lie at 37965 cm^{-1} and 43965 cm^{-1} above ground level. These UV frequencies can present a number of practical difficulties in successful direct gas laser generation.

The efficiency of a resonance scattering experiment diminishes rapidly as the lower level energy value increases above ground, due to the relatively sharp decrease in Boltzmann population at the low atmospheric temperature of 167°K at an altitude of 90 km. Although the infrared fundamental of nitric oxide has been lased successfully by means of both electronic and photodissociation of NOCℓ, the presently observed vibrational transitions in NO are 11-10 to 6-5, in CO 18-17 to 5-4 (maximum pulsed power 100 μW). Further development may result in lower vibrational states but with increasing difficulty, and the population difficulty for the probe application will increase at e^{-16} per vibrational level. Yet, it will be shown that signal level and detection background noise difficulties are already marginal for 5 millijoule pulses in the 1-0 band.

On the basis of recent GCA laboratory experiments, it appears that the shifting of ruby or neodymium laser lines to the nitric oxide resonance lines by harmonic generation and Raman shifting offers more promise of high power than a direct laser transition. Specifically, the fourth harmonic of the neodymium-glass laser has been produced at GCA at 10,608Å/4 = 2652Å at 50 millijoules per pulse, which matches the M(0,0) band of NO. Additionally, under high power laser outputs have been demonstrated at GCA at the resonance lines of Na, Ba, K, Li, Zr, and Rb by these tuning techniques.

In selecting the most useful lasing wavelength to investigate, the following comments apply. In considering the utility and possibility of developing a successful minor constituent atmospheric probe, the two most important considerations are (1) the ratio of the resonance scattering signal to the Rayleigh scattering signal and (2) the ratio of the resonant scattering signal to the detector and background noise problem (i.e., measure of the S/N). Concerning (1) the resonant/Rayleigh ratio has been treated in detail in Section 2.2.1; the pertinent results of that discussion are summarized in Table 2-1. For the γ-bands, a strong permitted electronic transition, the line strength, α, is generally of the order of 10^{-16} cm; the tabulated resonant/Rayleigh ratios are 690 (γ 0,0), 2400 (γ 1,0). For any other electronic (UV) transitions, losses in line strength, population factor, or fluorescent efficiency degrade these moderate magnitude ratios. For example, the M(0,0) band is 10^{-7} weaker in line strength (unfavorable Franck-Condon factor as well as prohibited transition), and 10^{-3} weaker in fluorescent efficiency. The

M(0,4) band is somewhat more favorable with respect to both these factors, but has no significant population in the lower level fourth vibrational state. Therefore, only the γ (n,0)bands or the vibration-rotation bands (1-0), 2-0, or 2-1) represent possible probe selections from the standpoint of resonant/Rayleigh ratio alone. This requires lasing in the extreme UV or IR, where various practical difficulties involving the availability of optical components, atmospheric transmission or emission, and laser technology are much more unfavorable than in the visible or near IR spectral regions.

Concerning requirement (2) above, the estimates of absolute signal and noise for the IR (1,0), γ (0,0) and γ (1-0) bands are summarized in Table 3-1. The values were calculated on the basis of the parameter-values indicated in the table. Reasonable values of scattered return photons per 1 joule pulse are presented in line (16). However, it is estimated that immediately practical shift tune techniques can produce at best 3 millijoules at 5.3 microns (from second harmonic CO_2 laser) or 50 millijoules at the γ bands. The final estimated photons/pulse are shown on line (18). The practical possibilities for immediate performance of the indicated experiments will be discussed in the next sections.

It should be noted that the quantity listed as "photons/pulse" is also calculated for a single range resolution element, which is 3.8 km in the 0.26 microsecond lifetime of γ (1,0). Therefore, by electronically lengthening the receiver time constant to 1 microsecond, for example, one obtains four times the signal in photons per resolution element. Now the resolution is 15 km or about the halfwidth of the peak NO concentration at 90 km. In addition, since the background from all sources is a fraction of an electron per pulse, statistical integration of several pulses can be employed to obtain useful data even at a return as low as 1 electron per pulse per resolution element.

On this basis, it appears that a promising laboratory possibility exists for generating the required γ (1-0) 2155Å radiation by means of a dye laser at 8620Å (ADP second harmonic) – (KDP fourth harmonic). The feasibility (Ref. 16) of this lasing technique has been demonstrated previously for the 2652Å m (0,4) band.

In the present case involving the generation of 2155Å radiation, it appears that the attainment of 50 millijoules, as in the previous two-step process may be difficult, although 1 to 5 millijoules is feasible. This will result in about 1 to 10 received electrons per pulse, per 0.5 microsecond of range gate, with a resolution of 3.8 km. Perhaps it will be required that a number of pulses be integrated to obtain acceptable statistical data.

In practice, it is suggested that a laboratory scattering experiment from a resonance cell be performed which should test most of the calculated performance parameters, except atmospheric transmission. Specifically, it would demonstrate the feasibility of both achieving the

TABLE 3-1

ABSOLUTE SIGNAL ESTIMATES

(1) $S^1(t) = \left(\frac{J}{\Delta t_F}\right)\left(\frac{A_R}{4\pi R^2}\right)(\tau^2 \eta p)\left(\frac{\alpha[NO]\,\Delta h}{\Delta \nu_D}\right)$ if $\frac{2\Delta h}{c} \ll \Delta \tau_F$

Constant Terms:

(2) $J = 1$ joule (reference laser pulse energy)
(3) $A_R = 1000$ cm^2 (telescope area)
(4) $R = 90$ km, $R^2 = 81 \times 10^{12}$ cm^2 (range)
(5) $\tau = 1$ (reference atmospheric transmission)
(6) $[NO]\,h = 1.7 \times 10^{14}$ molecules/cm^2
(7) $J \frac{A_R}{4\pi R^2} \tau^2 [NO]\,\Delta h = 167$

Terms a Variable Function of Transition:

	BAND	IR(1,0)	γ(0,0)	γ(1,0)
	LINE	P6	P6	P6
	$\lambda(\mu)$	5.33	0.2269	0.2155
	ν(cm^{-1})	1876	44,100	46,450
(8)	Δt_F, lifetime(sec)	0.088	0.26×10^{-6}	0.26×10^{-6}
(9)	η, fluor. eff.	0.53	0.073	0.154
(10)	p, population	0.069	0.069	0.069
(11)	α (cm), strength	4.27×10^{-18}	3.5×10^{-16}	7×10^{-16}
(12)	$\Delta\nu_D$(cm^{-1}), Doppler	1.5×10^{-3}	3.5×10^{-2}	3.7×10^{-2}
(13)	Relative $\frac{\eta p \alpha}{\Delta \nu_D \Delta t_F}$	1.18×10^{-15}	1.93×10^{-10}	7.7×10^{-10}
(14)	$S^1(t)$, Signal (watts)	2.0×10^{-13}	2.5×10^{-11}	1.0×10^{-10}
(15)	" (photons/sec)	5.3×10^{-6}	2.8×10^{7}	1.1×10^{8}
(16)	" (photons/joule pulse)	4.7×10^{5}	1.9×10^{3}	7×10^{3}
(17)	Available pulse (joules)	3×10^{-3}	50×10^{-3}	50×10^{-3}
(18)	New photons per pulse	1400	95	350
(19)	NEP (watts)	1.6×10^{-11} (Δt= 0.088) (300°K Background)	10^{-10}	10^{-16}

match can be achieved and holding it sufficiently stable to tune the source through the resonant line. By this method then, dissemination can be achieved between resonance and the background due to all other sources. In addition, in a short-range resonance cell experiment, no problem will be encountered with either the energy threshold, or signal-to-noise.

A promising shift-tuning possibility exists for generating losing action in the IR 5.3-micron band. This may be accomplished by generating the second harmonic of the CO_2 laser 10.6-micron radiation.

Both possibilities (γ-band,and IR 5.3-micron bands) are discussed in greater detail below.

3.2.1 Matching NO-5.3 microns with harmonic of CO_2-10.6 microns. — A promising possibility is available for generating 5.3-micron radiation by generating the second harmonic of the CO_2 laser 00^o1-10^o0, R-branch, J = 24. In Figure 3-5 the best values are presented for 2ν of the CO_2 lines which have been reported and the lines of NO(1,0). NO(1,0) = R(J = 1) matched to 0.02 cm^{-1}, which is essentially the accuracy of the available data. The accidental precise match is required in the case of two molecules, since the narrow lines cannot be shifted far, as in the case of the wide fluorescent bands of ruby, neodymium, or dyes, which can be tuned continuously by cavity mode selection.

This harmonic doubling experiment of the CO_2 laser has been performed by Patel (Ref. 49, 50) and others. The nonlinear medium employed is a single crystal of tellurium.

The vertical absorption of a relatively dry atmosphere is about 80 percent at 5.3 microns. Initial probe experiments should be performed using CW, with a coded chopper at about a hundred cps and a phase sensitive detector (Princeton Research Associates). This is suggested owing to the long lifetime of the nitric oxide IR transition, i.e. 88 milliseconds. Although this approach does not result in fine range resolution, it may provide a measurement of total nitric oxide along the path, by careful analysis of the phase changes in the modulation. Because the average power in the CW CO_2 lasers is comparable with that in the best pulsed CO_2 lasers of high repetition rate, the modulated -CW type radar probe experiment is essentially as sensitive as the pulsed radar type. The CO_2 laser mirror Q-switched at 120 cps yields 10-kW peak power at 300-nanoseconds pulsewidth, or 3 millijoules per pulse, 3.6-watts average power. The tellurium harmonic yields 3 microjoules per pulse. A 10-watt CW CO_2 laser interrupted at 100 microseconds gives the millijoule/pulse. Interruption at 10 milliseconds (50 cps square wave) yields 100 millijoules/pulse; at the NO(1,0) lifetime of 88 milliseconds, this amounts to 0.880 joules/pulse. The former approach is more promising since it can be accomplished more easily with the present GCA laboratory facilities.

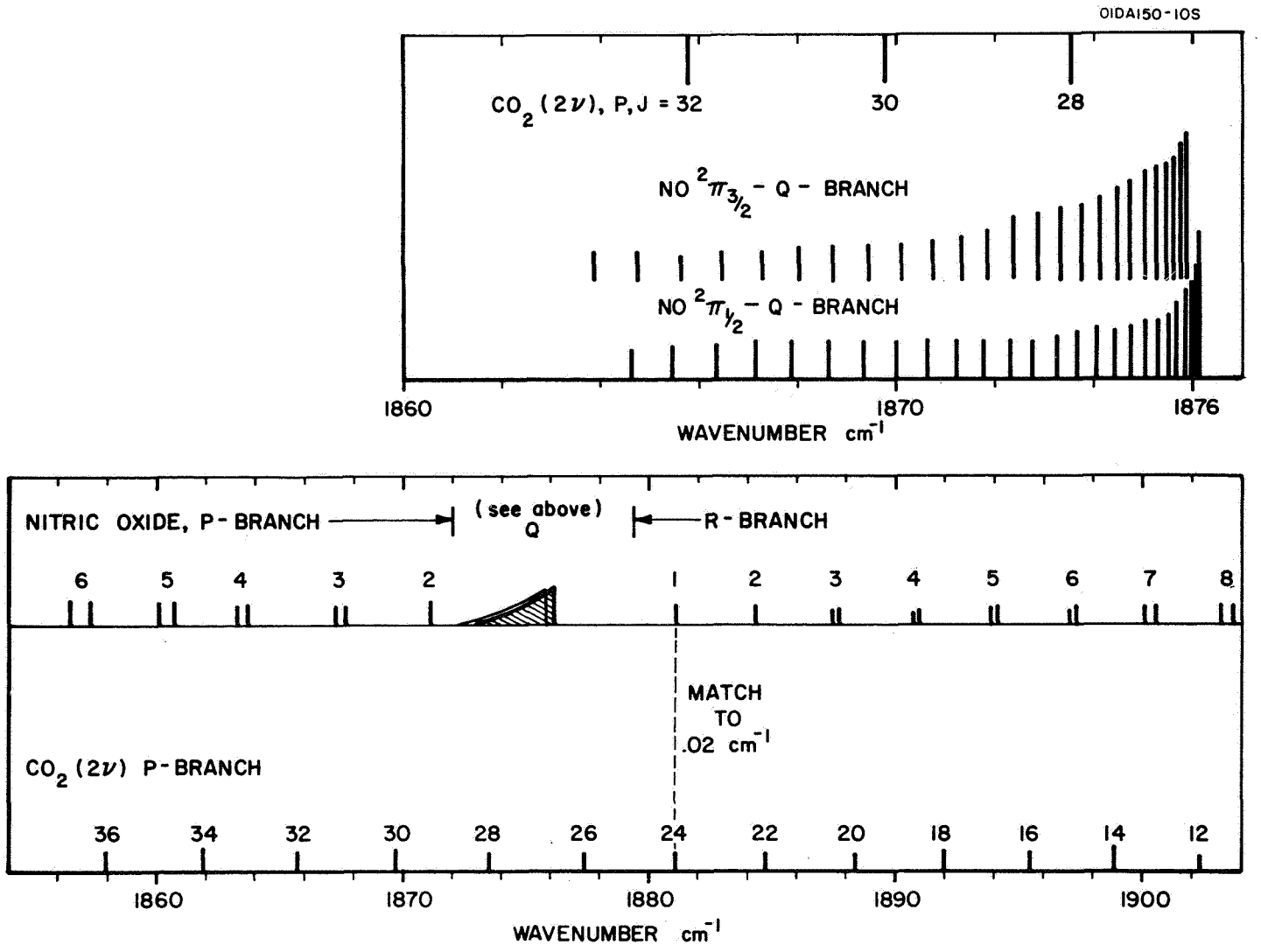

Figure 3-5. Harmonic of CO_2 - 940 cm^{-1} matched with NO - 1876 cm^{-1}.

The above discussed shift-tuning possibilities have been investigated under the present program effort. A description of the general laboratory techniques involved and the experimental data and results are presented in the following section of this report.

3.2.2 The matching of NO resonance lines by shift-tuning ruby or neodymium lines via harmonic generation and/or Raman shifting. – Since there are no lasers available with an output at the 2155Å NO band, a most promising method of producing a usable output is by starting with a laser which delivers substantial power at other wavelengths and using nonlinear optical techniques to generate an output at the wanted wavelength. The two laser materials which have been employed to produce sufficient power output when Q-switched to give high efficiency in nonlinear optics are ruby with an output at 6943Å and neodymium-doped glass at 10,600Å. However, if the output of the latter laser can be shifted to 10,775Å, the fifth harmonic will be shifted to 2155Å. Owing to the broad fluorescent line of Nd-doped glass, such tuning is possible. Broude, et al. (Ref. 51) have indeed reported tuning from 10,500Å to 11,000Å which includes the region of interest at 10,775Å. This tuning was performed with a glass prism in the laser cavity which acted as a disperser to select the output wavelength. By combining this technique with mode selection, it is possible to generate a narrow line output tunable over a broad region.

The second, third, and fourth harmonic generation of the neodymium-doped glass laser have been reported (Ref. 52) and second and fourth harmonic generation have been performed at GCA (Ref. 25). Although the fifth harmonic could theoretically be generated directly by the fifth-order nonlinear susceptibility, this is so small that it is more efficient to employ the second-order susceptibility; i.e., second harmonic generation and mixing of two frequencies to generate higher order harmonics. Therefore, "fourth" harmonic is obtained by generating the second harmonic of the second harmonic and the "fifth" harmonic can then be obtained by mixing the fourth harmonic and the fundamental.

To generate the fifth harmonic efficiently, the wave vector of the second-order polarization wave, ${}_e k_5'$, which is equal to the fourth harmonic plus fundamental mixed light wave must be made equivalent to the fifth harmonic second-order light wave, ${}_e k_5$, to provide phase matching of the two wave (Ref. 53) or:

$$ {}_e k_5' = {}_e k_5 = {}_o k_4 + {}_o k_1 \qquad (3\text{-}30) $$

and

$$ k_i = \frac{n_i \omega_i}{c} $$

where n_i is the index of refraction at the wavelength of the i-th harmonic, ω_i is its angular frequency, and c is the speed of light.

The subscripts e and o indicate that the fifth harmonic is an extraordinary wave in the crystal and the fundamental and fourth harmonic are ordinary waves, respectively. This permits the phase difference due to dispersion to be cancelled by the bi-refringence of a uniaxial crystal such as potassium dihydrogen phosphate (KDP) or ammonium dihydrogen phosphate (ADP). The angle, θ, at which phase matching occurs is given by (Ref. 54):

$$\sin^2 \theta = \frac{({}_e k_5' \lambda_5)^{-2} - {}_o n_5^{-2}}{{}_e n_5^{-2} - {}_o n_5^{-2}} \tag{3-31}$$

where ${}_o n_5$ and ${}_e n_5$ are the ordinary and extraordinary indices of refraction, respectively, at the fifth harmonic wavelength, and $\lambda_5 = \lambda_5/2\pi$ where λ_5 is the wavelength of the fifth harmonic. Then Equations (3-30) and (3-31) may be rewritten as

$${}_e k_5' = \frac{{}_o n_1 \omega_1 + {}_o n_4 \omega_4}{c} \tag{3-32}$$

$$\sin^2 \theta = \frac{\frac{(\omega_1 \, {}_o n_1 + \omega_4 \, {}_o n_4)^{-2}}{\omega_5} - {}_o n_5^{-2}}{{}_e n_5^{-2} - {}_o n_5^{-2}} \tag{3-33}$$

where ω_5 is the angular frequency of the fifth harmonic.

In order that $\sin \theta < 1$:

$${}_e n_5 < \frac{\omega_1 \, {}_o n_1}{\omega_5} + \frac{\omega_4 \, {}_o n_4}{\omega_5} = 0.2 \, {}_o n_1 + 0.8 \, {}_o n_4 \, . \tag{3-34}$$

The problem is that in the ultraviolet region, the dispersion is so great that for most materials, the above condition cannot be satisfied in general. The index values for ADP and KDP calculated from Zernike's empirical equation (Ref. 54) which is accurate to 10^{-4} are presented in Table 3-2. As can be seen, neither ADP nor KDP fulfill the condition for phase matching at any angle. However, potassium dideuterium phosphate (KDDP) has a lower dispersion in proportion to its bi-refringence than KDP (Ref. 55) and, therefore, should permit phase matching since KDP is so close to it. Unfortunately, no index values are available for KDDP in the ultraviolet of sufficient accuracy to permit exact calculation of the phase matching angle. The strong possibility of being able to accomplish phase matching using KDDP, suggests that an appropriate series of experiments should be performed in order to test this possibility as will be discussed in greater detail in Section 4.1.3.

TABLE 3-2

INDEX VALUES FOR ADP AND KDP

Material	$_{o}n_{1}$	$_{b}n_{4}$	$0.2\ {}_{o}n_{1} + 0.8\ {}_{o}n_{4}$	$_{e}n_{5}$
ADP	1.5071	1.5800	1.5654	1.5711
KDP	1.4943	1.5602	1.5470	1.5484

In the event that the "fifth harmonic" of the neodymium laser cannot be tuned directly to the 2155Å NO line, there are a number of ways in which harmonic generation, sum frequency generation, and Raman shifting can be combined to yield the desired frequency. The exact order can be determined by the characteristics of the Raman material and selected in order to maximize the conversion efficiency at each step. Regardless of the order, the frequency involved can be characterized as follows: let ν_o be the initial laser frequency, ν_1 is the Raman frequency shift, and $\bar{\nu}$ is the final desired frequency. Then

$$\bar{\nu} = n\nu_o \pm m\nu_1 \quad . \tag{3-35}$$

For the neodymium-in-glass laser $\nu_o = 9418 \pm 10\ cm^{-1}$ ($\pm 10\ cm^{-1}$ represents the amount by which the laser can be tuned) and $\bar{\nu}(2155Å) = 46389\ cm^{-1}$. Here it is assumed that n = 5 and one is only interested in Stokes Raman lines so that the minus sign is employed. Then:

$$\nu_1 = -\frac{1}{m}(\bar{\nu} - 5\nu_o) \tag{3-36}$$

$$\nu_1 = \frac{1}{m}(701 \pm 50)\ cm^{-1}$$

Taking m-values 1 through 5, yields the following required Raman frequencies with the indicated possible materials:

m	ν_1	Material (MP/BP °C)	Expected Raman Shift
m = 1	ν_1 = 701 ± 50	TeF_6 (-36/35.5)	697 cm^{-1}
		SeF_6 (-46/-35)	710 cm^{-1}
m = 2	ν_1 = 350 ± 25	$A\ell_2\ C\ell_6$ (subl 117.8)	340 cm^{-1}
		$Si_2\ C\ell_6$ (-1/145)	354 cm^{-1}
m = 3	ν_1 = 234 ± 17	$Sn\ Br_4$ (31/303)	220 cm^{-1}
		$Ge\ Br_4$ (26/186)	234 cm^{-1}
		$Sn\ C\ell\ Br_3$ (1/73)	235 cm^{-1}
		$Si\ Br_4$ (5.4/154)	249 cm^{-1}
m = 4	ν_1 = 175 ± 12	$Sn\ H\ Br_3$	180 cm^{-1}
m = 5	ν_1 = 140 ± 10	$A\ell_2\ I_b$ (191/360)	146 cm^{-1}

Under another contract program, the stimulated Raman effect in SF_6, $C\ C\ell F_3$, $Sn\ C\ell_4$, $Si\ C\ell_4$, $Si\ Br_4$, and $Ge\ C\ell_4$ has been observed. This suggests that experiments be performed with SeF_6 or TeF_6 with the Raman shift generated after the first second harmonic step in the following basic manner:

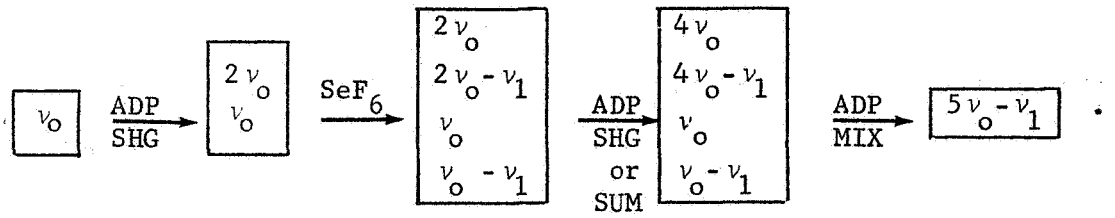

Only the more important of the many resulting frequencies are shown in the four-step process.

Similar analyses suggest using the ruby laser which offers two possibilities. The first involves the Stokes Raman shift of 2790 cm^{-1} from the ruby laser followed by a second harmonic step using ADP, and a fourth harmonic step using KDP or some other crystal. However, there exists the lack of a good Raman material yielding a shift of 2790 cm^{-1} and a crystal which affords good phase match for the second step of harmonic generation.

The second ruby laser approach involves the coupling of an equivalent third harmonic generation with anti-Stokes Raman shift. This would require the production of a strong anti-Stokes line using the ruby laser and a subsequent summing with the laser harmonic.

It is known that significant anti-Stokes components can be produced in gases as Raman materials due to the low dispersion of the gas (Ref. 56). It is possible in a gaseous medium that the phase matching condition (Ref. 57) for anti-Stokes production is almost satisfied. This anti-Stokes production can be copious if the phase mismatch

$$\Delta K = 2K_{\ell} - K_s - K_a$$

(with K the propagation vector, ℓ - laser, s - stokes, a - anti-Stokes) is small. At small phase mismatch, the intensity of the anti-Stokes wave approaches that of the Stokes wave (Ref. 58). This has been demonstrated in several gases (Ref. 59, 60). These results seem to be supported also in the GCA investigations of the gases sulfur hexafluoride, chlorotrifluoromethane, and hexafluoroethane. In such an approach, the Raman frequency required to generate output at 2155Å is 3195 cm^{-1}. A list of expected stimulated Raman shifts (derived from the literature on spontaneous Raman measurements) contains no materials with a 3195 cm^{-1} shift. The literature on observed stimulated Raman effect lists a shift of 3182 cm^{-1} for γ-picoline (Ref. 61) (4-methyl pyridine — a liquid) although the frequency error limits are ± 10 percent. This shift is the C-H vibration and, unfortunately, the basic ring vibration at 1016 cm^{-1} is also reported. However, to generate radiation at the 7(0,0) bands, 2260Å shift of 864 cm^{-1} is required by this "third harmonic" ruby method. Carbonyl sulfide (COS) has a shift of 858 cm^{-1} and is a readily available gas about which much information (Ref. 62) is available. If significant anti-Stokes Raman conversion is possible, th s method offers some advantages over that involving the "fifth harmonic" equivalent of neodymium-glass laser.

The final suggested technique in this category involves the use of dye lasers. Recent developments (Ref. 63-76) indicate that the generation of radiation at 2155Å or at 2269Å can be accomplished by a one-step second-harmonic generation of either a flash lamp pumped or ruby harmonic pumped dye laser. A dye for this purpose might be 3-ethyl-aminopyrene 5, 8, 10-trisulfonic acid in the appropriate solvent. The problem with harmonic generation in this application is the same as that encountered earlier with regard to the "fourth harmonic" generation of a Raman shifted ruby laser, i.e. lack of a good nonlinear material in which phase matching can be accomplished for the 4310Å-2155Å harmonic step. An additional problem with the dye lasers is the broad line output so that work would be required on line width reduction. However, considering the satisfactory results already achieved with the Ne-glass laser one could be optimistic about achieving similar results with dye lasers. Once this is achieved, there is then a strong possibility that a flash lamp pumped laser with an output near 6465Å (such as 3,3′- diethyloxadicarbocyanine iodide) could be employed as a source for "third harmonic" $[(\nu_o + \nu_o) + \nu_o]$ generation with available crystals such as ADP.

4. EXPERIMENTAL PROGRAM

4.1 Laboratory Survey of Lasing Techniques

The previous discussions presented in Sections 3.1 and 3.2 have suggested a number of possibilities for generating lasing action in a variety of systems. Of these, the more promising schemes have been selected for further laboratory investigation in order to evaluate their feasibility for application as an atmospheric probe. Owing to the limited scope of the program, it was decided to survey a number of possibilities rather than single out any particular scheme for detailed investigation at the present time. As such, the program involved preliminary measurements for a number of systems. Specifically, the program included laboratory investigations involving the following systems: (1) CW and pulsed discharge experiments with NO and/or NO_2 with mixtures containing various partial pressures of N_2 and/or He, (2) afterglow experiments involving active nitrogen and oxygen, (3) attempts to generate the second harmonic of CO_2 (10.6μ) to match NO IR 5.3-micron radiation, and (4) the tuning of neodymium laser lines by both harmonic generation and Raman shifting.

Laboratory investigations on systems (1) and (2) represent attempts to achieve direct lasing of NO at the required transitions whereas systems (3) and (4) represent possibilities of tuning other lasers to the desired frequency. Thus, for convenience the results are discussed in these two general categories.

4.1.1 Direct lasing of NO at the required transitions. — Of the large number and variety of possibilities to obtain direct lasing of NO (see Section 3.1) the present laboratory effort restricted the investigation to CW and pulsed discharge experiments involving a large number and variety of gaseous mixtures and some preliminary work on afterglow studies. For these purposes a suitable experimental apparatus was designed and constructed; a schematic of the gaseous laser apparatus shown in Figure 4-1.

The apparatus shown was constructed of standard 2-inch glass pipe components permitting relatively simple (and low cost) modification of either the length or diameter. The gold coated mirrors in the cavity have a radius of curvature of 1.75 meters. The output energy is removed through an output coupling hole bored through the axis of one mirror and an optical flat of irtran IV which makes the vacuum seal on the mirror flange. The end (mirror) flanges may be adjusted for optical alignment in a near confocal arrangement by the micrometric screws anchored to the optical bench rail.

A 1500/liter/minute Precision Model D-1500 mechanical pump is employed evacuating the apparatus. The gas mixtures can be regulated

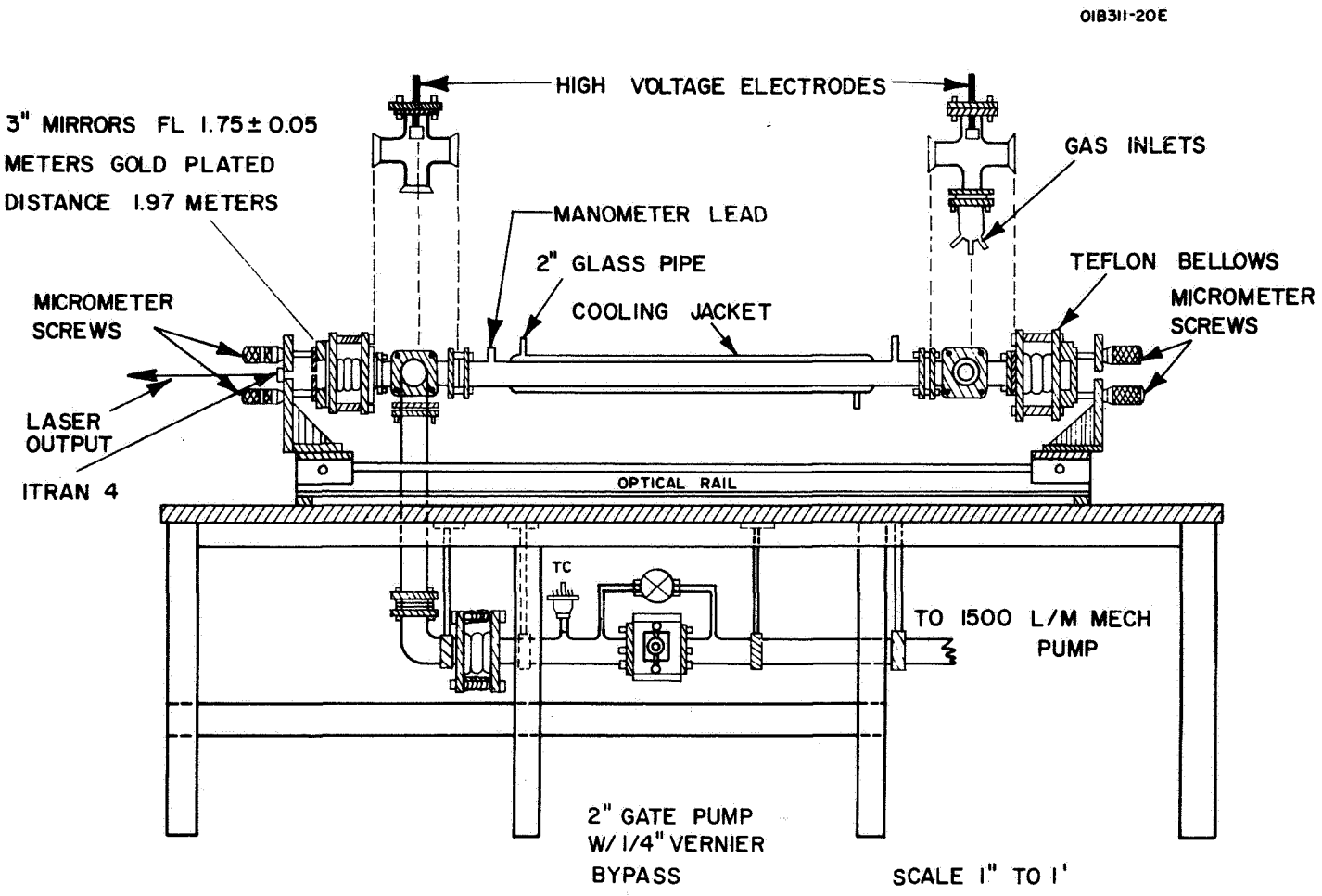

Figure 4-1. Schematic diagram of experimental apparatus for gaseous lasers (NO and CO_2 experiments).

and varied with calibrated Edwards high vacuum valves. A Wallace and Tiernan vacuum gauge (0-20 mm) was employed to check the composition of the gas mixtures.

For CW operation, a rated 10-kV, 150-mA commercial power supply was employed. For the 2-inch diameter, 2-meter long discharge tube, the breakdown voltage varied from 4 to 7 kV depending on gas mixture. For some experiments a 5-kV, 250-mA power supply was used.

For pulser operation the circuit shown in Figure 4-2 was employed. The RC-charging circuit had a time constant of 0.003 seconds (approximately 1/5 the repetition rate), thus leading to nearly full power supply voltage on condenser for each discharge. The stored energy for each discharge was $1/2\ CV^2 \approx 2$ joules per pulse for a 4-kV supply. This is more energy than in the pulser used by Patel (Ref. 49), though the GCA discharge time was about 10 μsec as observed by oscilloscope. Patel reports his pulser as 15-kV, 15-A initial amplitude and 1 μsec duration, thus 0.25 joules per pulse.

The radiation detector employed for this experimental phase was an Eppley Thermopile No. 3630 with a 10-second response time. Absolute calibration of the thermopile was accomplished by comparison of its response against an NBS standard lamp. The results indicated a sensitivity of 0.056 μV/μW per cm^2. Unfortunately, this particular thermopile has a 1-mm LiF window which reduces its sensitivity at 9.5μ and 10.5μ by factors of 10 and 100, respectively. These calibration results were checked against a TRG Model 107 calorimeter employed with a CO_2 - CW laser output. In any case, this detector was employed as indicated for the discharge and afterglow experiments discussed below.

Prior to the performance of the indicated laser experiments involving a variety of gases, it was necessary to establish the operating characteristics of the apparatus and its capability. This task was performed by successfully lasing CO_2 in the 9.5μ to 10.6μ band in accordance with Patel (Ref. 49 & 50). The results of these tests established the proper functioning of the following:

(1) mirror alignment and stability of all mechanical components,
(2) calibration and testing of flow and vacuum systems,
(3) check and calibration of power output measuring devices (i.e., thermocouple, and calorimeter, and
(4) other general operational tasks.

Subsequent to these initial tests, a number of CO_2-N_2-He partial pressure combinations were investigated. It was found that the optimum partial pressures for this system were 0.4 mm CO_2, 1.2 mm N_2 and 2.4 mm He. It was found that lasing power output increased with discharge current up to about 40 mW at 40-mA current; thereafter it was constant to the power supply limit of 150 mA.

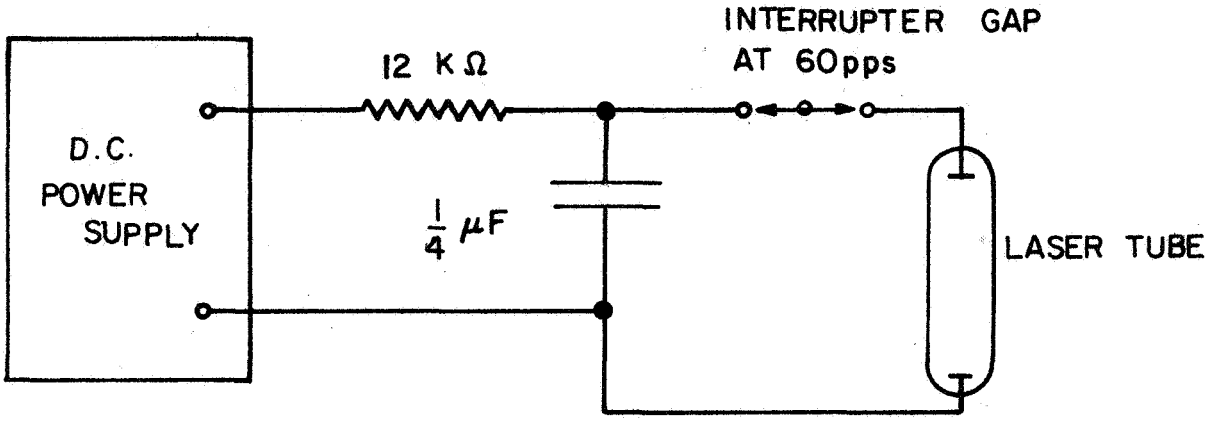

Figure 4-2. Interrupter gap pulse discharge source, 60 pps

The N_2-CO_2 system would still lase CW without use of buffering helium gas, but the output was about 10 percent of the 40 mW obtained with helium. The N_2-CO_2 system also lased only at low discharge currents, about 15 to 20 mA, the output decreasing rapidly to zero as the current was increased to 50 mA.

Finally, a brief attempt was made to observe CO lasing radiation; with generally negative results. Since Patel (Ref. 49) had demonstrated that the expected radiation intensity is about 1 percent of that from the CO_2 laser, it appears that the present system detection capability lies between 0.4 and 40 mW. In any case, subsequent to these test and performance capability studies, the laser apparatus was employed to investigate the CW and pulsed discharge experiments as well as the afterglow experiments described subsequently below.

4.1.1.1 CW and pulsed discharge experiments. – The rationale for performing CW and pulsed discharge experiments involving NO and/or NO_2 was discussed previously in Sections 3.1.1 and 3.1.2. The specific experiments were selected on the basis of simplicity and the possibility of gaining some scientific insight into the NO vibrational-rotational excitation processes since investigations of vibrational transfer systems under steady state discharge conditions are attractive from this point of view.

The CO_2 laser apparatus was employed to perform brief laboratory surveys of spectral output in the 5-micron region as a function of total and partial pressure and current density for the following gases and mixtures:

(a) pure NO at pressures of 0.1 to 1.0 torr (typical lasing for pressures),
(b) mixtures of NO and N_2 where the partial pressure of NO varied from 0.1 to 1.0 torr and the total pressure was maintained at 1.0 torr,
(c) mixture of NO and He as in (b),
(d) mixtures of NO with N_2 and/or He as buffer gases. Here the partial pressures of NO again varied from 0.1 to 1.0 torr while the total pressure was always maintained at 1.0 torr. In all cases the buffer gas was a 50-50 mixture of N_2 and He.
(e), (f), (g), and (h) mixtures involved NO_2 as the lasing gas [in place of the NO in (a), (b), (c), and (d)] with analogous use of the buffer gases.

The individual mixtures [involved in Items (a) through (h)] were formed and fed into the "gas inlet" of the apparatus previously shown in Figure 4-1. For the cases investigated, the input power was varied from about 2 to 8 joules/pulse. In no case, was lasing action observed or detected in the 5-micron region by the thermopile. It may be suggested that these negative results may be attributable to the relatively long time constant of the thermopile detector employed and/or the longer

pulse discharge time constant. In any case, in light of the disappointing results, it was decided not to pursue this possibility further in view of the requirement to examine the other schemes as described below.

4.1.1.2 Afterglow experiments. – A detailed discussion of the general scheme of generating lasing action by chemical reactions involved in afterglow discharge phenomena was presented in Section 3.1.4. In addition, some specific possibilities of lasing NO by this scheme were enumerated. Thus, a number of afterglow experiments were performed to test the feasibility of the above described mechanisms.

The apparatus employed was similar to the laser setup shown in Figure 4-1. A number of preliminary afterglow experiments were performed whereby a Raytheon microwave generator (Model No. MW/200) was employed to generate the required N and O atoms which were fed into the position marked "gas inlet" in Figure 4-1. Pulsed and CW discharges were attempted between 5 and 15 kV. The pressures of the gases were varied from 0.25 to 3.0 mm. No lasing was detected in the 5-micron region with the Eppley thermopile. A Bass Kessler wide aperture spectrograph was used to determine the spectra of the gas discharges. A Hg spectrum was employed for the calibration and the wavelength of the emission lines were calculated. No atomic lines of oxygen or nitrogen could be identified from the spectra, but a least four lines (band heads) in the molecular spectra of O_2 and N_2 were identified. On the basis of these results, it was concluded that the antenna which was used on the microwave generator probably did not produce N atoms or O atoms with sufficient efficiency. Therefore, these experiments were repeated using a microwave cavity coupled with the microwave generator as the excitation source as described below.

The final set of afterglow experiments were performed in which an electrodeless discharge was generated within an Evensen cavity which in turn was coupled to a Raytheon diathermy unit operating on 2450 Mc 100 watt maximum. The cavity was tuned to optimum power using a Bendix Model 725 RF power meter which allows measurement of both the incident and reflected power delivered to the microwave cavity. The experimental arrangement (for generating the N and O atoms) which was attached to the "gas inlet" position is indicated in Figure 4-3. In addition, this equipment was also employed for the detection and monitoring of N and/or O atom concentrations described below.

After passing through the microwave discharge, the mixture of N_2 and N (Reaction 1) was titrated with nitric oxide to give molecular nitrogen and oxygen atoms (Reaction 2):

$$(1)\ N_2 \xrightarrow{\text{MW discharge}} N_2 + N\ (1\ \text{percent})$$

$$(2)\ N + NO \longrightarrow N_2 + O$$

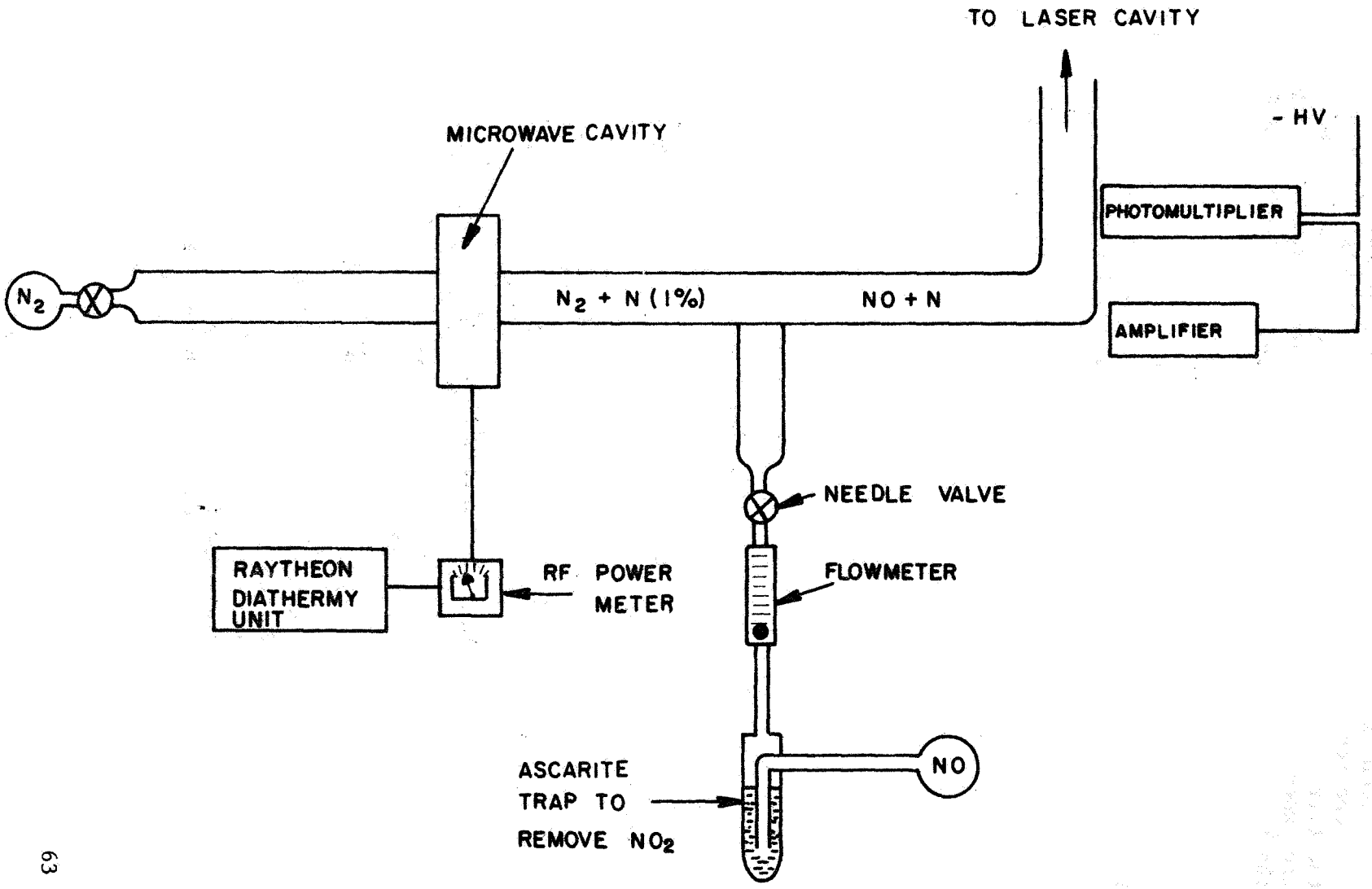

Figure 4-3. Experimental equipment for generating and detecting N and O atoms.

The nitrogen afterglow was monitored with a photomultiplier at a distance of 15 cm from the mixing point. A plot of the photomultiplier reading as a function of the nitric oxide concentration is presented in Figure 4-4. The reaction between nitrogen atoms and NO is very fast as evidenced by the titration plot data. The minimum represents the end point in titration where the nitrogen and oxygen atom concentrations are equal. At the titration, the following end point reaction becomes important

$$N + O \rightarrow NO^*$$

The discharge in the laser cavity was triggered and maintained with the Sorensen 3-kW power supply operating between 15 and 150 mA. The detector was again the Eppley thermopile with a Keithley microvolt amplifier readout.

At each pressure employed a similar NO titration was performed, and the discharge in the laser was initiated when the oxygen and nitrogen atom concentrations were equal (titration end point). The total pressure was varied between 1 and 8 torr (the usual pressure range for gas lasers) but still no lasing was detected with the thermopile. Helium was then added as a buffer gas and the total pressure was varied between 2 and 8 torr with no detectable increase in the signal. These experiments yielded negative lasing results from this system when conducted at both the CW and pulsed modes.

4.2 Shift Tuning of Other Laser Lines to Generate 5.3μ and 2155Å Lasing Radiation

In addition to the laboratory efforts described in the previous section, considerable emphasis was placed upon investigating the shift-tuning methods discussed in Section 3.2. Specifically, two programs were investigated: (1) the production of 5.33-micron radiation by generating the second harmonic of CO_2 laser radiation at 10.6μ and (2) the production of 2155Å radiation by generating a frequency approximately five times that of the neodymium-glass laser, 10,600Å.

4.2.1 Production of 5.3μ radiation via harmonic generation of the CO_2, 10.6μ lasing radiation. — The close coupling (within 0.02 cm^{-1}) between 2ν of the CO_2 lines and the 5.3μ lines of the NO (1,0) vibrational-rotational transition have been emphasized in Section 3.2.2.

Patel (Ref. 49,50) achieved experimental verification of this process by observing frequency doubling of the 10.5μ radiation from a 1-watt output CO_2 laser. The doubling was accomplished by passing the radiation through a tellerium crystal cut at the collinear index matching angle of 14 degrees. The process was noted to occur with a low efficiency, i.e., about 10^{-5}. Thus, these results suggested that an initial task would be to increase the laser output above the 40 mW previously achieved (see Section 4.1.1) to at least 1 watt prior to attempting to experimentally observe second harmonic generation.

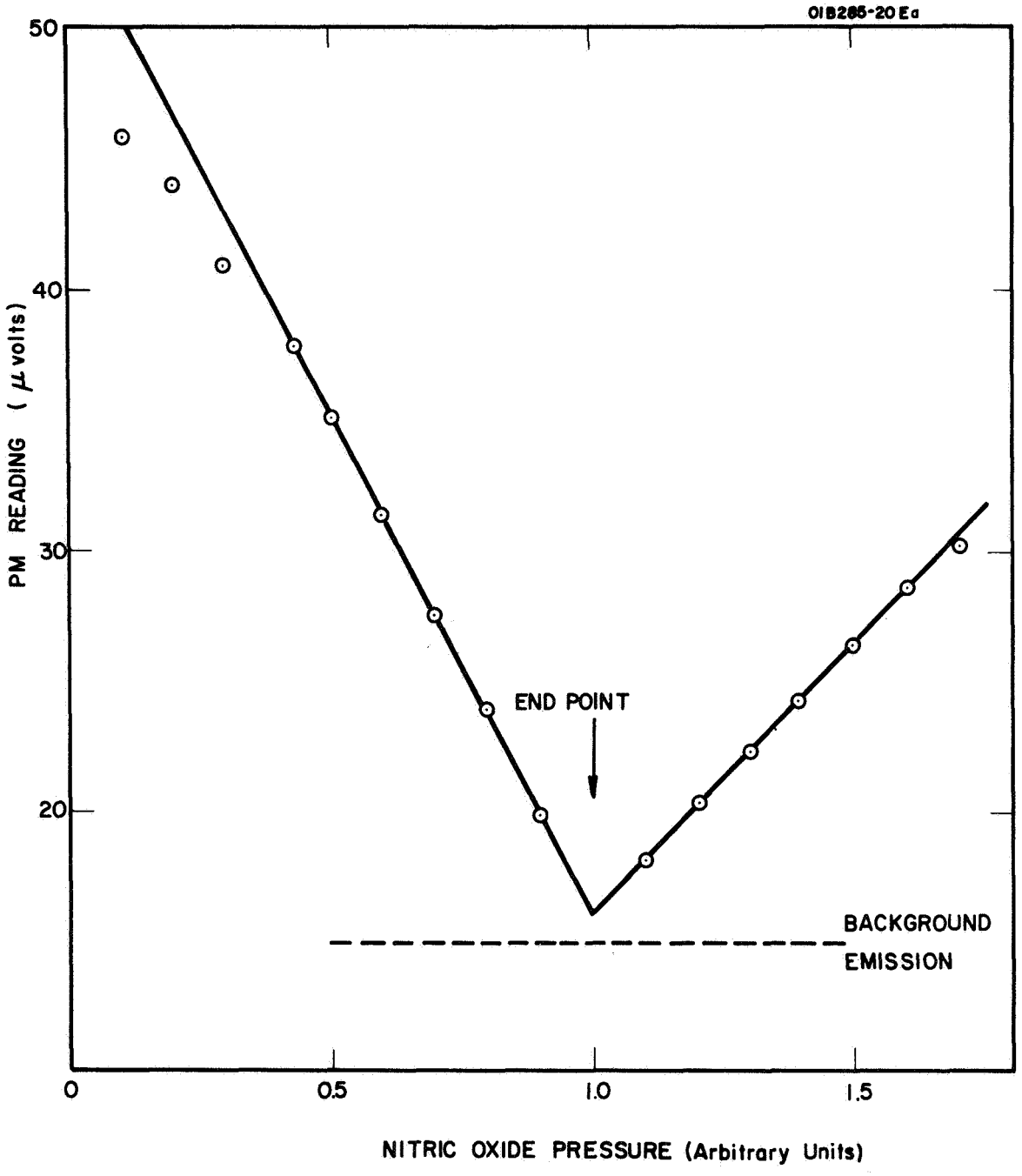

Figure 4-4. Nitric oxide titration.

4.2.2 Power output optimization of the CO_2 10.6μ lasing radiation. — A major factor involved in increasing the 10.6μ output (from the previous 40-mW value) to about 0.8 watts is the diameter change of the output coupling hole in the mirror from the original 2 mm to about 6 mm. Horrigan (Ref. 77) has reported that for hole coupling, a hole 0.6 times the tube diameter seemed to provide the optimum coupling. Thus, in principle, if the diameter of the output coupling hole is increased to 30 mm, one should be able to derive about 85 to 100 watts of power at 10.6μ. This is in agreement with the general estimated output of 50 to 75 watts per meter for CO_2 lasers.

Rigden and Moller (Ref. 78) have concluded that the gas mixture which yielded the optimum power for the CO_2 laser was helium, 80 percent; nitrogen, 15 percent; CO_2, 5 percent. The above premixed gas was purchased from Suburban Welders. The output power was measured as a function of the partial pressure of each gas added to the initial mixture (see Figure 4-5). Small increases in the amounts of the gases increased the output only slightly until finally quenching occurred at higher pressures. The optimum mixture then is essentially equivalent to that reported by Rigden and Moller (Ref. 78).

Higher laser outputs of the laser are observed with increasing power input up to a maximum (usually about 100 to 125 mA) then a gradual decrease as shown in Figure 4-6). The output power was measured as a function of pressure for the 80 percent helium, 15 percent nitrogen, and 5 percent CO_2 mixture (the values plotted in Figure 4-7 represent the peak powers obtained at the particular gas pressure). The laser power rises sharply with increasing pressure and peaks at 6 mm. At higher pressure, the output power and the efficiency decrease considerably. The actual values might not vary as much as suggested in Figure 4-7 since the level lifetimes are pressure dependent.

The efficiency (which is not corrected for the power dissipated at the electrodes) is only 0.31 percent at 6 torr total pressure. This is low compared to the 10 to 15 percent efficiencies reported for this laser; however, as indicated previously, optimum output coupling does not prevail here. If the efficiency is plotted as a function of power output (watts), it is evident that the efficiency decreases with increasing power as shown in Figure 4-8. Qualitatively, at least, these results resemble those obtained by Rigden and Moller (Ref. 78).

It has been reported that the addition of water vapor to the CO_2 laser leads to an increased efficiency through a de-excitation mechanism (Ref. 79). This experiment was attempted and a reduction in power of about 75 percent was observed for which no ready explanation is offered. No further effort was directed toward this phase.

The divergence was measured for the laser beam which is coupled through a 6-mm hole in the mirror (Figure 4-9). This was performed by

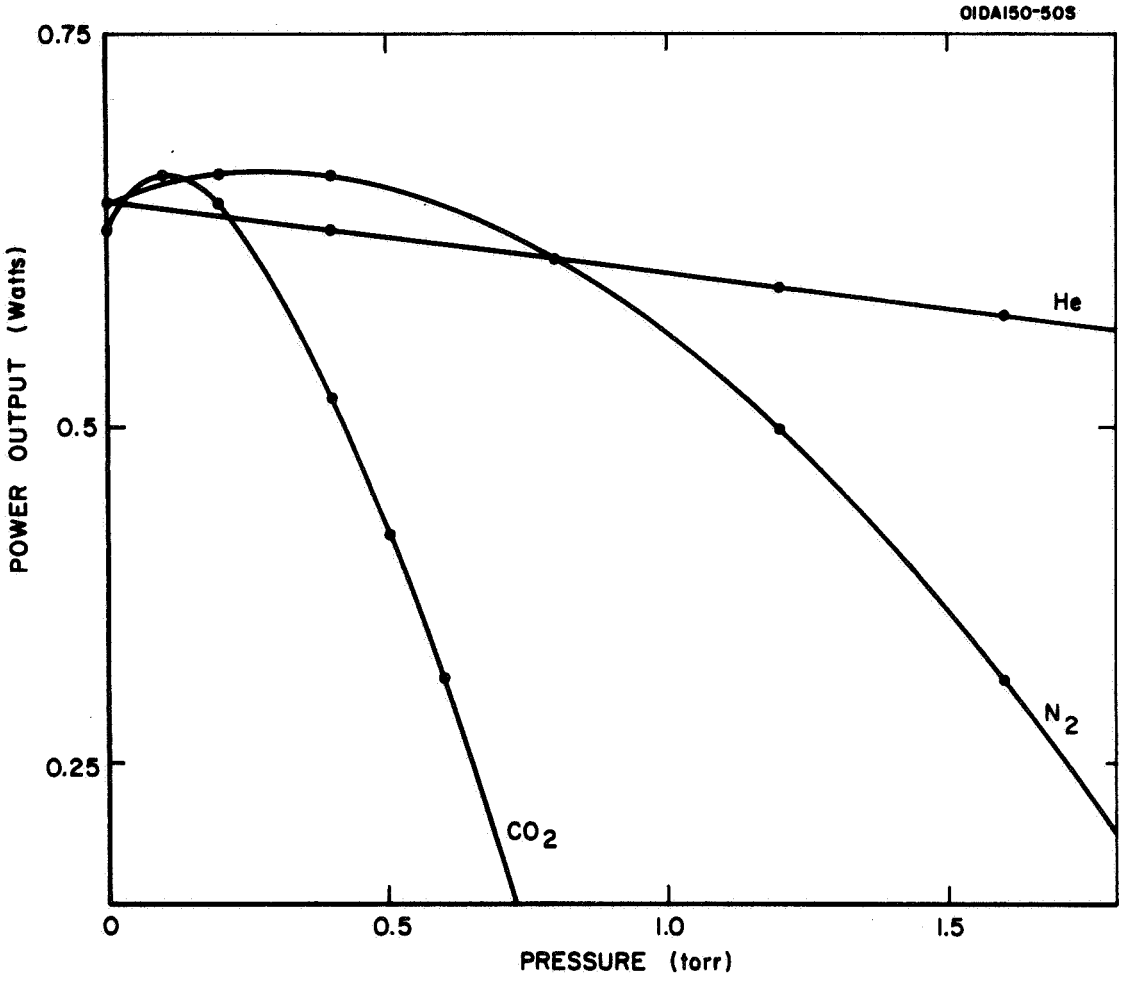

Figure 4-5. Variation of power output as a function of added gases for 80% He, 15% N_2, 5% CO_2 mixture

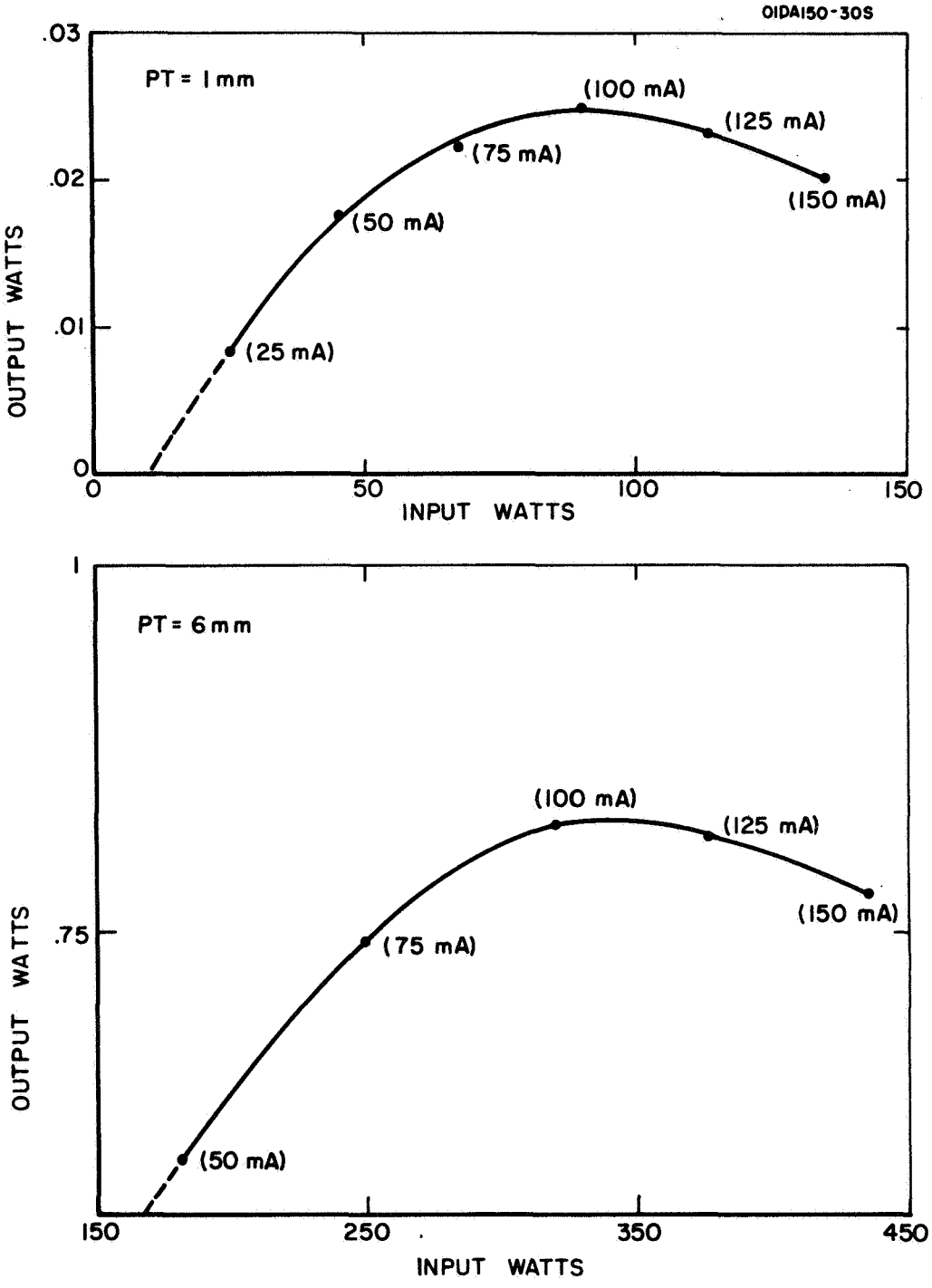

Figure 4-6. Variation of laser power with discharge current.

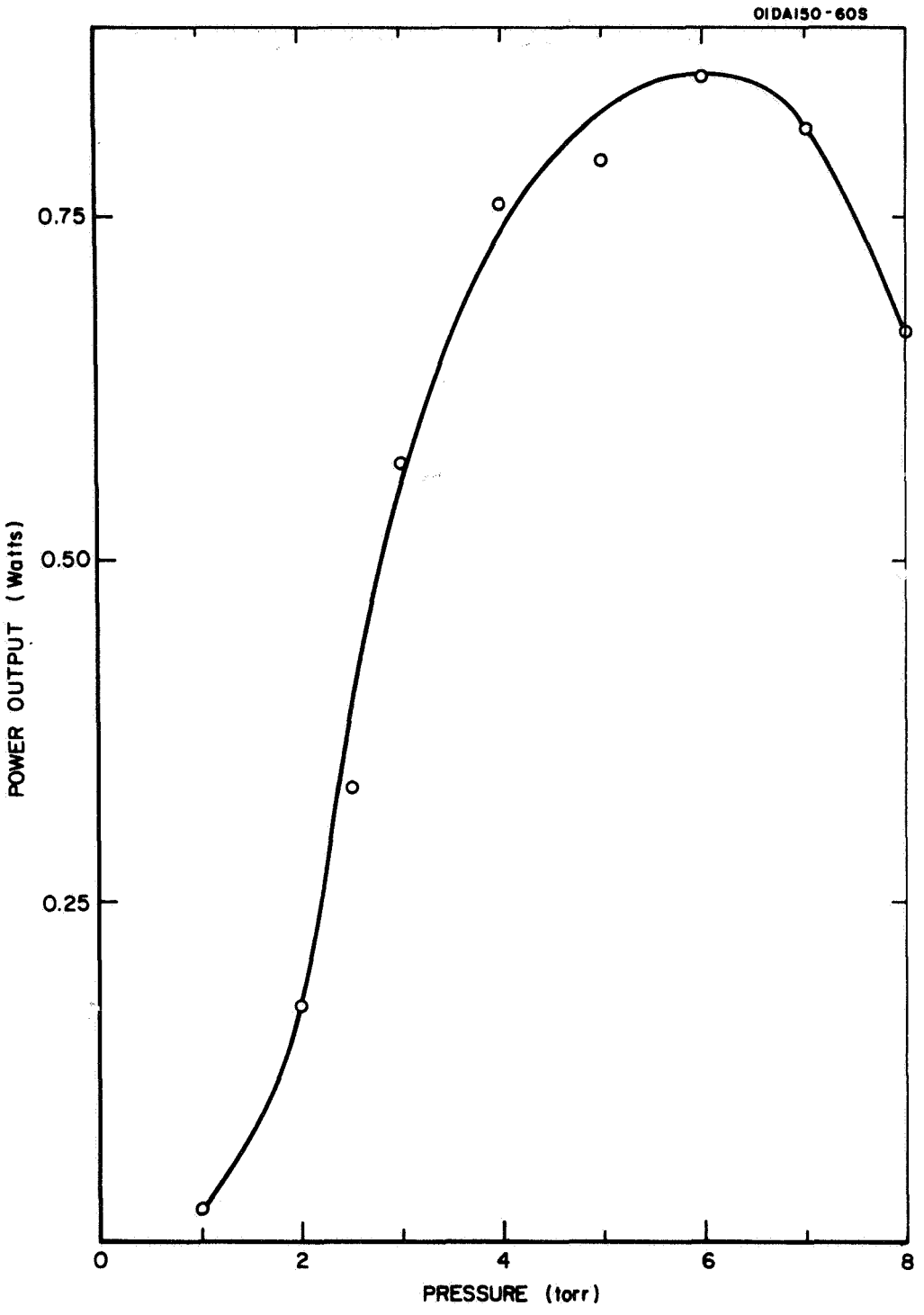

Figure 4-7. Optimum laser power versus pressure for (80% He, 15% N_2, 5% CO_2) gas mixture. (Input power was varied to give maximum output at each pressure.)

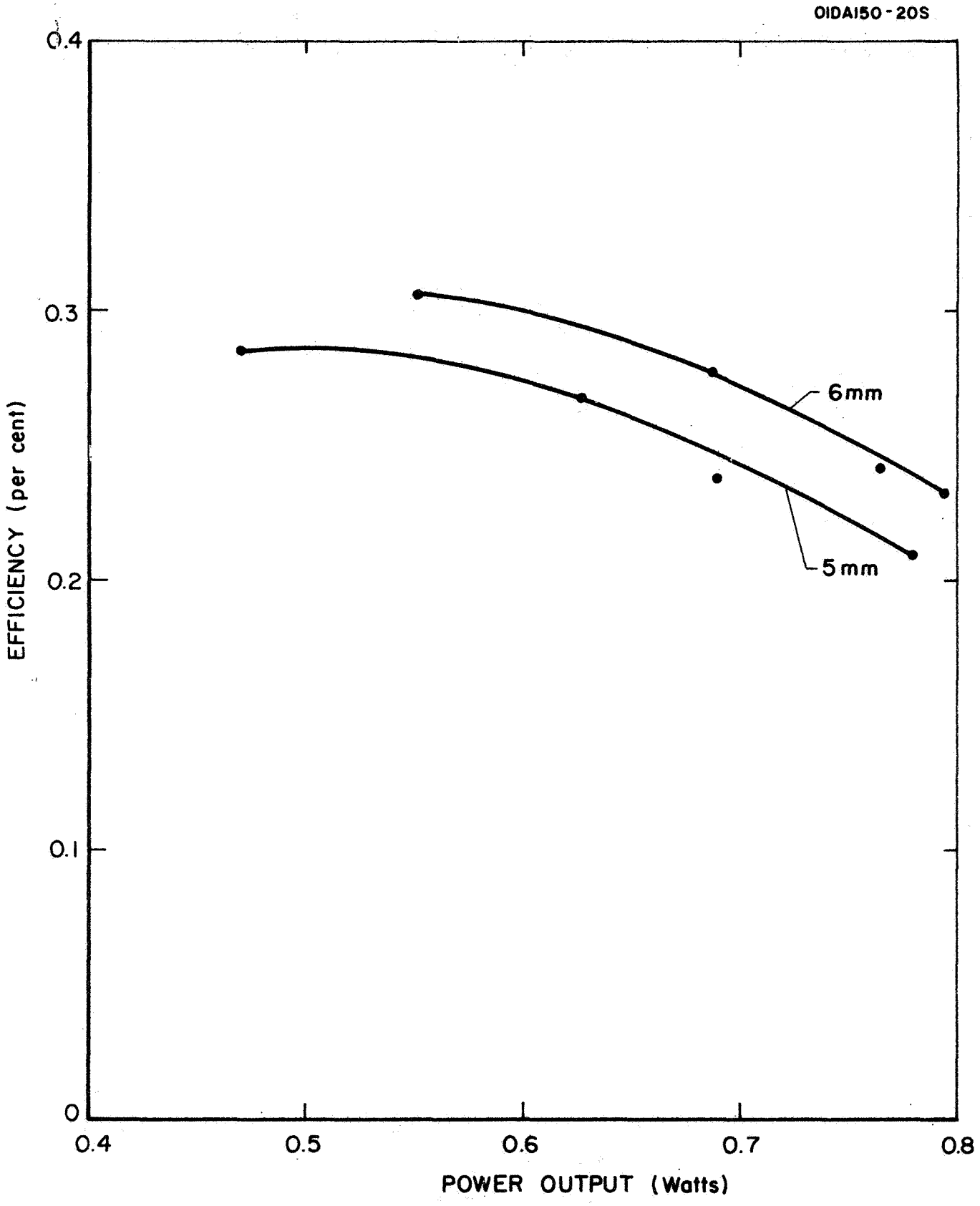

Figure 4-8. Efficiency versus power output for the CO_2 laser.

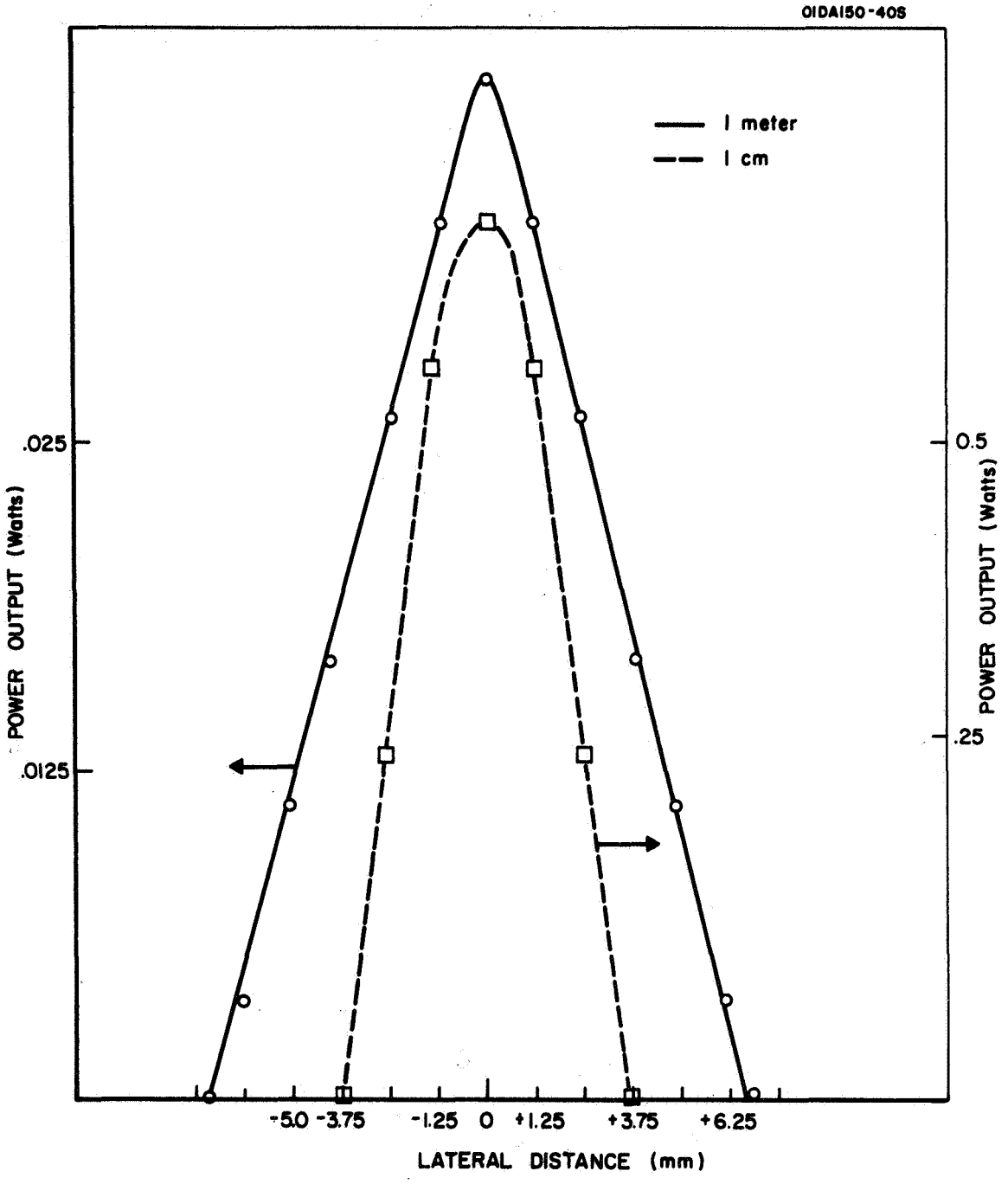

Figure 4-9. Scan of output beam width of CO_2 laser with thermopile.

racking the thermopile across the beam parallel to the mirror and measuring the power as a function of the distance traversed.

In any case it is evident that at this stage a power output of approximately 1 watt was achieved which was considered sufficient to perform the initial experiments on second harmonic generation which are described below.

4.2.3 CO_2 second harmonic generation. – The isolation of 2ν of the CO_2 laser was attempted with the equipment illustrated in Figure 4-10. Specifically, the 5.3-micron region was isolated by combining a 4.5μ long pass filter with a sapphire window. The band pass of this filter combination shown in Figure 4-11 was successful in eliminating the CO_2 discharge emission at 4.3μ as well as the 10.6μ laser signal.

The IR measurements were performed with the Texas Instruments IR-10A mercury-doped germanium detector which operates at liquid-helium temperatures. The signal was amplified with a Tektronix preamplifier and displayed on a Princeton Applied Research HR8 phase-sensitive detection amplifier chopped at 600 cps. With this detector and amplifier, the sensitivity is limited only by the magnitude of the thermal (room temperature) radiation. Lower sensitivities were attained by nulling out the thermal signal with a 0.1-watt resistor which could be regulated by a variac. The responsivity of this detector is 5×10^4 volts/watt.

Patel (Ref. 49, 50), using a 1 watt CO_2 laser and a tellurium crystal as the nonlinear medium, achieved 10^{-5} watts of second harmonic generation (SHG) power. Therefore, the initial experiments utilized the CO_2 laser operating CW at a maximum power of 0.8 watts. The thermal background signal which limited detectability was of the order of 10^{-9} watts. Thus a signal which was four orders of magnitude small than that observed by Patel could be detected.

The experiments with the 0.8 watt source indicated that a small signal ($\sim 3 \times 10^{-9}$ watts) passed the combination of both filters. This "apparent" SHG signal failed to demonstrate the dependence of SHG power on the orientation of the crystal which Patel observed in his experiment. Since this signal was marginal especially for a resonance scattering experiment, an attempt was made to increase the "apparent" SHG power. The most obvious method for improvement involves increasing the laser power output. It should be noted (by comparing area increase with power increase) that there is an increase in power density as well as an increase in total output power. Owing to the basic nonlinearity of second harmonic generation, the harmonic conversion efficiency is power density dependent while the total power out is a function of both total power in and power density. Therefore, the SHG signal might be increased by as much as two orders of magnitude with the tenfold power increase of the laser.

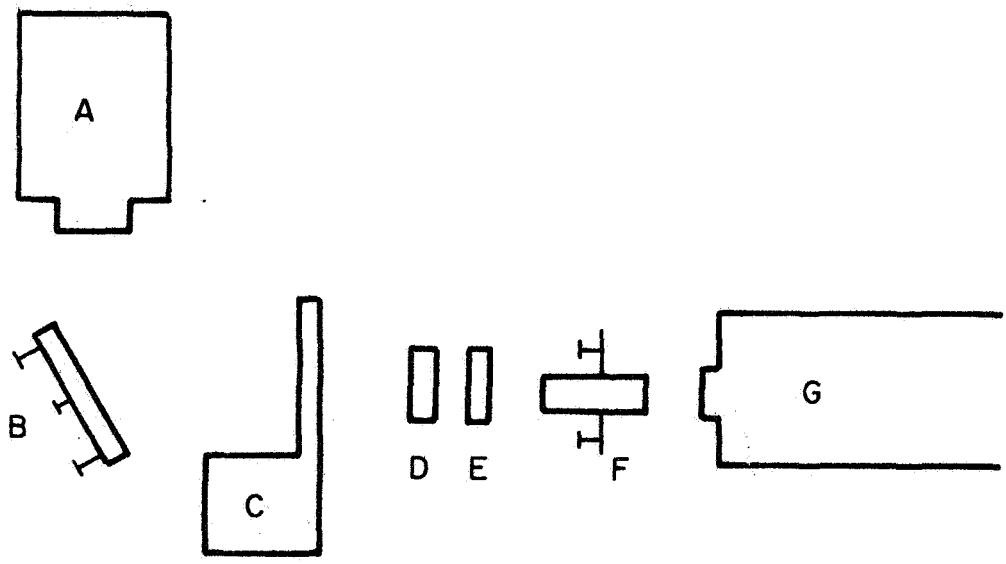

A - Hg Doped Ge Detector
B - Mirror
C - 600 cps Chopper
D - 4.5μ Long Pass Filter
E - Sapphire Filter
F - Tellurium Crystal
G - CO_2 Laser

Figure 4-10. CO_2 2nd harmonic detection system

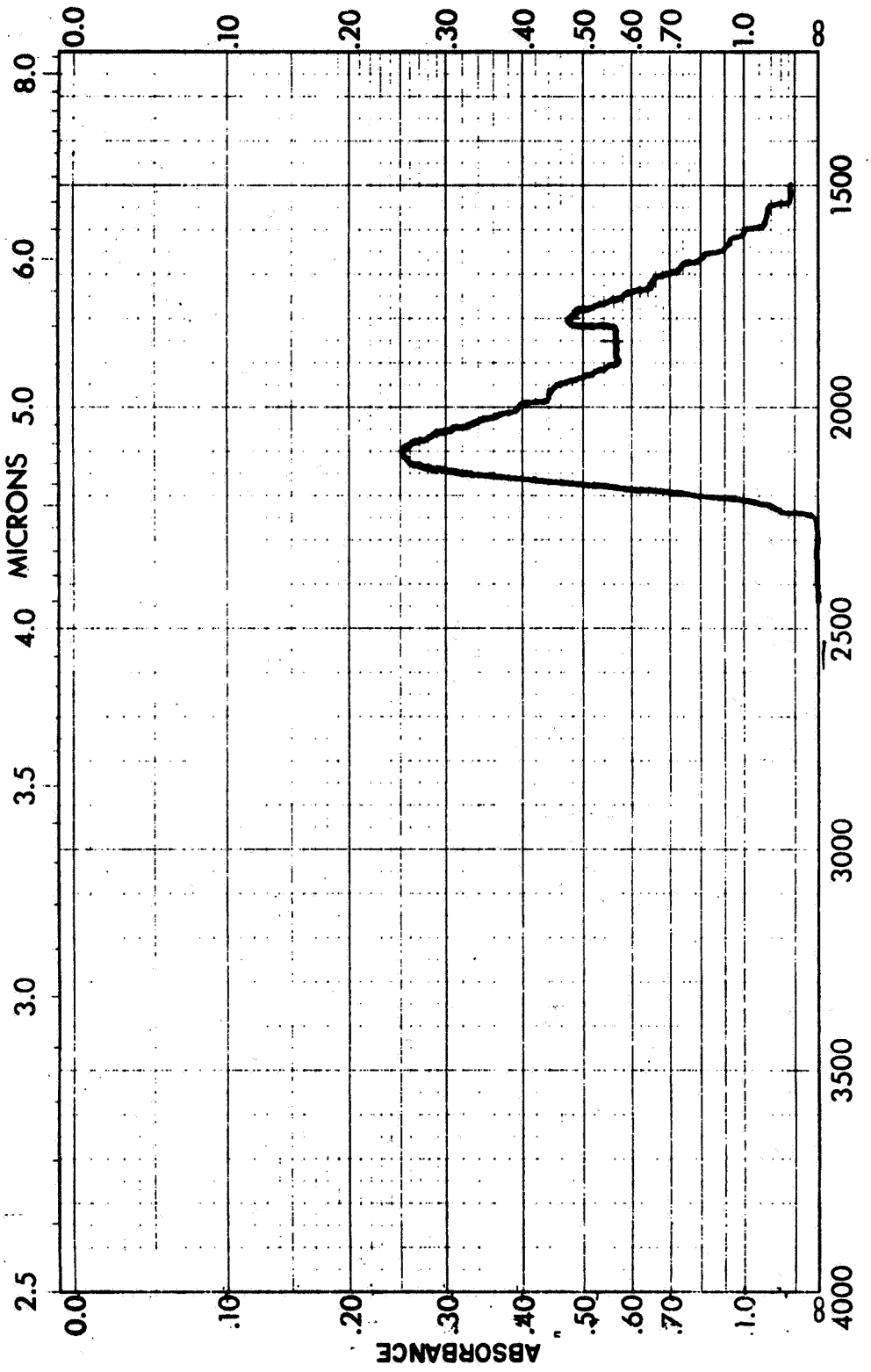

Figure 4-11. Band pass of sapphire + 4.5μ filter.

Owing to the results indicated above, it was decided to attempt further power output optimization. Thus, a separate investigation was performed in order to determine the increase of power output with increase in the hole size of the output coupling mirror. The results are summarized briefly as follows:

Mirror Coupling Hole (mm)	Peak Power (watts)
2	0.1 - 0.2
6	1
15	12
24	16

On the basis of employing a mirror coupling hole of slightly less than 15 mm, it was possible to achieve an output power of approximately 10 watts. Thus, a second series of SHG experiments were conducted involving this new power capability. In spite of this improvement, analogous results were obtained, i.e., no increase in apparent SHG signal was observed. From this result and the absence of the angular dependence in the crystal orientation, it was concluded that the "signal" obtained in earlier experiments (involving lower power output) could not have been due to second harmonic radiation of the CO_2 laser.

Finally, a series of experiments were performed whereby a 2-inch focal length germanium lens was used to focus the laser 5.3-micron radiation. However, these experiments failed owing to the excessive heating of the tellurium crystal. This concluded this category of laboratory effort involving second harmonic generation (5.3μ) of CO_2 10.6 m laser radiation. The laboratory effort program was then directed toward generating 2155Å [$\gamma(1,0)$] radiation from shift tuning of the neodymium-glass laser as described in the following section.

4.2.4 Shift tuning of the neodymium line (10,600Å) to the $\gamma(1,0)$ lines 2155Å. – In Section 3.2.1 the feasibility was demonstrated for for investigating shift tuning techniques to generate NO resonance lines. In particular, it was shown that an initial attempt should involve the generation of the fifth harmonic in neodymium (10,600Å) to produce 2155Å radiation to match the $\gamma(1,0)$ band in NO. For this purpose, it was suggested that potassium dideuterium phosphate (KDDP) be employed owing to its relatively low dispersion/birefringence ratio. On this basis, a series of shift tuning experiments were performed to test the feasibility of accomplishing the required frequency shifts as described below.

4.2.4.1 Experimental Program. – The experimental arrangement used in these tests is shown in Figure 4-12. A typical series of tests started by optimizing the 5300Å output power by adjustment of the angle of the second harmonic crystal for phase match, indicated by maximum output. The crystal was mounted in a gimbal which permitted angular adjustments to the required $\pm$ 1 minute of arc. A photodiode and oscilloscope were employed to monitor output. After peaking the 5300Å output,

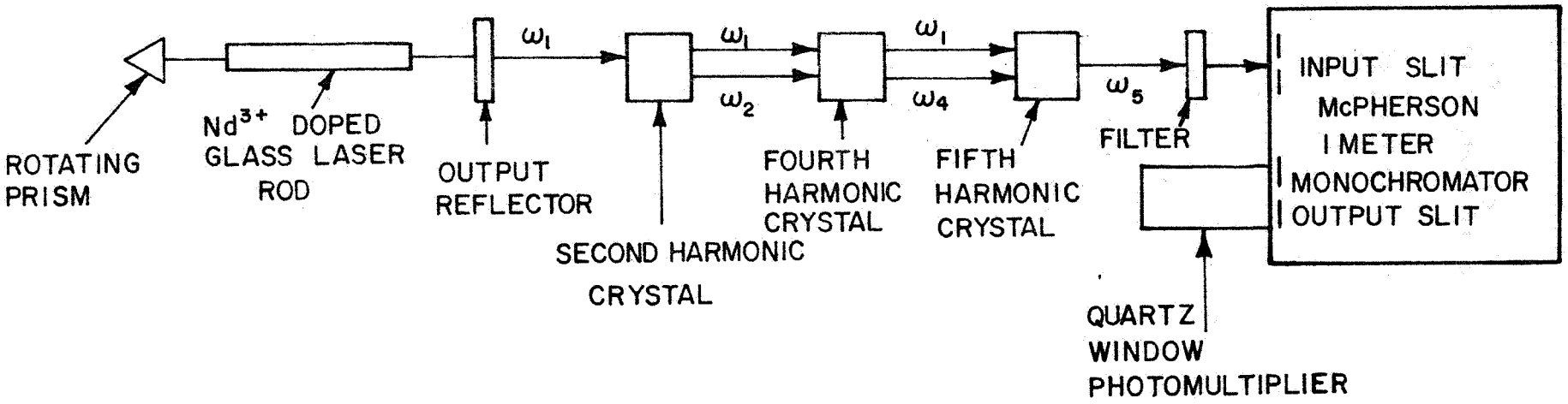

Figure 4-12. Experimental arrangement used in the generation of the 5th harmonic of neodymium to produce 2155Å.

the procedure was repeated for the fourth harmonic crystal used to generate the 2650Å output. Finally, the crystal to be tested for fifth harmonic generation was placed in the beam and its output was adjusted to pass through the interference filter to the input slit of the McPherson Model 216, 1-meter monochromator. The sensitivity of the quartz window photomultiplier at the output of the monochromator was adjusted until a small signal, due to leakage through the filter and scattering in the monochromator, was observed. The fifth harmonic crystal was then rotated through a series of angles including the value at which phase matching was expected to occur. An oscilloscope photograph of the photomultiplier output was obtained for each laser pulse.

The laser had a 3/8-inch diameter by 3-inch pumped length Kodak ND 11 Nd^{3+} doped glass laser rod which was Q-switched by a rotating prism. The power output was 20 MW in a 13-ns pulse. The second harmonic at 5300Å was generated with a phase matched ADP crystal and a power output of 1.7 MW was measured with an EGG Lite Mike. The fourth harmonic at 2650Å was generated in another phase matched ADP crystal and the power output was measured with a calibrated photomultiplier using a sodium salicylate (Ref. 80) coating to convert the UV into visible radiation. An output of about 20 kW was measured at 2650Å.

As discussed previously, KDDP represents the most promising material for fifth harmonic generation. Initial experiments were conducted using an available sample of KDDP. Unfortunately, this sample was cut a 45 degrees to the x-axis and close to 90 degrees orientation was required for phase matching. This made it difficult to get the beam through the crystal. The technique normally adopted is to immerse the crystal in a liquid of the same index of refraction contained in a cell with fused quartz windows. This eliminates the necessity for a high quality polish on the crystal and prevents moisture from attacking it. However, few liquids exist with sufficiently low absorption at 2120Å. After a search of the literature, acetonitrile was chosen, though its index of 1.35 did not represent a good match for KDDP at 1.5.

Detection of the fifth harmonic was first attempted using the 1-meter McPherson spectograph and Polaroid 3000 speed film, with no success. However, it was subsequently found that the film gelatin was somewhat absorbing below 2500Å, thereby reducing its sensitivity. For this reason, the calibrated photomultiplier with the sodium salicylate coating was employed subsequently with an interference filter have a 10 percent transmission at 2120Å. The beam was attenuated by allowing it to impinge on a magnesium oxide block and observing a portion of the diffuse scattered light. It was found, however, that the interference filter transmitted sufficient second and fourth harmonic radiation to mask any fifth harmonic.

In order to reduce this leakage the filter was combined with the McPherson spectrograph set up as a monochromator at 2120Å. This reduced the leakage of 5300Å and 2650Å radiation to below the sensitivity limit of the sodium salicylate coated photomultiplier. However, no fifth

harmonic was detected. In order to extend the sensitivity further, an EMI 9558Q photomultiplier with a quartz window was then tried in the monochromator but again no fifth harmonic was detected. A check of the transmission of the KDDP indicated that it was transmitting only about 25 percent at 2120Å and, because of this and the incorrect angle of this KDDP sample it was decided to order a new crystal at the correct orientation and of higher purity. The experiment was repeated using the new crystal but fifth harmonic was still not detected. A calculation of the detection sensitivity indicated that the maximum amount of fifth harmonic present was less than 10-mW peak.

5. SUMMARY AND CONCLUSIONS

The results of the investigation presented in the preceeding sections of this report are summarized below under three general categories.

1. A theoretical study to determine transitions of the ambient atmospheric nitric oxide molecule which offered the greatest promise for laser probing of the atmosphere by the mechanism of resonance scattering.

2. A developmental program wherein various methods were examined for producing laser radiation from NO gas at transitions where the terminal state both corresponded to a well populated state in atmospheric NO and whose characteristics made probing possible.

3. An experimental program to explore techniques of suitably tuning existing lasers to the appropriate resonance wavelengths with sufficient output energy to provide reasonable signal-to-noise ratios.

The theoretical investigation centered on calculations of the ratio of integrated resonance scattering cross section to the Rayleigh scattering cross section for the ambient atmospheric molecules, termed the resonant/Rayleigh ratio. This parameter was employed as a figure of merit to select candidate transitions from among those for which pertinent data were available. It was concluded on the basis of this criterion that the $\gamma(n,o)$ bands, or the vibration rotation bands (1-0, 2-0, or 2-1) constituted the only likely candidates for a laser probing scheme. In turn, this restricted operations to the far UV or the far IR, where both practical laser technological difficulties exist such as the availability of optical components as well as the presence of atmospheric transmission or emission problems are encountered.

5.1 Direct Production of NO Resonant Frequencies

The results of the development program demonstrate that operating a direct NO laser at either of the above spectral regions is not promising particularly for electronic transitions in the UV. Moreover, the IR laser energy already produced in NO in the ground state by photodissociation of $NOC\ell$ is on higher vibration rotation levels than required for a resonant probing experiment. Further development may result in lasing of lower vibrational states, although increasing difficulties may be involved.

5.2 Indirect Frequency Shifting Techniques for Producing NO Resonant Frequencies

The experimental work performed under the program involved the shift-tuning of known high power lasers using harmonic generation, sum frequency, generation, stimulated Raman shifting, and parametric oscillation. These techniques appear to offer reasonable means of generating radiation at the lines of interest.

5.2.1 Evaluation of Frequency Shifted $\gamma(1,0)$, 2155Å Laser Probe.- At the $\gamma(1,0)$ 2155Å transition, a return signal of 350 photons was calculated for an assumed 50 millijoule pulse. At this wavelength, low-noise photomultipliers are available with a quantum efficiency of 0.2 (thus 70 electrons per pulse). At room temperature, typical thermionic electrons are about 100 per second, or only about 10^{-4} electrons per 0.26μ sec lifetime of the $\gamma(1,0)$ transition. The imposition of moderate cooling reduces this relatively low background even further. At this wavelength, no additional optical backgrounds of significance should exist, certainly not at night or in the presence of moderate filtering of the photomultiplier.

Two major difficulties exist with respect to this experiment: (1) the atmospheric transmission cutoff, and (2) the problem of producing 50 millijoules at the shift-tune wavelength.

It happens that the 2155Å wavelength matches an absorption minimum between the oxygen and ozone absorptions. Although the atmosphere is opaque at sea level, a transmission of about 70 percent exists through the vertical at about 40,000 feet, as demonstrated from observed solar spectra from an aircraft. Although the inconvenience of mounting the relatively massive laser generator and 12 inch telescope receiver on an aircraft with transmitting window at 2155Å (high quality fused quartz) is a relatively serious problem, it represents the best possibility for the operation of an NO probe on an electronic transition.

Experimental attempts to date to produce 2155Å radiation employing sum-frequency generation of a 20 MW Neodymium-glass laser were generally unsuccessful. However, it is felt that the method is still somewhat promising and the use of higher powered lasers is recommended.

5.2.2 Evaluation of Frequency Shifted NO Fundamental 5.3μ Laser Probe.- For probing at the 5.33μ transition, use can be made of the accidental match between the second harmonic of the CO_2 laser transition on the $00^01 - 10^00$, P-branch, J = 24 and the NO $(\bar{1},0)$, R branch, J = 1. In this case, the atmospheric transmission is about 20 percent although the major difficulty involves the thermal background radiation.

While high power CO_2 laser operation has been demonstrated, resonance scattering in NO using the harmonic was not observed. Furthermore, the conversion efficiency into the harmonic was significantly less than both theory and the results of others would indicate. This result is attributed to a poor quality tellurium crystal. Unfortunately, an acceptable replacement could not be acquired during the contract performance period.

Another method of producing radiation at the 5.3μ NO transition involved the use of stimulated Raman shifting from the Neodymium-glass or Neodymium calcium-tungstate lasers. Nd-glass lasers have an output

between 9410 cm^{-1} and 9458 cm^{-1}. The range of NO frequencies to be probed is between approximately 1850 cm^{-1} and approximately 1900 cm^{-1} which requires a Raman shift of between 7510 cm^{-1} and 7610 cm^{-1}. The third Stokes line of a material having a shift between 2503 cm^{-1} to 2536 cm^{-1} could be employed. Alternatively, if H_2 gas ($\Delta\nu$ = 4156 cm^{-1}) is used to produce a first Stokes line, this in turn could produce a first Stokes line in a material with Raman frequency between 3354 and 3454 cm^{-1}. It was found that the N-H bond in aliphatic compounds has a frequency in this range.

Considering the rapid advances in CO_2 laser technology and the general state of knowledge concerning the stimulated Raman effect, it is recommended that future efforts be placed on shift tuning to the vibration-rotation (1,0) transition for NO atmospheric probing.

REFERENCES

1. Nicolet, M., "Nitrogen Oxides in the Chemosphere", J. Geophys. Res. 70, (3 February 1963).

2. Nicolet, M., "Ionospheric Processes and Nitric Oxide", J. Geophys. Res. 70, (3 February 1963).

3. Barth, C. A., "Rocket Measurements of the Nitric Oxide Day-Glow", J. Geophys. Res. 69, 3301 (August 1, 1964).

4. Barth, C. A., Planet. Spa. Sc. 14, 623 (1966).

5. Smith, L. G., "Ionization By Lyman-α in the E-region at Sunrise," J. Atmos. Terr. Physics 28, 1195-1205 (1966).

6. Barth, C. A., "Chemical Reactions in the Lower and Upper Atmosphere," Interscience N-Y, 303 (1961).

7. Jursa, A. S., Tonaka, A. and LeBlanc, F., "Nitric Oxide and Molecular Oxygen in the Earth's Upper Atmosphere," Planet. Spa. Sci. 1, 161-172

8. Collis, R.T.H., "Lidar Observations of Clouds," Science 149, 978 (1965).

9. Collis R.T.H. and Ligda, M.G.H., "Note on Lidar Observations of Particulate Matter in the Stratosphere," J. Atmos. Sci. 23, 255 (1966).

10. Collis, R.T.H., Fernald, F. G. and Ligda, M.G.H., "Laser Radar Echoes from a Stratified Clear Atmosphere," Nature 203, 1274 (1964).

11. Fiocco, G. and Colombo, G., "Optical Radar Results and Meteoric Fragmentation," J. Geophys. Res. 21, 1795 (1964).

12. Fiocco, G. and Grams, G., "Observations of the Aerosol Layer at 20 km by Optical Radar," J. Atmos. Sci. 21, 323 (1964).

13. Fiocco, G. and Smullin, L. D., "Detection of Scattering Layers in the Upper Atmosphere (60-140 km) by Optical Radar," Nature 199, 1275 (1963).

14. Grams, G. and Fiocco, G., "Stratospheric Aerosol Layer During 1964 and 1965," J. Geophys. Res. 72, 3523 (15 July 1967).

15. Barrett, E. W. and Ben-Dov, O., "Application of the Lidar to Air Pollution Measurements," J. Appl. Meteorology 6, 500 (June 1967).

16. Hirono, M., "On the Observation of the Upper-Atmosphere Constituents by Laser Beams," J. Radio Res. Labs (Japan) 11, 58 (1964).

17. Young, R. A., "Optical Radar Study of the Upper Atmosphere," Faraday Soc. (London) Disc. 37, 118 (1964).

18. Cooney, J. A., "Measurements on the Raman Component of Laser Atmospheric Backscatter," Appl. Phys. Letters 12, 40 (15 January 1968).

19. Leonard, D. A., "Observation of Raman Scattering from the Atmosphere Using a Pulsed Nitrogen Ultraviolet Laser," Nature 216, 142 (14 October 1967).

20. Brynes, K., Crozier, E., Hurd, A., Pike, C., Sargent, B., and Schuler, C., "Laser Mapping of Bomb Debris Atmospheres," Final Report on Phase II, Contract DA-49-146-XZ-350, GCA Corporation (March 1968).

21. Deutsch, T. F., Appl. Phys. Letters 9, 265 (15 October 1960).

22. Huber, M., Phys. Letters 12, 102 (1964).

23. Penndorf, R., JOSA 47, 176 (1957).

24. Carpenter, R. O'B., Pressman, J., and Berger, A., "Evaluation of Active Probe for Atmospheric Nitric Oxide," Quarterly Progress Report No. 1, Contract NAS 12-85 (April 1966).

25. Carpenter, R. O'B., and Driscoll, J. N., "Evaluation of Active Probe for Atmospheric Nitric Oxide," Quarterly Progress Report No. 5, Contract NAS 12-85 (15 April 1967).

26. Gilmore, F. R., JQSRT 5, 369 (1965).

27. Broida, H. P. and Peyron, M., J. Chem. Phys. 32, 1068 (1960).

28. Carpenter, R. O'B. and Franzosa, M., JQSRT 5, 465 (1965).

29. Nicholls, R. W., Annide Geophys. 20, 144 (1964).

30. Nicholls, R. W., J. Res. NBS 68A, 535 (1964).

31. Schuoin, B. and Clough, S. A., J. Chem. Phys. 38, 1855 (1963).

32. James, T. C., J. Chem. Phys. 40, 762 (1964).

33. Breene, R. G., J. Chem. Phys. 29, 512 (1958).

34. Herzberg, G., Molecular Spectra and Molecular Structure, Vol. I, p. 124," Spectra of Diatomic Molecules," 2nd Edition.

35. Bennett, App. Opt. Supp. "Chemical Lasers" (1965).

36. Schawlow, A. and Townes, C. H., Phys. Rev. 112, 1940 (1958).

37. Patel, C.K.N., Phys. Rev. 136A, 1187 (1964).

38. Patel, C.K.N. et al., Appl. Phys. Let. 5, 81 (1964).

39. Patel, C.K.N., Phys. Rev. 141, 71-83 (January 1966).

40. MacFarlane, R. A. and Howe, J. A., Phys. Let. 19, No. 3, 208-210 (15 October 1965).

41. Legay-Sommaire, N., and Legay, F., Le J. de Phys. 25, 59 (1964); Legay-Sommaire Henry, Legay, and Kastler, C. R., Acad. Sci. Paris 260, 3339 (1965).

42. Polanyi, J. C., Applied Optics, Supplement 2: Chemical Lasers, 109-127 (1965).

43. Muller, M. W., Sher, A., Solomon, R. and Dow, D. G., Appl. Phys. Letters 2, 86 (1963).

44. Shuler, K. E., Carrington, T. and Light, J. C., Appl. Optics, Supplement 2: Chemical Lasers 81 (1965).

45. Bosco, N., and Norris, R.G.W., Proc. Roy. Soc. (London) A268, 291 (1962).

46. Calbar, A. B., Proc. Roy. Soc. (London) A276, 401 (1963).

47. Wells, J., Appl. Phys. 36 (9 September 1965).

48. Heil, H. and Wagner, W. G., Atomic Collision Processes, Amsterdam North-Holland Publishing Co.

49. Patel, C.K.N., Phys. Rev. Let. 15, 1027 (1965).

50. Patel, C.K.N., Phys. Rev. Let. 16, 613 (1966).

51. Broude, V. L., Krarchenko, V. I., Prokopyuk, N. F., and Soskin, M. S., JETP Letters 2, 324 (1965).

52. Akhamanov, S. A., Kobirigin, A. I., Piskarskas, A. F., Khokhlov, R. V., JETP Letters 2, 141 (1965).

53. Miller, R. C. and Savage, A., Phys. Rev. 128, 2175 (1962).

54. Zernnike, F., J. Opt. Soc. Am. 54, 1215 (1964).

55. Phillips, R. A., "Temperature Variation of the Index of Refraction of ADP, KDP, KDDP," J. Opt. Soc. Am. 56, 629 (1966).

56. Garmire, E., Panderese, E. and Townes, C. H., "Coherently Driven Molecular Vibrations and Light Modulation," Phys. Rev. Letters 11, 160 (August 1963).

57. Bloembergen, N., Nonlinear Optics, W. A. Benjamin, Inc., New York (1965).

58. Glass, A., "Design Considerations for Raman Laser," IEEE J. Quant. Elect. QE-3, 249 (abstract) (June 1967).

59. Minch, R. W., Terhune, R. W. and Rado, W. G., "Laser Stimulated Raman Effect and Resonant Four-Photon Interactions in Gases H_2, D_2 and CH_4," Appl. Phys. Letters 3, 181 (November 1963).

60. Johnson, F. M., Duardo, J. A. and Clark, G. L., "Complex Stimulated Raman Vibration - Rotational Spectra in Hydrogen," Appl. Phys. Letters 10, 157 (March 1967).

61. Martin, M. D. and Thomas, E. L., IEEE J. Quant. Elec. QE-2, 196 (August 1966).

62. Matheson Gas Data Book, The Matheson Company, East Rutherford, New Jersey, Third Edition, p. 91 (1961).

63. Sorokin, P. P. and Lankard, J. R., "Stimulated Emission Observed from an Organic Dye, Chloro-aluminum Phthalocyanine," IBM J. of Res. and Dev. 10, 162 (March 1966).

64. Spaeth, M. L. and Bortfeld, D. P., "Stimilated Emission from Polymethine Dyes," Appl. Phys. Letters 9, 179 (1 September 1966).

65. Schafer, F. P., Schmidt, W. and Volze, J., "Organic Dye Solution Laser," Appl. Phys. Letters 9, 306 (15 October 1966).

66. Sorokin, P. P. Culver, W. H., Hammond, E. C. and Lankard, J. R., "End-pumped Stimulated Emission from a Thiacarbocyanine Dye," IBM J. of Res. and Dev. 10, 401 (September 1966).

67. Sorokin, P. P. Lankard, J. R., Morizzi, V. L., and Hammond, E. C., "Organic-Dye-Stimulated Emission Spectra," Bull. Am. Phys. Soc. 12, 90 (January 1967).

68. Schafer, F. P., Schmidt, W. and Marth, K., "New Dye Lasers Covering the Visible Spectrum," Phys. Letters 24A, 280 (27 February 1967).

69. Sorokin, P. P., Lankard, J. R., Hammond, E. C. Morizzi, V. L., "Laser-pumped Stimulated Emission from Organic Dyes: Experimental Studies and Analytical Comparisons," IBM J. Res. and Dev. 11, 130 (March 1967).

70. Sorokin, P. P. and Lankard, J. R., "Flashlamp Excitation of Organic Dye Lasers: A Short Communication," IBM J. Res. and Dev. 11, 148 (March 1967).

71. McFarland, B. B., "Laser Second-Harmonic-Induced Stimulated Emission of Organic Dyes," Appl. Phys. Letters 10, 208 (1 April 1967).

72. Soffer, B. H. and McFarland, B. B., "Continuously Tunable, Narrow Band Organic Dye Lasers," Appl. Phys. Letters 10, 266 (15 May 1967).

73. Bass, M. and Deutsch, T. F., Appl. Phys. Letters 11, 89 (1 August 1967).

74. Gibbs, W.E.K. and Kellock, H. E., IEEE J. Quant. Elect. QE-3, 419 (October 1967).

75. Snavely, B. B., Peterson, O. G., and Reithel, R. F., Appl. Phys. Letters 11, 275 (1 November 1967).

76. Miyazoe, Y. and Maeda, M., Appl. Phys. Letters 12, 206 (1 March 1968).

77. Horrigan, F., Final Report, U. S. Army Missile Command, Contract DA-01-021-AMC-12427 (Z) (March 1966).

78. Rigden, J. D. and Moeller, G., IEEE J. Quant. Elect. QE-2, 365 (September 1966).

79. Witteman, W., IEEE J. Quant. Elect. QE-2, 375 (September 1966).

80. Samson, J.A.R., Vacuum Technique of Vacuum Ultraviolet Spectroscopy, John Wiley and Sons, New York (1967).